Advanced Manufacturing Research Centre

MACHINABILITY STUDY AND FEM ANALYSIS OF UD-CFRP COMPOSITE MTM 44-1 MATERIAL UNDER ORTHOGONAL CUTTING CONDITION

(Orthogonal Experimental Cutting tests and FE Modelling of UD-CFRP material)

Thesis

Submitted for the Requirements of

Master of Philosophy

Written By: Davide Lazzarato

Submission Date: January 2014

Abstract

Several engineering applications in the aerospace, marine, military and automotive industries have introduced modern synthetic composites as a substitute to metals due to their high specific strength and stiffness. Furthermore, their high corrosion resistance and lightweight make the aerospace industry the largest beneficiary of these materials.

While the advantages of using composite materials are well known designers have to face their limitations. Being relatively new materials further studies are still required to better understand their actual limits, related to the high materials cost and the manufacturing process complexity when compared to metals.

The aim of this project was to analyse some of the machinability challenges set by Carbon Fibre Reinforced Polymer (*CFRP*) and provide a better understanding of the relationship between a number of process parameters and relative cutting forces generated during the machining process. A Finite Element Model (*FEM*) was created to predict cutting forces during orthogonal cutting of Unidirectional Carbon Fibre Reinforce Polymer (*UD-CFRP*) composite material. The material analysed was a *MTM 44-1* low density toughened epoxy matrix system particularly suited for the production of both primary and secondary aircraft structures. The work-piece was considered as an Equivalent Orthotropic Homogeneous Material (*EOHM*) alongside with a failure mechanism model using the Chang-Chang criteria. Experimental tests were performed on a lathe machine tool in order to compare and validate simulation results. Polycrystalline diamond (*PCD*) inserts were used to carry out the tests. Work-pieces with a ring shape were used for experimental tests to obtain suitable data. The specimens were carefully designed and built at the Advance Manufacturing Research Centre (*AMRC)* based in Sheffield. Six different fibre orientations, two cutting speeds and four feed rates have been used to generate a full set of experimental data.

The cutting force results highlighted a dependency between cutting parameters and fibre orientations of the *CFRP* specimens. The results have shown that fibre orientation is a key factor that governs failure mechanisms, chip formations, surface integrity and cutting forces.

Abstract

Both the experimental tests and the *FEM* analysis have confirmed the influence that the feed rate has on the cutting forces. Conversely, negligible effects were observed when increasing the cutting speed at the tested cutting conditions.

Acknowledgements

The author would like to express his appreciation to those who have made contributions throughout the duration of this work.

First of all I would like to express my gratitude for my supervisors, Dr. Sam Turner for his invaluable support and guidance throughout this project, for his precious advice and for the time he dedicated to read this thesis.

I would like to thank Dr. Sabino Ayvar-Soberanis for the guidance and help in this research.

Particular thanks go to Prof. Jeong Whan Yoon and Mariana Paulino who shared their knowledge in *FEM* Analysis during the time I spent at the *AMRC* at the Swinburne University in Melbourne.

I would also like to thank the colleagues with whom I shared the office during the four years I spent in the *AMRC* part of the University of Sheffield.

Finally, special thanks must go to my family, to Jaleh, to Davide, to Gianluca and to all of my friends for sharing with me the good and the bad moments I have been through during these four years I have lived in Sheffield.

Contents

Contents

Nomenclature

UD-CFRP	*Uni-Directional Carbon Fibre reinforced Polymer*
EOHM	*Equivalent Orthotropic Homogeneous Material*
FEM	*Finite Element Method*
FRP	*Fibre Reinforced Polymer*
CFRP	*Carbon Fibre reinforced Polymer*
ALE	*Arbitrary Lagrangian Eulerian*
PCD	*Poly-Crystalline Diamond*
CTE	*Coefficient of Thermal Expansion*
DOC	*Depth of Cut (mm)*
CZM	*Cohesive Zone Model*
UMAT	*User Define Material Model*
DEM	*Discrete Element Method*
GFRP	*Glass Fibre Reinforced Polymer*
OoA	*Out of Autoclave*
θ	*Fibre orientation angle (deg)*
α	*Rake angle (deg)*
γ	*Relief angle (deg)*
r	*Edge Radius (mm)*
f	*Feed rate (mm/rev)*
Vc	*Cutting speed (m/min)*

Nomenclature

Fc	*Principal cutting force (N)*
Ft	*Thrust force / Feed force (N)*
$\sigma_{11}{}^{T}$	*Longitudinal tensile strength*
$\sigma_{11}{}^{C}$	*Longitudinal compressive strength*
$\sigma_{22}{}^{T}$	*Transverse tensile strength*
$\sigma_{22}{}^{C}$	*Transverse compressive strength*
σ_{12}	*In-plane shear strength*
$e_i^{t,c}$	*Failure criterion ratio*
X_T	*Maximal tensile strengths along fibre direction*
X_C	*Maximal compressive strengths along fibre direction*
Y_T	*Maximal tensile strengths along matrix direction*
Y_C	*Maximal compressive strengths along matrix direction*
Sab	*Allowable shear strengths in the principal material directions*
ADC	*Automated Dynamics system composite center*
SRATE	*Strain rate effects*
FAIL	*Failure criteria*
EOS	*Equation of state required for 3D solid and 2D continuum elements*
THERM	*Thermal effects*
ANISO	*Anisotropic orthotropic*
DAM	*Damage effects*
TENS	*Tension handled differently that compression in some manner*

Nomenclature

D	*Material stiffness parameters*
ε_{ij}, γ_{ij}	*Strain along axis i and j*
E_i	*Young modulus along axis i*
G_{ij}	*shear modulus in direction j*
v_{ij}	*Poisson's ration*
DFAILT	*Maximum strain for fibre tension*
DFAILC	*Maximum strain for fibre compression*
DFAILM	*Maximum strain for matrix*
DFAILS	*Maximum shear strain*
TFAIL	*Time step limit*
EFS	*Effective strain*
FBRT	*Crush front strength reducing parameter*
YCFAC	*Softening compressive fibre factor after matrix failure*
SOFT	*Young modulus reduction parameter*
MID	*Material identification number*
RO	*Mass*
AOPT	*Material axes optional parameter*
A1, A2, A3	*Vector component for material axes for AOPT=2*
D1 D2 D3	*Vector component for material axes for AOPT=2*
CRIT	*Failure criterion used (MAT54, MAT55)*
CFC	*Channel Frequency Class*

Nomenclature

SEM	*Scanning Electron Microscope*

List of figures

List of figures

List of tables

CHAPTER 1 OVERVIEW AND PROJECT AIM

1.1 Introduction

The use of Carbon Fibre Reinforced Polymer (*CFRP*) composite has grown considerably over the recent years. Although their creation ascends to a half century ago, their use was initially limited to few niche aerospace and defence applications due to their high manufacturing costs. This can be attributed to their high production costs as well as to the fact that carbon fibres are a very expensive raw material.

The development of new and innovative production technologies has reduced carbon fibre cost promoting their use across different industries. During the last decades *CFRP* have earned huge importance for applications in many industrial sectors such as automotive, sporting, wind energy, nuclear, construction, naval, biomedical and offshore oil and gas applications.

One of the emerging opportunities and challenges in carbon fibres manufacturing is to move *CFRPs* from low to high volume production within the next decades. This is due to an increase in industry demand driven by the need of finding lightweight materials that can comply with more stringent legislation requirements for greenhouse gas emission reduction.

CFRPs are well suited for several engineering applications thanks to their superior corrosion resistance, lightweight and specific strength and stiffness. Despite the fact that composite parts are fabricated near-net shape, machining operations such as trimming and drilling are still required in order to achieve close fit tolerances and component design requirements.

The *CFRP* machining aspects differ significantly from those of traditional and well known metal materials. Although the theory of cutting has been mainly developed for homogeneous materials, the cutting mechanisms for Fibre Reinforced Polymer (*FRP*) are largely unexplored. Their anisotropy and non-homogeneity nature makes them "difficult-to-machine" materials.

CHAPTER 1 **OVERVIEW AND PROJECT AIM**
- Introduction -

The *CFRP* cutting process is highly dependent on the properties of the *CFRP* main constituents, the matrix and the fibres, which significantly affect the machining process. From a structural point of view, the matrix phase is the constituent that provides load transfer and structural integrity, while the reinforcing phase enhances the mechanical properties of the material.

Extensive experimental campaigns have been performed to understand the cutting mechanisms of *CFRP* materials. One of the main problems that limit their machinability is related to the fact that *CFRPs* are extremely abrasive. Therefore the selection of suitable cutting tools is essential to limit tool wear, machining costs and to improve structural quality of final components. As a matter of fact, if unsuitable cutting tools or cutting conditions are used damage phenomena such as fibre pull out, delamination and debonding rapidly occur. For all these reasons the machining of composite structures creates discontinuities in the fibres which can negatively affect part integrity and performances.

Therefore, with the increasing use of *CFRP* materials in the industry, the need to develop optimised and economical machining processes has arisen.

Due to the complexity of these materials, which are constitute by two or more distinct elements having their own separate structural properties, the design of new cutting tools are mostly based on knowledge gained through experience and often require extensive and expensive trial and error testing, performed with the intention to reproduce the same cutting conditions the tool experiences during its real application. Being real applications focussed in practice over the oblique cutting of multidirectional *CFRP* structure, it is not possible to capture the correlation between the machinability aspects and the input process parameters without having a deep understanding of the process. Thus, although multidirectional composites have more practical interest than unidirectional ones, the latest lend themselves nicely for research investigation, because it is easier to relate their mechanical properties and machining characteristic to fibre orientation.

Many studies on the machinability of *CFRP* composites are discussed in literature. Some of them focus on real manufacturing applications (as drilling, milling, trimming,

turning, etc.) with the intention of investigating the quality of the cut surface and tool performances for different process conditions. Others are aimed to investigate the failure mechanisms that lead to chip formation. The former group is devoted to the study of a real cutting process under representative cutting conditions, where a 3-dimensional cut takes place on a multi-directional composite lamina. Whilst on the other hand, the latter group tends to use a simplified approach, where by a low speed 2-dimensional cut is performed on a uni-directional lamina.

The main aim of this study was to design a dynamic cutting operation, performed at representative cutting conditions, which enables the use of a simplified analysis approach. In these conditions, the machinability of a Unidirectional Carbon Fibre Reinforced Polymer (*UD-CFRP*) composite material was investigated. Turning cutting trials were performed under an orthogonal cutting condition. Representative cutting speeds and feeds were used by turning operations with a lathe. As a result, a better understanding of how the process parameters affect the cutting forces was found. This simplified approach enabled the performing of a 2D plane stress study which reduced complications in the chip formation analysis.

The work discussed in this thesis is a Boeing research project carried over at the *AMRC* of the University of Sheffield. Part of the activity was developed at the *AMRC* of the Swinburne University in Melbourne. The purpose of the study was to increase the expertise on machining of composite materials within the *AMRC* in Sheffield by combining the expertise of two groups operating within the company: the *AMRC* Composite Centre knowledge together with the knowledge on cutting processes developed by the Process Technology Group.

A preliminary numerical model was developed at the Swinburne University of Technology of Melbourne using LS-Dyna for comparison with the experimental data to provide an insight of the effects of the cutting parameters on the cutting forces.

1.2 Structure of the thesis

In **Chapter 2** a literature review on the machining of *CFRP* material is presented. An overview of the cutting process is given to provide the fundamental knowledge to understand the difficulties that arise when cutting *CFRP* materials; which differ significantly in many aspects from the machining of the well-known metal materials. The *FEM* techniques developed during the last decades are also described and discussed.

Chapter 3 focusses on the experimental tests describing machine tool set-up, designed procedures, used equipment and experimental results. In **Chapter 4** the data acquired from the cutting trials are compared with the results obtained from the developed FE model**.** Dynamic tensile tests and model calibration are included.

Conclusions are covered in **Chapter 5** while suggestions for future work are offered in **Chapter 6**.

CHAPTER 2 LITERATURE REVIEW

2.1 Introduction

In several engineering applications in the aerospace, marine, military, and automotive industries modern synthetic composites have been introduced as substitutes for metals due to their high specific strength (strength to weight) and stiffness (stiffness to weight) [1], [2].

Each of these sectors requires different qualities that composite materials must satisfy. Thanks to their high corrosion resistance, lightweight and their specific strength and stiffness, composite materials are not only used in the aerospace industry, but also in the sport sector which accounts as the second largest beneficiary of polymer composites. Application span from the production of large products such as boats and cars, to smaller items such as bicycles, tennis rackets, skis and fishing poles, just to mention few, amongst a growing range of products [3].

Composites consist of two or more distinctly different materials present in reasonable proportions, that when combined together have superior characteristics than each single constituent when taken alone. In nature there are many natural composites, such as wood, which consists of a cellulose fibre and lignin matrix, and bones, made up of collagen embedded in a mineral matrix. The use of composites, from a manufacturing point of view, can result in a significant reduction in the number of parts, tooling and assembly required for a specific component [4].

While the advantages of using composite materials are well known (structural properties, thermal insulation, conductivities, acoustic insulation, corrosion and fatigue resistance) designers have to face their limitations. Being relatively new materials, introduced into industry in the early 1900s, further studies are still required to better understand their actual limits, related to the high materials cost and the manufacturing process complexity (lack of simple analysis tools, reliable material properties data bases, easy to implement design rules) when compared to metals [3].

CHAPTER 2 **LITERATURE REVIEW**
- Introduction -

In the manufacturing industry, the composites are classified by the type of matrix material used, which can be metallic, ceramic or polymeric. The matrix material has a profound effect on the properties of the finished composite. The bulk role is to transfer the external loads applied to the reinforcement to support the structure during compression loading and to protect it from adverse environmental conditions. The reinforcement material can again be metallic, ceramic or organic. The combination between the bulk (matrix) and the reinforcement (fibres) generate a new material having properties that differ from the individual constituents [4].

These mechanical properties differ from metals because by modifying the structure and volume fraction of the reinforcing phase (fibres orientation) it is possible to obtain a material with isotropic, quasi-isotropic or anisotropic properties. Composites behave as quasi-isotropic materials when the mechanical properties of a component are independent from the force direction acting on the part. This condition is achieved when the reinforcement is formed of equiaxed fibres uniformly distributed. Materials with unequal dimensional reinforcement behave as quasi-isotropic, while composite with long fibre perfectly aligned behaves as anisotropic. Mechanical properties are also greatly dependent upon the manufacturing process used. Using fibres with a negative coefficient of thermal expansion (*CTE*) along the reinforcement axis gives designers the option to create components that can be designed with zero-dimensional change over a wide range of temperature [3].

FRP are a specific class of composite materials constituted by a polymeric matrix matched with a reinforcement of carbon, glass or aramid. *FRPs* possess high specific strength and stiffness with good corrosion and fatigue resistance under loading [5].

Despite the fact that composite parts are fabricated near-net shape, machining operations such as milling, trimming, drilling and grinding are still required in order to achieve close fit tolerances and component design requirements [6]. The *CFRP* machining aspects differ significantly from those of traditional and well known metal materials. Although the theory of cutting has been mainly developed for homogeneous materials, the cutting mechanisms of *FRP* are largely unexplored [7], [8].

Their anisotropy and non-homogeneity nature makes them "difficult-to-machine" materials. The cutting forces are not easy to predict [9] and the cut surfaces integrity, in terms of residual stresses, roughness and subsurface damage, is hard to control [10]. Moreover, cutting operations create discontinuities in the fibres which can result in a reduction of the part performances [8], [11], [12].

The increasing use of *CFRP* parts lead to the development of efficient cutting techniques that allowed a reduction of manufacturing costs, whilst preserving the structural integrity of the components after machining [2].

Due to the large number of factors that play a significant role when machining it is almost impossible to deal with such a complex scenario. The use of an experimental approach to investigate their connection with the process behavior is expensive and time consuming. Therefore mathematical simulations are considered a valid alternative when study chip-formation processes. Additionally, the advent of computers during the last decades enabled the use of sophisticate numerical techniques to model engineering phenomena such as elasticity, plasticity, fracture mechanics, heat transfer, lubrication, contact problems and metallurgy [13], [14].

Finite element methods are widely used for analysis of structural engineering problems. The main aim of a *FEM* is to predict displacements, strain and stresses in the work-piece along with temperature and loads acting on the tool under defined cutting conditions [13], [14].

2.2 Machining of composite materials

Although composite components are designed and manufactured near net shape, some machining operations are still required to remove excess material for fixturing purposes (to create holes, slots and other features that are not possible to obtain during the manufacturing phase) and for finishing tight-tolerance features. The most common machining operations when cutting composite components are drilling and milling, but even trimming, routing, countersinking, sawing, turning, abrasive cutting and grinding can be performed [3], [5], [6].

According to Mazumdar [5] the labour costs of the machining operation in the aerospace industry is one of the major factors, reaching 50% of the total manufacturing cost of current airframes. A fighter plane has between 250,000 and 400,000 holes while a bomber or transporter have between 1,000,000 and 2,000,000 holes.

Mainly due to their mechanical properties, machining of composite material is widely different from metal cutting even though the technology used (machine tools, tools and inserts) is the same [3], [5], [6].

FRPs machining differs from metal machining in several aspects, largely because they are inhomogeneous materials constituted of different phases. In the majority of homogenous and ductile metals, the cutting process is characterised by plastic deformation of the bulk material where a continuous chip is formed by the shearing action. Under fixed cutting conditions a steady state cutting process is reached and the cutting forces, temperature, induced surface damage and surface quality, can be predicted within a satisfactory level of accuracy. On the other side *FRPs* machining is characterized by fractures which oscillate with the intermittent rupture of the fibres, driven by phenomena which are not yet well understood [3], [15].

FRPs machinability is mainly determined by the physical and mechanical properties of the constituents, by the fibre orientation and the tool geometry. The surface quality of the machined edge is highly affected by the type of fibre reinforcement and its orientation. For example, glass and carbon fibres exhibit brittle behaviour while aramid fibres bend ahead of the advancing cutting edge. Also, because the strength of the matrix material is typically lower than the fibres, the generated cutting forces are primarily dependent on the type of fibre used, and also to its dimensions and volume fraction [4], [5].

The temperatures reached during the cutting process depend specifically on the *FRPs* thermal properties and on the fibre orientation. Carbon fibres have a higher thermal conductivity when compared to glass and aramid fibres, they are more capable of transferring heat along the fibres length, dissipating it away from the cutting zone. High localised long-lasting temperatures have to be avoided to preserve the polymeric matrix integrity. Localised heating can lead to burning in the machined surface of

thermosetting polymers and gumming of thermoplastic polymers. Moreover, different thermal expansion coefficients between the matrix and the fibres can lead, during the cutting process, to thermal stress which may deform and damage the composite structure. This can lead to nonconformity of tolerance features and structural quality issues [3].

The integrity of the machined surface is a fundamental factor in determining the machinability of *FRPs*. Their structural quality can be significantly affected during the cutting process where defects such as delamination, cracking, fibre pull-out, and burning can occur [8]. The most common problem is the delamination caused by the low strength of the structure along the laminates and the potentially high transverse forces created by the cutting process [16]. These forces can be reduced by matching the use of proper cutting tool geometry with the correct cutting parameters which allow the fibres to be sheared neatly. This can be achieved using extremely sharp inserts, with particular attention on the selection of the cutting material and relative coating. Ideally the tool used should present an extremely small corner radius and a positive cutting angle, while the tool material needs to be able to withstand the abrasiveness of the fibre. For these reasons *PCD* tools are generally preferred, however their use is limited due to their high cost [1], [13]. The finished surface and the cutting forces are strongly influenced by the fibres volume fraction, dimension and orientation. The machined surface quality is determined by the condition of the machined surface itself together with the extent of material damage caused by the cutting process. Standard to assess the surface integrity and quality of composite materials have not been developed yet. Another important consideration to take into account when cutting *CRFP* materials is the formation of dust and decomposition gaseous compounds which occur as results of the cutting process. These substances, if not properly removed through extraction systems, represents a threat for the health and safety of the workers and for the life of the machine itself [3].

One of the first machinability studies was conducted by Koplev et al [17] in 1983. According to their study, machining of *CFRP* materials can lead to a surface damage of up to 0.3 mm when fibres are oriented perpendicular to the tool direction. Conversely, when the fibres are parallel to the tool direction a better surface quality is achieved and

the cracks are significantly reduced. They found that the cutting force is determined by the Depth of Cut (*DOC*) and by the tool rake angle, while the relief angle and the tool wear determine the feed force.

In 1995 Wang et al [18] analysed the effect that rake and relief angle have on the machining forces and on the chip formation analysing trimming UD graphite/epoxy composite materials at different fibre orientations using *PCD* tools. They also considered the effects that the orientation of the fibre has on the cut surface. They asserted that the primary factor affecting the material removal mechanisms is the orientation of the reinforcement, as most of the following research on machining of *FRP* will confirm.

In 1997 Ramulu [12] observed a combination of cutting, shearing and fracture along the fibre/matrix interface during edge trimming of *UD* and *MD-FRP* composite material using *PCD* tools. The effects of different tool geometries, process conditions and ply distribution on cutting forces, chip formation mechanisms and on machined surface quality were analysed. Ramulu confirmed the strong dependency of the material removal mechanisms on the fibre orientation. Due to the inhomogeneity of composite materials it is critical to determinate the surface quality after machining. Ramulu stated that: "it is often desirable to supplement quantitative description provided by profilometry with a visual analysis of the surface morphology" concluding that, although limited influence is played on the material strength, the machining induced damage might affect the fatigue strength.

Due to the complexity of the *FRP* material removal process, understanding the chip formation mechanisms is fundamental. Having mechanical properties which vary considerably between the different constituents it is hard to control the quality of the machined surface and relative subsurface damage.

Wang [19] examined the effects that *DOC*, fibre orientations and rake angle have on cutting forces and surface roughness after orthogonal cutting of *UD-CFRP*. They confirmed that the orientation of the fibre is a key factor in determining cutting forces, subsurface damage and chip formation mechanisms. A study on fibre bouncing back phenomena was included to prove that the real and the nominal *DOC* have significant

differences when cutting *FRP* materials. The cutting tool radius and the fibre orientation were found to be the main cause of fibre bouncing back due to ineffective cutting. As expected the mechanical properties showed dependency with the curing process, which does not play any effect on the machined surface roughness.

The complexity of the subject requires developments of models capable to predict the correlation between the machinability output parameters (cutting forces, surface quality and part integrity) and the input process parameters (cutting parameters, cutting conditions, tool type and geometry).

Zhang [10] developed a mathematical model able to reflect the principal material removal mechanisms through an accurate characterisation of the matrix and reinforcement interaction, focussing on fibre and matrix deformation. Three distinct cutting zones were considered in the model: *chipping region*, *pressing region* and *bouncing region* (*Figure 1*), as identified by Sheikh-Ahmad [3] on a previous study. The total cutting force was calculated by the sum of the forces in the three cutting zones. Only test pieces having the orientation of the fibres between 0 and 90 degrees were considered in the study. Turning machining trials were performed for comparison with a mathematical model. Zhang stated that: "Due to the very different mechanical properties of the matrix and the reinforcement materials, the surface integrity of machined composites is hard to control, including surface roughness, residual stress and subsurface damages" [10].

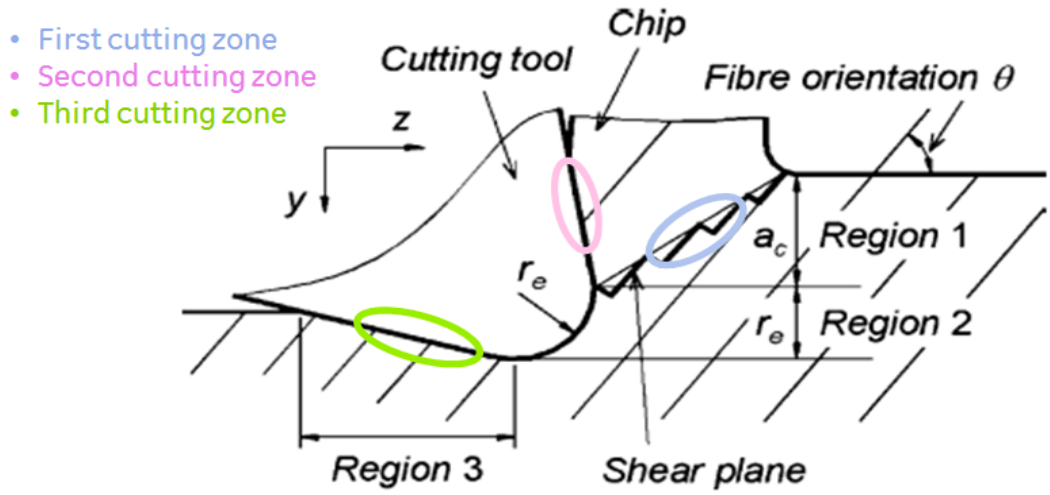

Figure 1: Deformation zones when cutting FRP [10].

A mathematical model based on response surface methodology based aimed to predict cutting power and specific cutting pressure was developed by Mata et al [20] in 2009. The machinability study was conducted on three different polyetheretherketone (PEEK) composite materials. In their work, the correlation between the process parameters (cutting speed and feed rates) and the machining responses (cutting power and specific cutting pressure) were highlighted. 12 experimental tests were planned in a full factorial design testing using three cutting speeds and two feed rates. *PCD* tools were used. The model accuracy was found to be within 9%. They concluded that, for a given constant cutting speed, the cutting power is directly proportional to the feed rates while the specific cutting pressure is inversely proportional.

Experimental studies are expensive, time consuming and valid exclusively for the experimental condition used. The lack of knowledge and understanding of the cutting mechanisms when machining *FRP* materials, as well as the limitation in cutting tool design, are the main obstacle in increasing the efficiency of the cutting removal process. For this reason numerical method aimed to predict the machinability characteristics of *FRP* materials have been developed to be used in the cutting tools design and for process optimization purposes.

In 1995 Arola et al [21] developed one of the first numerical models for composite materials. The aim was to verify the validity of the *FEM* in predicting the cutting forces of *UD* graphite/epoxide. Tsai hill and maximum stresses failure criteria were used. From the experiments they observed that trimming fibres oriented at an angle between 0 and 90 degrees initiates a fracture from the tool nose radius due to compression and shear stresses generated during the relative tool advancement. Although their two dimensional model did not have the capability to predict consistently the thrust force, they predicted the potentiality of the numerical model and their future utilization in the cutting tool design for the machining of *FRP*.

Nayak et al [22] presented a 2 dimensional micro mechanical Cohesive Zone Model (*CZM*) of the fibre matrix debonding that aimed to predict the sub-surface damage of *UD-FRP* composite materials. The cohesive zone was modelled with zero-thickness

elements. The fibre and the matrix were modelled separately as two distinct physical constituents with the fibre embedded in the matrix material.

Zitoune et al [23] worked on the orthogonal cutting of *UD* carbon/epoxy for four different cutting orientations, analysing the cutting forces and the temperature in the tool work-piece interface, together with the obtained chip shape, rupture modes and finishing surface quality. It was observed that compression was the dominant rupture when cutting lamina having the fibres oriented at 0 degrees. The chip was generated by laminate shearing for lamina at 45 degrees and bending/shearing for 90 degrees lamina. The failure mode could not be captured when cutting 130 degrees because severe cracks suddenly propagated inside the work-piece. The best surface quality was obtained for 45 degrees fibre orientation which is the configuration that presented the lowest cutting temperature.

A user-defined material model (*UMAT*) subroutine was developed in Abaqus/Standard by Knight [24] to describe the failure analysis of different composite materials. Different failure initiation criteria models were considered and described. The material degradation was applied to a material coefficient and not to the material mechanical properties. The progressive failure models implemented in the *UMAT* were shown in a single two-dimensional shell *FEM*. Once the Hashin failure criteria are detected they degrade both the in-plane normal coefficients and the in-plane shear term, leading to a conservative failure prediction.

Venu Gopala et al [25], [26] developed a 2 dimensional micro-macro *FEM* in Abaqus to study the orthogonal cutting of Unidirectional Glass Fibre Reinforced Polymer (*UD-GFRP*). Fibres and matrix were modelled separately. Fibres and matrix close to the cutting tool were considered respectively as elastic and elasto-plastic material while a macro scale approach was used to model the composite away from the cutting tool, modelled as Equivalent Orthotropic Homogeneous Material (*EOHM*). Zero thickness Cohesive Zone elements were used to capture interfacial debonding. In this work the effects of the fibre orientations, tool parameters and operation conditions over the cutting forces, the chip formation mechanisms, the interfacial debonding, matrix damage evolution and the subsurface damage were investigated. The cutting force and

the thrust force were calculated for different fibre orientations (15˚, 30˚, 45˚, 60˚, 75˚, 90˚), *DOC* (0.1, 0.15, 0.2 mm) and rake angle (5˚, 10˚, 15˚). They concluded that with the increasing of the fibre orientation and *DOC* the cutting forces increases significantly for both *CFRP* and *GFRP* while the rake angle effects are less significant.

Venu Gopala et al [27] validated a three dimensional macro-mechanical model able to predict cutting forces, induce surface damage and chip formation mechanisms when cutting *UD-CFRP* composite material at different fibre orientation varying the *DOC* and the tool rake angle. They observed that the cutting forces are highly dependent on the *DOC* and on the orientation of the fibres, while minor effects are played by the rake angle.

A detailed work was conducted by Mkaddem et al [28] which studied and simulated the effects that fibre orientation, *DOC* and rake angle have to the cutting forces during orthogonal cutting of *UD-GFRP*. The composite was modelled as *EOHM* using a micro-macro combined approach while Tsai Hill failure criteria were considered. An adaptive mesh technique and density was applied. In their work they identified the chip cutting ration as an important indicator for determining the mode of failure and relative damage propagation. The cutting ratio was found to be dependent on the orientation of the fibre. The cutting forces showed a proportional dependency on the *DOC* while they were found to be inversely proportional to the tool rake angle.

To provide a better understanding of the chip formation process and damage initiation and propagation, a 2D FE progressive failure analysis was developed by Lasri et al [6], investigating the effects of fibre orientation and failure criteria over *UD-CFRP* material. Hashin, Maximum stress and Hoffman failure criteria were considered and compared with experimental results from literature. Matrix cracking, fibre-matrix debonding and fibre breaking were simulated. They concluded that during the cutting process the failure initiates near the edge of the cutting tool while the damage propagates along the fibre direction. For this reason the extension of the induced surface damage is highly dependent on fibre orientation. The minimum surface damage was observed when simulating 30° fibre orientation and increasing beyond 45˚ fibre orientation. Fibre-matrix debonding was found to be the first failure that occurs when cutting *UD*

composites, followed by the matrix crashing and by fibre breaking. The prediction of the principal cutting force agreed well with the experimental test from literature, but the thrust force was highly underestimated. This underestimation was attributed to the bouncing back phenomenon.

Adapting mesh technique and dynamic explicit finite element analysis were used to simulate the chip formation during the orthogonal cutting of *UD-GFRP* [29]. The work-piece was considered as *EOHM*, avoiding the complications that occur when simulating the complex fibre-matrix interface in micro mechanical models. The maximum sub-surface damage value was predicted when simulating 90 degrees fibre angle work-piece.

A Discrete Element Method (*DEM*) simulation was created by Iliescu et al [30] to simulate the orthogonal cutting of *UD-CFRP* at 0, 45, 90 and 45 degrees of fibre orientation. The model agreed with experimental cutting tests, reproducing experimental aspects as cutting forces and chip formation. A high speed camera was used to validate *DEM* simulation results.

Calzada [7] compared the failure mechanisms that occur in micro-scale when cutting *UD-CFRP* composites at 0, 45, 90 and 135 fibre angle degrees with the results obtained when a macro-scale approach was used. To do this a micro-mechanical finite element model was created in Abaqus and failure theories, capable of explaining the failure mechanisms that occur throughout the chip formation process, are developed for each fibre orientation. The experimental tests, performed for validation purpose, were found to accurately represent the process of chip formation.

Santiuste et al [31] validated an *FEM* analysis in Abaqus/Explicit capable to capture the induced surface damage when cutting *GFRP* and *CFRP*. They affirm that, unlike when cutting *GFRP*, the induced surface damage obtained when cutting *CFRP* is limited to tool-work-piece interface, making this material more suitable for aeronautical applications than the glass fibres.

In their study Rentscha et al [32] developed two different modelling approaches to simulate the cutting of *CFRP* materials. The first approach consisted of a macroscopic implicit model using continuous anisotropic material properties. The second is a

microscopic explicit model having matrix and fibres modelled separately. Hashin failure criteria were considered. For both models cutting forces and chip formation mechanisms were predicted at 0 and 90 degrees fibre orientation. The cut surface was analyses and an induce surface damage of 200 micros was found for specimens with 90 degrees fibre orientation while no cracks appeared when cutting 0 degrees fibre orientation specimens. While the predicted chip formation mechanisms were consistent with experimental tests, the cutting forces were highly underestimated. This was attributed to the fact that in the simulation, when the compressive strength of the material is exceeded and the material is degraded, the elements are deleted, while in reality the yield material is still present between the insert and the work-piece itself and can still carry load in compression.

El-Hofy et al [33] studied the effects that process parameters, tool material and cutting environment have on surface integrity and quality after machining. They concluded that the cutting environment does not affect the surface roughness, while chilled air helps to prevent surface burning. They also found that *PCD* tools offer a tool life that is 95 times higher than coated carbide. The best surface roughness was obtained when cutting at low cutting speed and high feed rate.

Karpat et al [34] designed a mechanistic model to predict the cutting forces when slot milling a *UD-CFRP* with different polycrystalline diamond cutters. Additional pocket milling tests demonstrated the correlation between surface quality and cutting speed.

A macroscopic and a microscopic *CFRP* model were developed by Rentsch [35] to predict the material removal mechanisms under orthogonal cutting conditions. The calculated principal cutting forces agreed well with experimental results, while the thrust forces were highly underestimated. This was attributed to the fact that, while the *CFRP* material can still carry compressive loads once yield, in the *FEM* model a complete deleting of the elements occur.

The effect that machining operations have on material performance was investigated by Ghidossi [11] and Ramulu [12] for different cutting tools. They both concluded that the surface roughness does not represent a reliable factor to determinate the machining

quality of fiber composites and that the mechanisms responsible for the mechanical performance reduction are not clearly understood yet.

2.3 Process parameters

As the present study is focused on the orthogonal cutting of *UD-CFRP* the process can be simplified to a two dimensional problem which allows to perform a 2D plane stress study, avoiding complications in the chip formation analysis [15].

In orthogonal cutting the tool engages the work-piece perpendicular to the cutting direction, as shown in *Figure 2* below. The angle θ indicates the orientation of the fibres, α is the tool rake angle, γ the tool relief angle and r the edge radius of the tool.

In this cutting condition the cutting parameters are summarised by feed rates (*f*) and cutting speed (*Vc*).

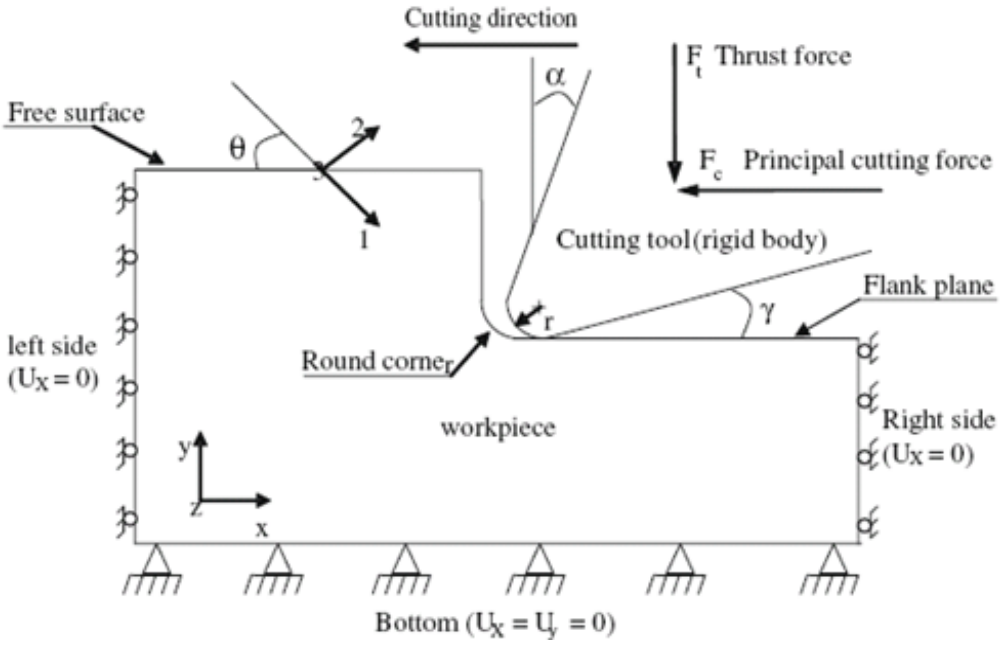

Figure 2: Orthogonal cutting model - tool geometry, work-piece and boundary condition [6].

The key process parameters which affect the cutting forces, the surface quality and the chip shape are: the tool geometry, the cutting parameters and the mechanical properties of the *CFRP* work-piece.

- Tool
  - *Rake angle - α*
  - *Relief angle - γ*
  - *Corner Radius – r*
  - *Material and surface quality*
- *CFRP* Material Properties
  - *Fibre orientation – θ*
  - *Young Modulus of both fibres and matrix*
  - *Fibres volume fraction and fibres diameter*
  - *Shear Modulus of both fibres and matrix*
  - *Tensile & Shear strength of both fibres and matrix*
- Cutting Parameters
  - *Feed rate - f*
  - *Cutting Speed – V_c*
  - *Depth of Cut - DOC*

Another important factor that characterises the cutting of *CFRPs* is the coefficient of friction which must account for all the tribological complexity of machining and varies with the different process parameters used. Friction on the tool face interacts with the shearing process, influencing the shear stress and strain in the shear plane, affecting the chip type produced. Several studies were made to investigate the friction coefficient between the cutting tool and the work-piece, when cutting *CFRP* materials.

Mkaddem et al illustrates the variation of the friction coefficient with fibre orientation (*Figure 3 (a)*), obtained using pin-on-disk tests on epoxy matrix and glass fibres [29]. From their study it was clear that the friction coefficient varies with monotony behaviour with the fibre orientation (from 0˚ to 90˚). Different friction coefficient behaviour is revealed by Jamal for *CFRP* materials [3] (*Figure 3(b)*).

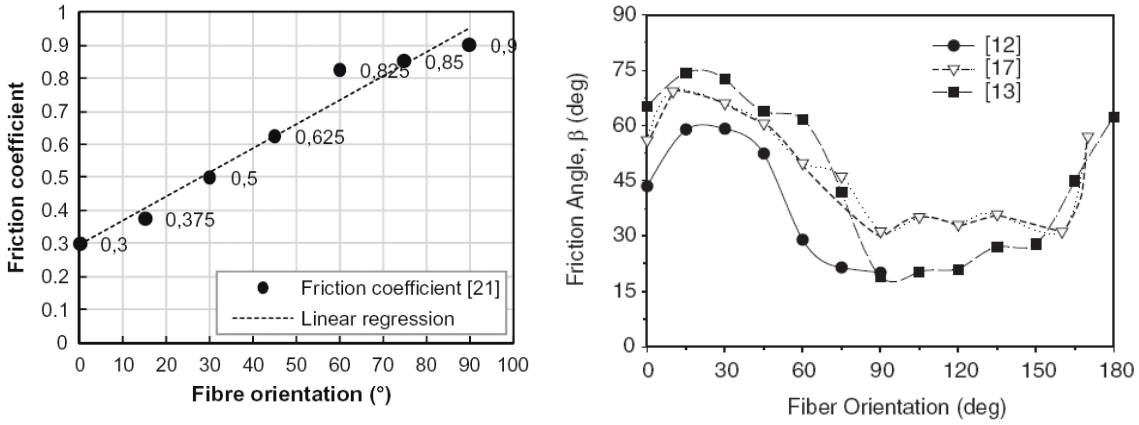

(a) (b)

Figure 3: Variation of friction coefficient vs. fibres orientation in an epoxy matrix and glass fibre (a) and for CFRP (b) *[3], [29].*

In one of the first studies on the machinability of *CFRP* Koplev et al [17] highlighted the dependency of the cutting forces on the friction coefficient. An average tool/work-piece fiction coefficient value was found to be 0.25.

Klinkova et al [36] developed a new rotary open tribometer specifically designed to better predict machining conditions of *CFRP* materials. Different sliding velocities (up to 120 m/min) were used during the tests under high contact pressure, while having a continuous regeneration of the contact surface. They observed that the friction coefficients of *CFRP* are significantly lower than the one obtained when cutting traditional metals. Moreover, a further reduction was observed when increasing the sliding velocity (from 0.25 to 0.1).

Same results were observed by Mondelin et al [37] who extended their research to study the effects of cutting fluid. They concluded that the implementation of lubricant (emulsion with 9% of mineral oil at 4 bar of pressure) drove to a further reduction of the friction coefficient (from 0.1 to 0.06) when cutting *CFRP*.

By taking in account these factors in the cutting simulation models more realistic results are possible.

2.4 Chip Formation

Although machining of composite materials is significantly different to metal cutting in terms of chip formation, cutting forces and heat transfer, the same cutting tool designs and techniques are still used for the majority of composite cutting processes.

When cutting *FRPs* there are several new failure mechanisms which do not exist when cutting metals. The damage consists of various failures modes as fibre breakage, matrix cracking, matrix crushing and fibre-matrix debonding or ply delamination.

In orthogonal cutting, there are five different modes of *FRPs* chip formation, based on the geometry of the insert, the polymer type and the cutting conditions [3], [7], [12], [18], [23], [27], [29], [30] and [31]. A continuous elastic chip with a thickness equal to the depth of cut is produced for ductile material that exhibit high elastic deformation at low cutting speed and positive tool rake angle. A continuous chip from plastic deformation is formed even when cutting some thermoplastic polymer. The chip shape is similar to the one obtained when cutting ductile metals, where the chip thickness is typically greater than the depth of cut. A discontinuous chip shape is formed when materials with brittle behaviour are cut with a large rake angle tool and large depth of cut. Even if the practical interest is focused on multidirectional fibre cutting, the actual lack of *FRPs* material knowledge leads the research to develop unidirectional composite as it is easier to relate their mechanical properties and machining characteristics to fibre orientation.

The variation of fibre orientation with respect to the cutting direction, as shown in *Figure 4*, is the most fundamental factor in the determination of the chip formation mode when cutting unidirectional *FRP* materials.

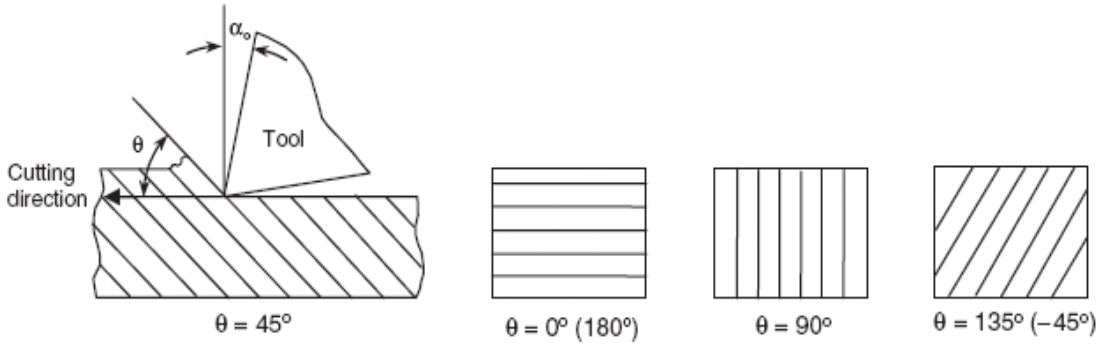

Figure 4: Schematic view of different fibre angle orientations [3].

In contrast to what is observed when cutting metals, material removal in CRFPs was found to be governed by a series of uncontrolled fractures which exhibited very little plastic deformation. When cutting at θ=90˚, with positive rake angles tool, the chips is formed by fibre cutting, while cutting with negative rake angles the chip is formed by macro-fracture [3].

Observations by other authors of the chip formation process during machining unidirectional *FRPs* composite have highlighted that fibre orientation and the cutting edge are the factors that mostly influence the chip type obtained. The chip modes can be categorised in 5 types [3], [12], [18].

Type I

Delamination: occurs when cutting 0˚ fibre orientation with inserts with positive rake angles. The crack, generated in the contact point between tool and work-piece, propagates along the fibre-matrix interface. A bending moment induced failure occurs ahead of the cutting edge perpendicularly to the fibre direction. The cutting force fluctuates widely with the repeating of Delamination-Bending-Fracture cycle.

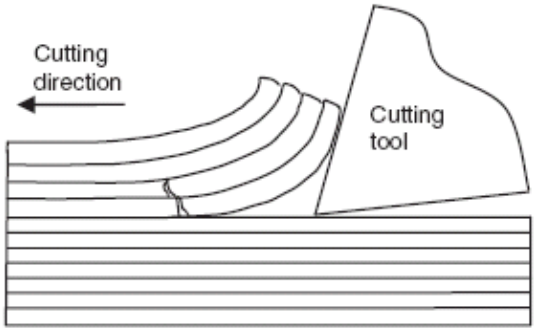

Figure 5: Chip formation mode for 0˚ fibre orientation cutting with positive rake angle [3].

Type II

Buckling: this mode is caused by the compression generated along the fibres directions from a negative rake angle insert when cutting 0˚ fibre orientation. The continuous advancement of the tool causes fracture at the fibre-matrix interface and successive buckling causes the fibre fracture in a direction perpendicular to the fibre length, not far from the cutting edge, generating a small discontinuous chip. The fracture cycle is much shorter than the one generated during delamination (type I) thus the cutting force fluctuation is smaller.

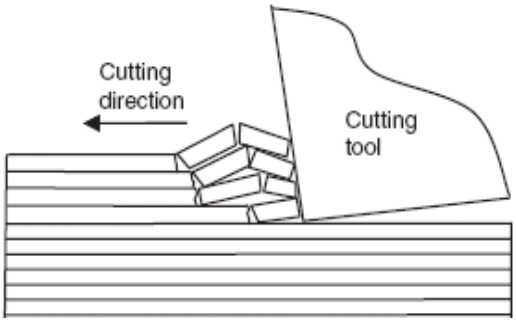

Figure 6: Chip formation mode for 0˚ fibre orientation cutting with negative rake angle [3].

Type III

Fibre Cutting: this mechanism occurs when machining material having fibre orientation angle between 0˚ and 90˚ with positive or negative rake angle tooling.

The chip formation process consists of a fracture caused by the compression along the fibre axis that shears the fibres. An interlaminate shear fracture occurs along the fibre-matrix interface during the cutting tool advancement.

The compression generates cracks in the fibres above and below the cutting plane. The cracks below the cutting plane remain in the surface after machining is completed and can be observed under the microscope.

The chip flows in a direction parallel to the cutting fibre when cutting at positive fibre angle, up to 90˚. The continuous chip generated in this condition is similar to the one that occurs when cutting metal, where the material is deformed by plastic shear as it passes across the shear plane, but with the absence of plastic deformation when cutting *FRPs*.

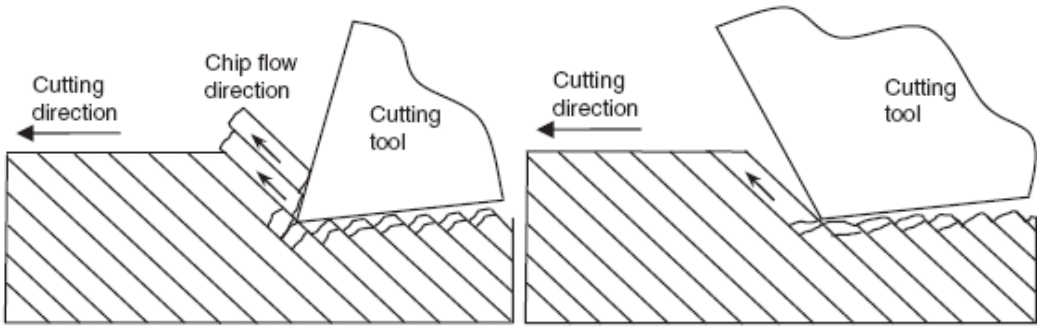

Figure 7: Chip formation mode for 45˚ fibre orientation [3].

Type IV:

Deformation: differs from the previous type (III) because at θ=90˚ a discontinuous chip is presented.

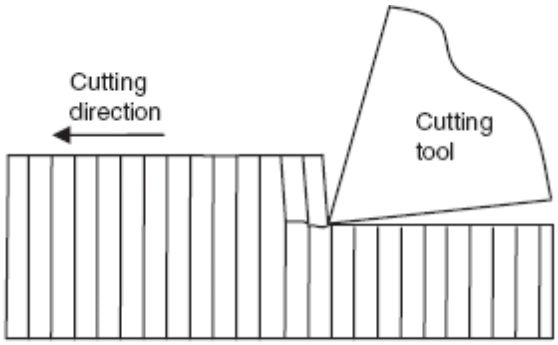

Figure 8: Chip formation mode for 90˚ fibre orientation [3].

Type V:

Shearing: occurs when cutting composite fibre with larger fibre orientation angles (105˚<θ<150˚). The compression forces caused by the tool advancing leads to deformation of the fibres leading to delamination, interlaminar shear along the fibre-matrix interface and out of plane displacement.

When the fibres face the advancing tool, elastic bending is observed. The compressive stress localised in the cutting edge generates the crack in the fibre-matrix giving rise to a discontinuous long chip, where the thickness of the chip is generally greater than the *DOC* (r < 1). When the chip is formed elastic recovery takes place and "bouncing back" of the material causes brushing between the relief tool surface and the cut surface.

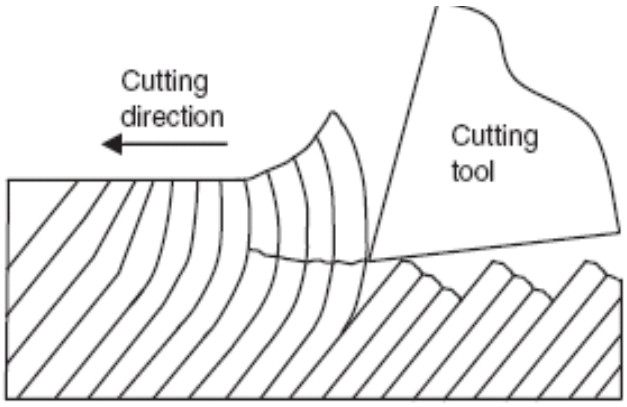

Figure 9: Chip formation mode for 135˚ fibre orientation [3].

2.5 Tool Geometry

Although the chip type is mainly related to fibre orientation, the tool geometry plays an important role in determining failure modes and surface integrity of a machine component [19], [21]. It has been observed by Sheikh-Ahmad [3] that, for fibre orientations between 0˚ and 75˚, the insert *rake angle* does not have a distinct effect on the chip formation mode, while it plays an important role in deciding whether a continuous or discontinuous chip is formed. A large positive rake angle favours creation of continuous chips, while smaller positive rake angles are more likely to cause discontinuous chips. It can be shown that surface topography and the machining quality improve with positive rake tool geometries, which reduces matrix smearing over the machined surface [38].

While the tool *clearance angle* does not affect the chip formation type produced to the same extent, machined surface quality enhancements are highlighted for large clearance angle. In their study Wang et al [39] found that the increase in clearance angle above 17° results in a reduction of the thrust force as well as in a reduction of tool performance.

Nose radius: The previous chip formation modes taken are obtained when cutting with relative sharp edge. For cutting operations with large cutting tool nose radii other mechanisms became prevalent, such as chipping, pressing and bouncing [19]. The material in the chipping area forms the cut chip which flows over the rake face in a direction parallel to the fibres plane [3], [28]. On the other hand the material in the pressing region is compressed by the tool nose radius under the cutting edge and then, because of the elastic recovery, bounces back once the tool is passed over (*Figure 10*). Wang et al [19] found a direct correlation between the tool nose radius and the bouncing back, concluding that the bouncing back is a key factor that contributes to the generation of the cutting forces.

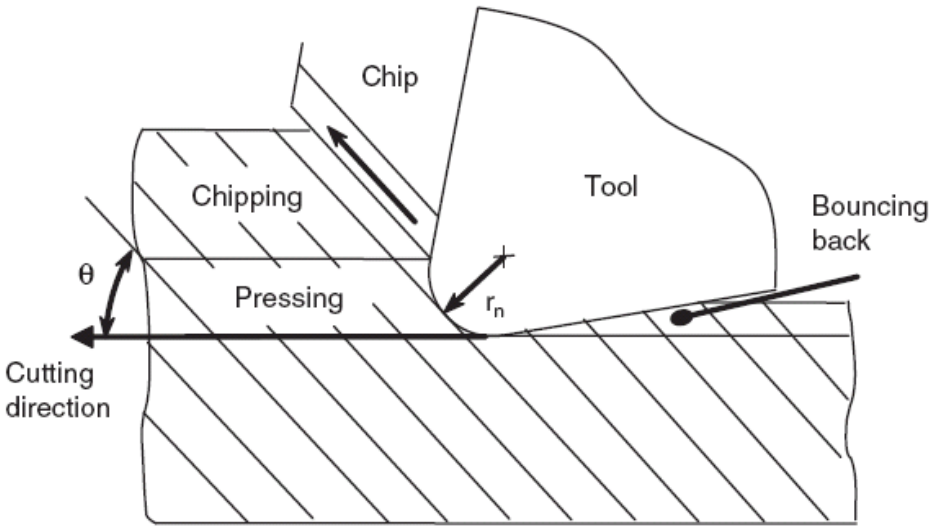

Figure 10: Influence of tool geometry on chip formation [3].

2.6 Modelling Techniques

Because experimental studies are frequently expensive and time consuming it is important to develop numerical methods that can predict the various output and characteristics of the cutting process. A *FEM* analysis provides approximate solutions to complex problems that are difficult to solve analytically. Such results can then be used in process and tool design with the aim of increasing the efficiency of the machining operation by improving working speeds, feed rates, tool life and reliability [13], [14].

During the last decades finite element methods have been widely used to analysis linear, nonlinear, static and dynamic analysis in structural engineering problems.

Three stages are common when developing a *FEM*, called: pre-processing, processing and post-processing. During the pre-processing boundary conditions, loads, material properties, connectivity and nodal coordinates are defined. In the processing phase the constitutive equations are solved while the post-processing deals with the presentation of the results. When studying machining processes the main aim of a *FEM* is to predict displacements, strain and stresses in the work-piece along with temperature and loads acting on the tool under defined cutting conditions [13], [14]. To be able to describe

these phenomena it requires that the properties of the material are accurately described [1].

On the basis of the interaction between mesh nodes and the material, mainly three different *FEM* formulations are used: Eulerian, Lagrangian and Arbitrary Lagrangian Eulerian (*ALE*) methods. In the Eulerian formulation the mesh is spatially fixed while the material is free to flow within the mesh control volume. The advantage of the Eulerian approach is that, due to the fact that the mesh is fixed, no excessive element distortion occurs. This approach is widely used in fluid dynamics but is not suitable to characterise the elevated material strain that occurs during chip-formation processes. In the Lagrangian algorithms, on the other hand, each individual node follows the associated material particle, being allowed to deform similarly to the actual mesh. This formulation is therefore used to analyse structural mechanic phenomena. Its limitations are related to excessive element distortion and the need of frequent remeshing that makes the model computationally expensive. The third method is a hybrid approach called Arbitrary Lagrangian Eulerian (*ALE*) that combines the advantages of both formulations. In this method the mesh is enabled to flow freely, being neither spatially fixed nor attached to the material [1], [40]. The three formulations are graphically shown in *Figure 11*.

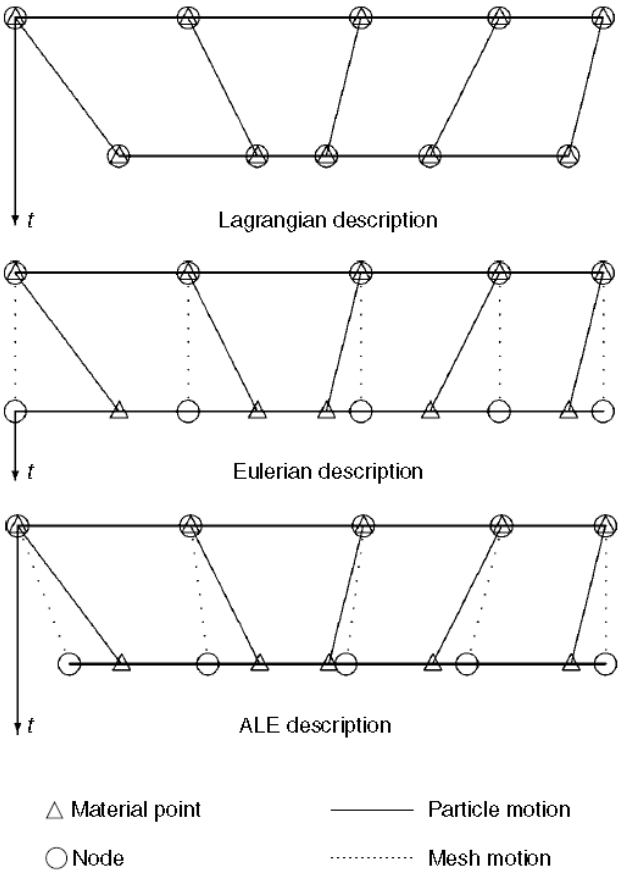

Figure 11: One dimensional example of Lagrangian, Eulerian and ALE mesh and particle motion [40]

The capability of the *ALE* formulation to accommodate distortion makes it the most suitable approach to simulate machining processes where high deformation is involved.

In a chip formation process the stress-strain response is calculated by constitutive equations which describe the dependency on work hardening, strain rate and thermal softening. Besides choosing a suitable constitutive equation the Lagrangian and the *ALE* formulations require to include a chip separation criterion to trigger the separation of chip from the work-piece. This can be achieved only through the use of an appropriate damage model that accurately describes the fracture mechanism of the examined material [1].

The authentication of the *FEM* when cutting *CFRPs* consists of understanding the nature of the issues related to those materials and finding an appropriate way to resolve them.

Several commercial codes (Abaqus, LS Dyna, Ansys, MSC, Marc, Deform, Thirdwave AdvantEdge, etc.) have been developed to support engineers in the practice of process and tool design.

When simulating *CFRP* it is necessary to understand the issues related to the complexity of these materials, having mechanical properties and failure mechanisms that differ from the ones found when traditional well known metal materials are used [9].

The machining of composite involves a significant number of physical parameters. Even though FE simulations offer a good opportunity to solve the technical difficulties and reduce the high cost of experiment studies, while providing valuable information to understand the cutting phenomena, few numerical studies have been successfully developed for *CFRPs*.

A further way to categorise simulations is based on the modelling method used to characterise the work-piece. Two types of models can be distinguished. *Macro-mechanical models* where the composite material is generally modelled as an *EOHM* [27], [29], [32] and *micro-mechanical models* where the fibres and the matrix are modelled separately [7], [10], [22], [25], [26], [28], and [32].

Due to the extremely small dimension of the fibres this technique needs a complex model of the fibre-matrix interface requiring many approximations and sometimes becomes highly complex due to the number of variables required to be considered. However, if constructed correctly they offer a better estimation when compared to the macro-mechanical models, which are limited to the prediction of global responses, such as estimations of cutting forces, being not capable of predicting the local effects at the fibre-matrix interface [25], [26].

2.6.1 Re-meshing technique and Failure Criteria

A simple way to adopt micro-mechanical model is the re-meshing technique where an adaptive mesh is controlled in the contact zone between the tool and the work-piece updating the node location in the deformed zone as the elements reach a certain distortion limit [29]. This distortion is caused by the continuous tool advancement which generates a load increase and guarantees better control of the results once the tool moves forward. Failure occurs in the element once failure criterion is exceeded.

The chip is generated as a result of the deformation process and the tool motion while failure occurs where the failure criteria used exceeds a set parameter. Different failures criteria can be used when simulating *FRPs* such as: Hashin, Chang/Chang, Maximum Stress, Offman, Tsai-Hill, Tsai-Wu, Punk, etc. [16], [29], [41], [42], [43].

Being non-interacting failure criteria the Hashin, Chang/Chang and the Maximum stress offer the advantages of considering each failure mode separately [6], [24] and [42]. Under a given load, the stresses at each integration point in the composite structure are calculated in the material coordinate system and then computed into the failure criteria. If any failure occurs, the material properties at that point are degraded accordingly to the mode of failure used.

Using Maximum Stress, Chang/Chang and Hashin failure criteria allows the model to adopt a selective stiffness reduction at failed nodes and a better prediction of cutting forces is possible [6].

The maximum stress criteria are as follows [24]:

$$e_1^t = \frac{\sigma_{11}}{X_T} \; for \; \sigma_{11} \geq 0 \tag{1}$$

$$e_1^c = \frac{|\sigma_{11}|}{X_C} \; for \; \sigma_{11} \leq 0 \tag{2}$$

$$e_2^t = \frac{\sigma_{22}}{Y_T} \; for \; \sigma_{22} \geq 0 \tag{3}$$

$$e_2^c = \frac{|\sigma_{22}|}{Y_C} \; for \; \sigma_{22} \leq 0 \tag{4}$$

$$e_3^t = \frac{\sigma_{33}}{Z_T} \; for \; \sigma_{33} \geq 0 \tag{5}$$

$$e_3^c = \frac{|\sigma_{33}|}{Z_C} \; for \; \sigma_{33} \leq 0 \tag{6}$$

$$e_4 = \frac{|\sigma_{12}|}{S_{12}} \tag{7}$$

$$e_5 = \frac{|\sigma_{23}|}{S_{23}} \tag{8}$$

$$e_6 = \frac{|\sigma_{13}|}{S_{13}} \tag{9}$$

When the ration $e_i^{t,c}$ reaches and exceeds 1 the failure occurs and the material degradation is applied. Each one of the failure mode can fail individually at different level of load. In the maximum stress criteria the failure is set accordingly:

$$\mathrm{f_i^{MS}} = \begin{cases} 0 \text{ for } \mathrm{e_i^{t,c}} \leq 1 \\ \pm 1 \text{ for } \mathrm{e_i^{t,c}} \geq 1 \end{cases} \text{for i} = 1,6 \tag{10}$$

In the Hashin criteria the failure modes included are as follows:

1. Tensile fibre failure ($\sigma_{11} \geq 0$)

$$(\mathrm{e_1^t})^2 = \left(\frac{\sigma_{11}}{\mathrm{X_T}}\right)^2 + \frac{\sigma_{12}^2 + \sigma_{13}^2}{\mathrm{S_{12}^2}} \begin{cases} \geq 1 \text{ failure} \\ < 1 \text{ no failure} \end{cases} \tag{11}$$

2. Compressive fibre failure ($\sigma_{11} < 0$)

$$(e_1^c)^2 = \left(\frac{\sigma_{11}}{X_C}\right)^2 \begin{cases} \geq 1 \; failure \\ < 1 \; no \; failure \end{cases} \tag{12}$$

3. Tensile matrix failure ($\sigma_{22} + \sigma_{33} > 0$)

$$(e_2^t)^2 = \left(\frac{\sigma_{22} + \sigma_{33}}{Y_T^2}\right)^2 + \frac{\sigma_{23}^2 - \sigma_{22}\sigma_{33}}{S_{23}^2} + \frac{\sigma_{12}^2 + \sigma_{13}^2}{S_{12}^2} \begin{cases} \geq 1 \; failure \\ < 1 \; no \; failure \end{cases} \tag{13}$$

4. Compressive matrix failure ($\sigma_{22} + \sigma_{33} < 0$)

$$(e_2^c)^2 = \left[\left(\frac{Y_c}{2S_{23}}\right)^2 - 1\right]\left(\frac{\sigma_{22} + \sigma_{33}}{Y_C}\right) + \frac{(\sigma_{22} + \sigma_{33})^2}{4S_{23}^2} + \frac{\sigma_{23}^2 - \sigma_{22}\sigma_{33}}{S_{23}^2} + \frac{\sigma_{12}^2 + \sigma_{13}^2}{S_{12}^2}$$

$$(e_2^c)^2 = \begin{cases} \geq 1 \; failure \\ < 1 \; no \; failure \end{cases} \tag{14}$$

5. Interlaminar tensile failure for $\sigma_{33} > 0$

$$(e_3^t)^2 = \left(\frac{\sigma_{33}}{Z_T}\right)^2 \begin{cases} \geq 1 \; failure \\ < 1 \; no \; failure \end{cases} \tag{15}$$

6. Interlaminar compression failure for $\sigma_{33} < 0$

$$(e_3^c)^2 = \left(\frac{\sigma_{33}}{Z_C}\right)^2 \begin{cases} \geq 1 \; failure \\ < 1 \; no \; failure \end{cases} \tag{16}$$

σ_{ij} indicate the stress components while T and C denote the tensile and compressive allowable strengths for lamina respectively. X_T, Y_T, Z_T represent the maximal tensile strengths along the three material directions as X_C, Y_C, Z_C represent the maximal compressive strengths in the three respective material directions. S_{12}, S_{13} *and* S_{23} denote allowable shear strengths in the respective principal material directions [24], [42].

Similar to maximum stress criteria when any of these failures exceed 1 the failure occurs at that material point and the degradation model is applied. Each one of the

failure mode can fail individually at different level of load. In the failure criteria the failure is set accordingly:

$$f_i^H = \begin{cases} 0 \; for \; e_i^{t,c} \leq 1 \\ \pm 1 \; for \; e_i^{t,c} \geq 1 \end{cases} for \; i = 1,3 \tag{17}$$

In the Chang/Chang the failure modes are:

For tensile fibre mode,

$$\sigma_{11} < 0 \; then: e_c^2 = \left(\frac{\sigma_{11}}{X_C}\right)^2 - 1 \begin{cases} \geq 0 \; failed \\ < 0 \; elastic \end{cases} \tag{18}$$

For compressive fibre mode,

$$\sigma_{11} < 0 \; then: e_c^2 = \left(\frac{\sigma_{11}}{X_C}\right)^2 - 1 \begin{cases} \geq 0 \; failed \\ < 0 \; elastic \end{cases} \tag{19}$$

For tensile matrix mode,

$$\sigma_{22} > 0 \; then: e_m^2 = \left(\frac{\sigma_{22}}{Y_T}\right)^2 + \left(\frac{\sigma_{12}}{S_C}\right)^2 \begin{cases} \geq 0 \; failed \\ < 0 \; elastic \end{cases} \tag{20}$$

For compressive matrix mode,

$\sigma_{22} < 0 \; then:$

$$e_d^2 = \left(\frac{\sigma_{22}}{2S_C}\right)^2 + \left[\left(\frac{Y_C}{2S_C}\right)^2 - 1\right]\frac{\sigma_{22}}{Y_C} + \left(\frac{\sigma_{12}}{S_C}\right)^2 - 1 \begin{cases} \geq 0 \; failed \\ < 0 \; elastic \end{cases} \tag{21}$$

In Maximum Stress, Chang/Chang and Hashin failure criteria simulations the elastic properties are described by three field variables *FV1, FV2* and *FV3*, which indicate the failure of the matrix, the failure of the fibre and the fibre-matrix interface.

The Hoffman criterion instead is constituted by a unique failure mode and it is not able to detect the failure orientation, so the non-selective stiffness reduction scheme must be

applied. In this case, once the failure criterion is satisfied, all of the stiffness terms are degraded.

$$e_{Hoffman} = \frac{\sigma_{11}^2}{X_t X_c} + \frac{\sigma_{11}\sigma_{22}}{X_t X_c} - \frac{\sigma_{22}^2}{Y_t Y_c} + \frac{X_t + X_c}{X_t X_c \sigma_{11}} + \frac{Y_t + Y_c}{Y_t Y_c \sigma_{22}} + \frac{\sigma_{12}^2}{S_c^2} \geq 1 \qquad (22)$$

Initially in the undamaged state the variable values are set equal to zero. After a failure index has exceeded 1.0 the associated user-defined field variables is set to 1.0 and remains at this value until the end of the process where a completed chip is formed.

The mechanical properties of the damaged area are changed once a failure is generated according to the degradation model applied. These failure modes can be applied both for macro-mechanical and micro-mechanical models.

2.6.2 Discrete Elements Method

A different micro-mechanical model, based on a Lagrangian description, is the *DEM* where the displacements that occur in each particle are calculated by the interaction of the fundamentals laws of dynamics.

The *DEM* is particularly well suited to help the understanding of the basic physical phenomena. Its ability to simulate the cutting of *CFRP* was investigated by Ilescu et al [30], where cutting forces, contact pressure and frictional shear at the tool-fibre interface were calculated and validated with experimental tests. Ilescu demonstrated that the *DEM* model gave a good representation of the experimental tests, describing reliably the physical composite cutting mechanisms in all the fibre orientations analysed. The evolution of the predicted cutting forces was also in general agreement with the experimental work although the model frequently over or underestimated the actual value.

When cutting 90˚ fibre orientation angle work-pieces with an insert which has a rake angle, α=0 the material initially bends ahead of the tool opening through the work-piece along the fibre/matrix interface. The damage is represented by the fibres detachment and the multi-cracking of the composite surface.

Once the material has been cut the fibres return elastically to their initial position rubbing against the tool clearance face, causing tool wear. The pressure located below the nose radius area leads to in-depth crack generation in the work-piece surface. In *Figure 12* the contact distribution and connection forces are shown. Indicated in red are the compression forces, in green are indicated the tensile forces while in blue the matrix between two fibres is represented. The simulation shows high compressive forces generated from the tool advancement, leading to bending and ultimately fibre delamination.

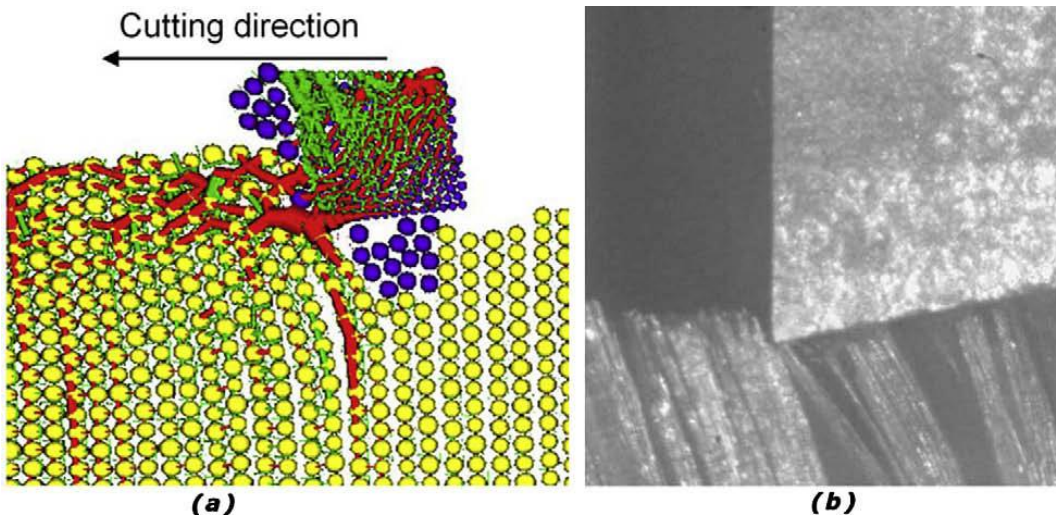

Figure 12: Chip formation in orthogonal cutting of UD-CFRP at θ=90˚.
(a) Virtual chip from DEM simulation. (b) High speed video image [30].

For work-piece with the fibres oriented at 0˚, chips are generated combining delamination (mode I) and fibre buckling (mode II). In mode I rupture along the fibre-matrix interface is generated, while in mode II fibre buckling is caused by the compressive forces created by the tool advancement. The chip separation occurs at an angle perpendicular to the fibre axis direction under the tool pressure.

In Iliescu's model, consistently with previous literature review, the chip produced when cutting at 0˚ is longer than that produced for other fibre orientation angles.

In their study they have proven that a *DEM* simulation has the capability to accurately describe high compression, bending and delamination of the fibre bundles, while calculating the cutting forces with the final results very close to reality.

2.6.3 Cohesive Zone Model

The need to harness the advantages of both the macro and the micro mechanical model leads to the develop of another model called the Cohesive Zone Model (*CZM*) where only the regions of the work material close to the chip formation zone are modelled as micro-mechanical [22], [25], [26]. The portion of the work-piece adjacent to the tool is modelled using fibre and matrix separately, whereas portions away from the tool have been modelled as *EOHM* (*Figure 13*) to simplify the model and reduce computational time. The interface between the matrix and fibres is modelled using zero thickness cohesive elements, allowing for debonding to occur once the interfacial fracture energy between the fibre and matrix is exceeded.

The benefits of this method lie in its ability to model the process in close details, performing a parametric study.

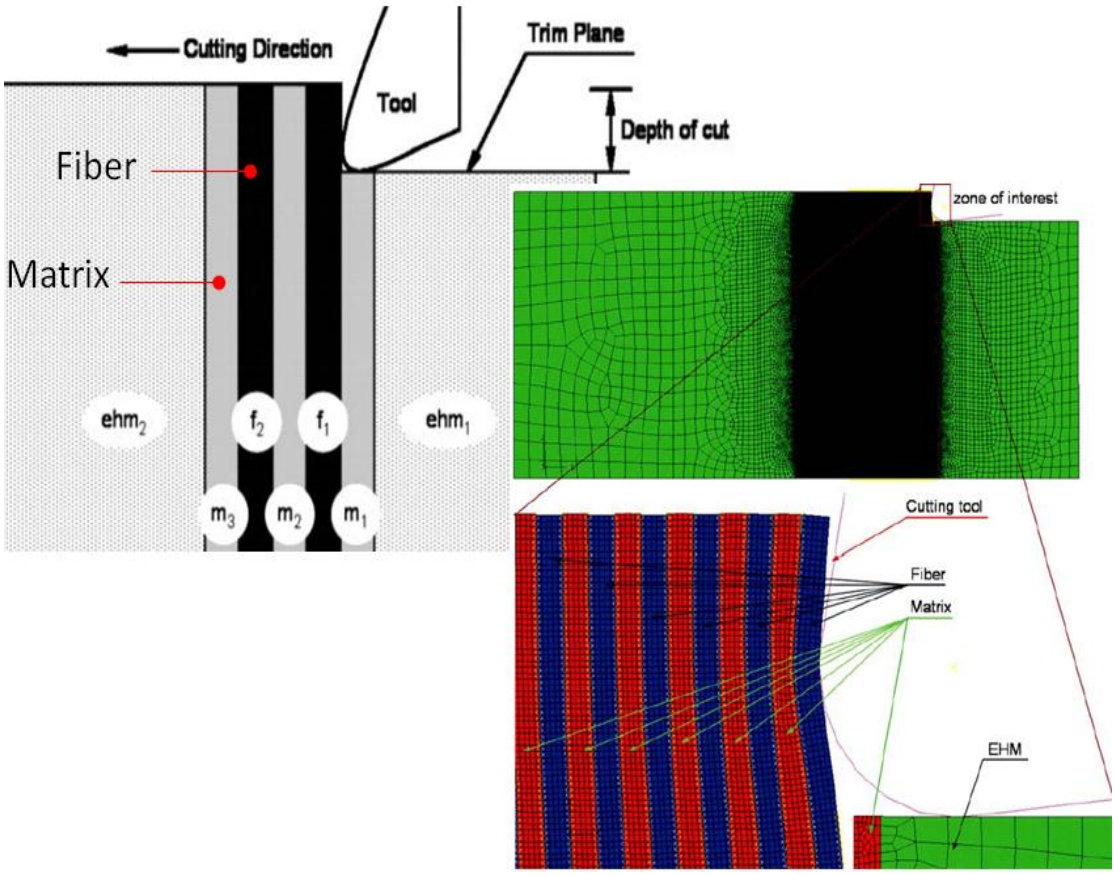

Figure 13: Schematic view of fibre, matrix and EOHM zones used in finite element modelling [25].

Calzada [7] investigated the failure mechanisms that occur in the micro-scale when cutting *CFRP* in a range of different fibre orientations (0˚, 45˚, 90˚, 135˚) for composites with 5-8 μm diameter fibres and 60% fibre volume fraction.

The matrix was modelled as an elasto-plastic isotropic material while the fibres were modelled as an anisotropic elastic material. The carbon fibres were modelled to fail at the onset of stress-induced damage. To deteriorate the epoxy material properties a progressive damage model available in ABAQUS was used.

In the material area far from the zone of interest the plasticity or failure modes did not take place since no failure occurs in the *EOHM* zone, which was modelled as elastic and anisotropic.

In the Calzada simulation cutting forces, fibre failure modes and chip dimension were investigated. *Figure 14* shows the fibres once failure occurs.

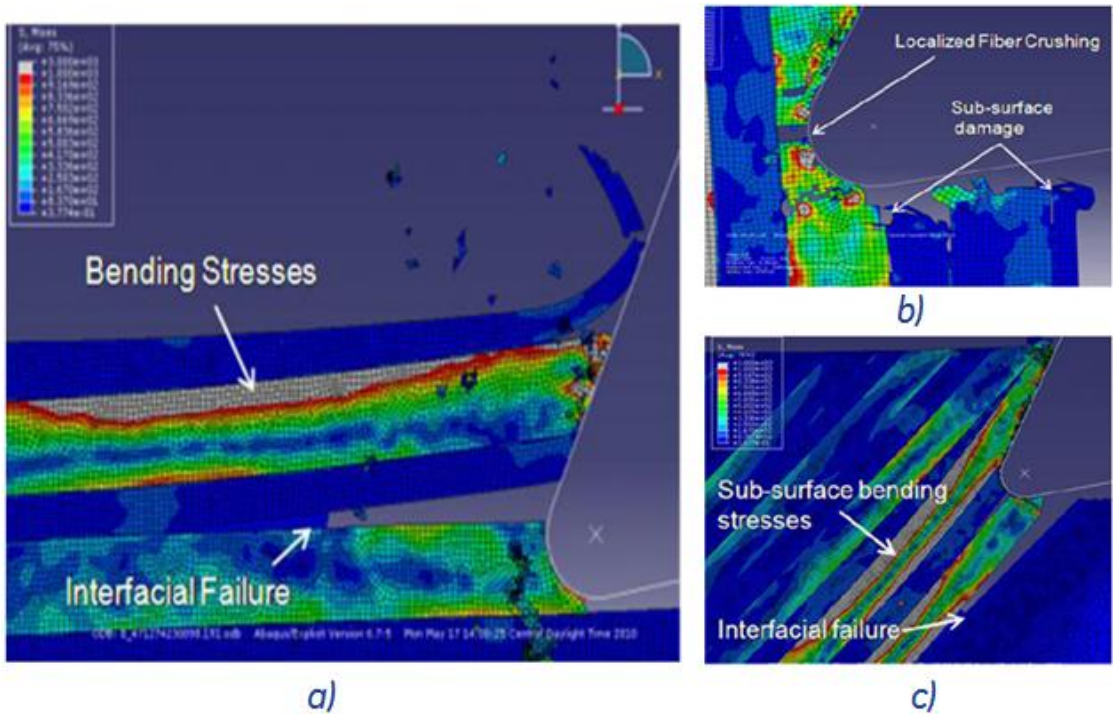

Figure 14: simulation results for different fibre angles work-piece a) 0˚, b) 90 ˚, c) 135˚ [7].

When simulating 0˚ fibre orientation work-piece the matrix/fibre phase separates due to interfacial failure that occurs as soon the tool enter the work-piece, leading to chip formation. The bending stress takes place ahead of the cutting tool until failure of the fibre in a direction perpendicular to the fibre axis.

It was shown that when cutting 0˚ fibre orientation the failure mode is not affected by the *DOC* as expected, since the chip failure occurs away from the point of contact with the tool. On the other hand, the chip length is around 120 μm for both the *DOC*.

When simulating 45˚ and 90˚ fibre orientation angles, the fibres crush as soon as the tool approaches the work-piece, failing in correspondence to the insert contact point as shown in *Figure 14 (b)*. Bending stresses occur also below the cutting plane without leading to sub-surface fibre failure but resulting in sub-surface damage as delamination between fibres and the matrix.

When simulating 135˚ fibre orientation work-piece (*Figure 14*(c)) the insert advancement peels the fibres from the work-piece due to failure that occurs in the fibre-matrix interface below the cutting plane. After adequate fibre peeling and separation the bending stress arose below the cut surface leading to fibre failure in a zone below the cutting plane. Even in the configuration at 135˚ the *DOC* does not affect the chip failure mode, but it does however affect its size.

The reason why the chip length becomes longer than the *DOC* value was attributed to the geometrical position of the fibres (135 degrees) and to the fact that the failure occurs below the cutting plane.

The cutting forces revealed a large variation among the different simulation configurations with the highest force variability when simulating the fibres at 90 and 135 degree.

The thrust forces predicted are significantly lower than those in the cutting direction. A common problem when analysing the thrust forces is the difficulty of predicting them accurately when simulating machining operations with finite element methods.

2.7 Summary

In this chapter the basic principles of orthogonal cutting of *UD-CFRP* materials were analysed. The influence of material properties, fibre orientation and process parameters on chip formation mechanisms was examined. In contrast to the cutting of traditional metals, the machining of *CFRP* is characterised by fracture and discontinuous chip formation. The surface quality and the cutting forces are primarily determined by the orientation of the fibres and then by the tool rake angle. Five different fibre chip types are formed during the machining process depending on the fibre orientation and tool geometry.

To minimise expensive and time consuming experimental studies, numerical methods that can predict the various output and characteristics of the cutting process were developed. In the FE simulation two types of models can be distinguished, *macro-mechanical models*, where the composite material is generally modelled as *EOHM*, and *micro-mechanical models*, where fibres and matrix are modelled separately.

The authentication of the *FEM* when cutting *CFRPs* consists of understanding the nature of the issues related to those materials and finding an appropriate way to resolve them. Different failure criteria with the aim of describing the fracture of *FRP* were considered.

CHAPTER 3 EXPERIMENTAL CUTTING TRIALS

3.1 Work-piece

The material under investigation was the *MTM 44-1* out-of-autoclave (*OoA*) composite. This material is a high performance toughened epoxy matrix system particularly suitable for the production of both primary and secondary aircraft structures. MTM 44-1 offers a high damage tolerance level and a low density, providing at least a 3% weight saving when compared to standard aerospace matrix materials (*Appendix A*).

Table 1 Mechanical properties(Appendix A)

Test	Test Method	145gsm 12k HTS5631 UD	268gsm 24k IMS5131 UD	283gsm 3k HTA5131 CF0604 5-HS Fabric
0° Tensile Modulus - GPa (msi)	D3039	128.9 (18.6)	174.6 (25.3)	62.6 (9)
0° Tensile Strength - MPa (ksi)	D3039	2159 (313)	2738 (397)	927 (134.4)
0° Compression Modulus - GPa (msi)	ASTM D695 (mod)	123.2 (17.8)	147.2 (21.3)	59.4 (8.6)
0° Compression Strength - MPa (ksi)	ASTM D695 (mod)	1330 (192.8)	1459 (211.5)	729 (105.7)
In-Plane Shear Modulus - GPa (msi)	D3518	4.11 (0.6)	3.60 (0.5)	3.98 (0.58)
In-Plane Shear Strength - MPa (ksi)	D3518	112.7 (16.3)	76 (11)	133 (19.3)
0° Flexural Modulus - GPa (msi)	CRAG	121.9 (17.7)	154.9 (22.4)	57.1 (8.2)
0° Flexural Strength - MPa (ksi)	200	1958 (238.9)	1874 (271.7)	1181 (171.2)
0° ILSS - MPa (ksi)	D2344	106.6 (15.4)	109.4 (15.8)	75.4 (10.9)

To measure the cutting forces during the machining trials, various *CFRP* tubes were made at different orientations relative to the cutting edge (0˚, 22.5˚, 45˚, 67.5 ˚, 90˚, 112.5°, 135˚ and 157.5˚; with a variation of ±5˚ among the fibres). In order to make the tubes, the *MTM 44-1* material was manufactured using the Automated Dynamics (ADC) system of the *AMRC* composite centre as shown in *Figure 15.*

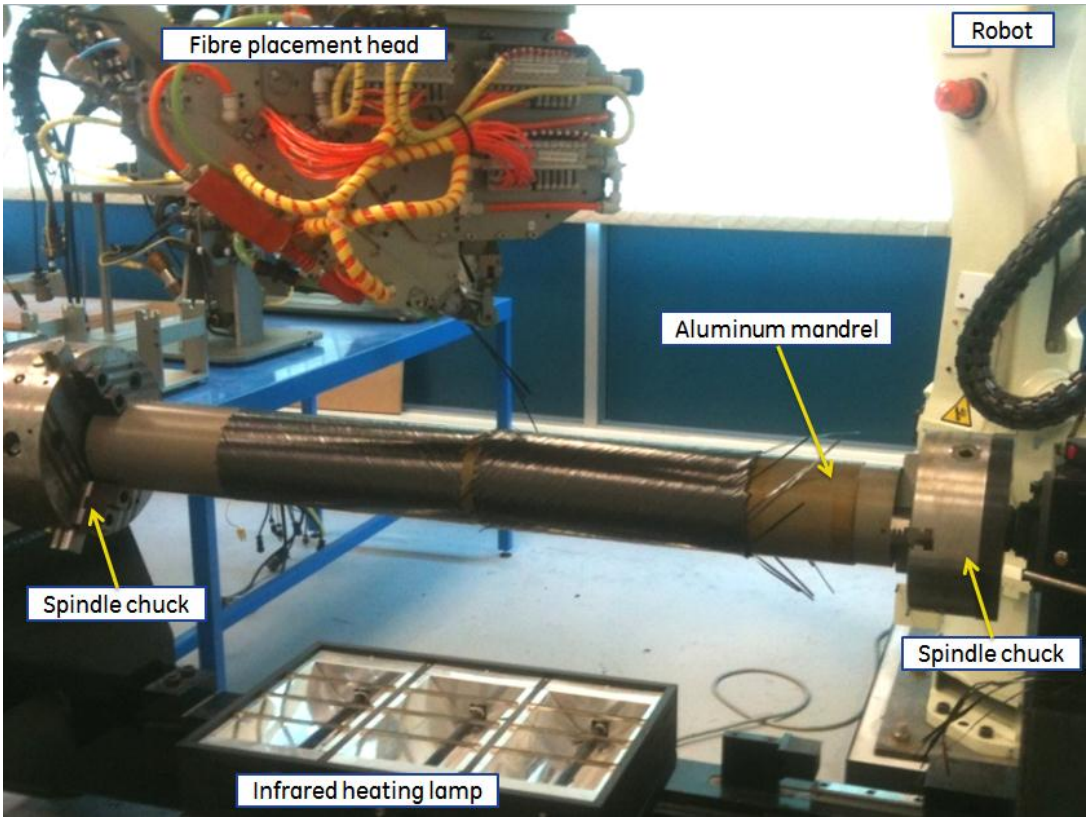

Figure 15: AMRC Composite Centres ADC fibre placement machine.

Once the 67.5˚, 90˚ and 112.5˚ fibre orientation work-pieces were manufactured, it was not possible to extract them from the aluminium mandrel. This was due to the fact that the direction of the work-pieces thermal expansion matched the direction of the aluminium mandrel thermal expansion. Therefore, it was not possible to extract the tubes without them being damaged. During their extraction severe cracks propagated along their fibre orientation. Only the work-piece with a 90° fibre orientation was repaired due to restrained fractures. The repair was made by gluing the epoxy matrix along the fracture.

Once the tubes were manufactured in the ADC system, they were cured at 180˚C for 2 hours to develop the maximal mechanical properties (*Table 1*); with a fibre volume fraction of approximately 58% having a tolerance of ±3%. The process parameters used are shown in the *Table 2* (*Appendix A*). The tubes were then cut into a number of test pieces having a length of 100 mm. The dimensions of the test pieces were selected as shown in *Figure 16* to guarantee adequate stiffness during the cutting trials in order to

avoid any influence in the machining cutting responses. It was noticed that after the curing process the thickness of the test pieces varied from 3.45 to 3.65 mm (6% variation).

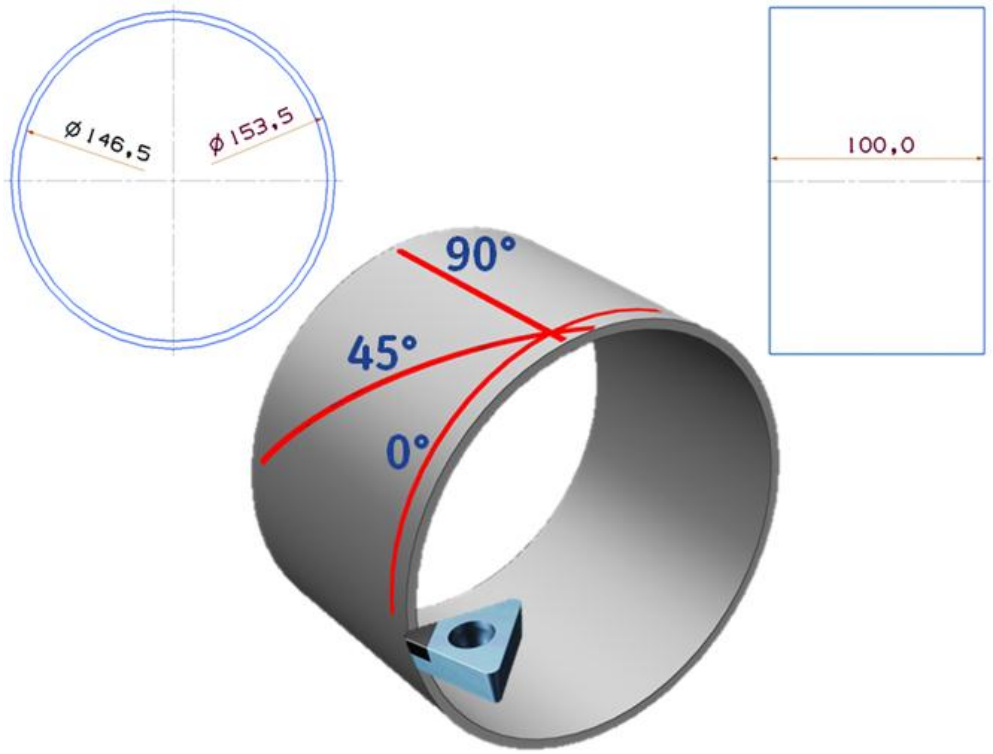

Figure 16: Work-piece dimensions.

Table 2 Autoclave process parameters MTM 44-1(Appendix A)

	Autoclave Processing
Ramp Rate	1 to 2°C/minute (1.8 to 3.6°F/minute)
Pressure	3 to 7bar
Vacuum Pressure	>0.75bar
Cure Time	4 hours @ 130°C (266°F) or 2 hours @180°C (356°F)

3.1.1 Experimentation Set Up

All the machining trials were carried out on a MAG Cincinnati Hawk 300 CNC lathe machine (*Figure 17*). A Kistler data acquisition system was installed on the machine to record the cutting forces in each test. This equipment consisted of:

- KISTLER 9121 - Quarz three-component dynamometer
- KISTLER 5017 - Multichannel charger amplifier
- DynoWare software installed in a laptop

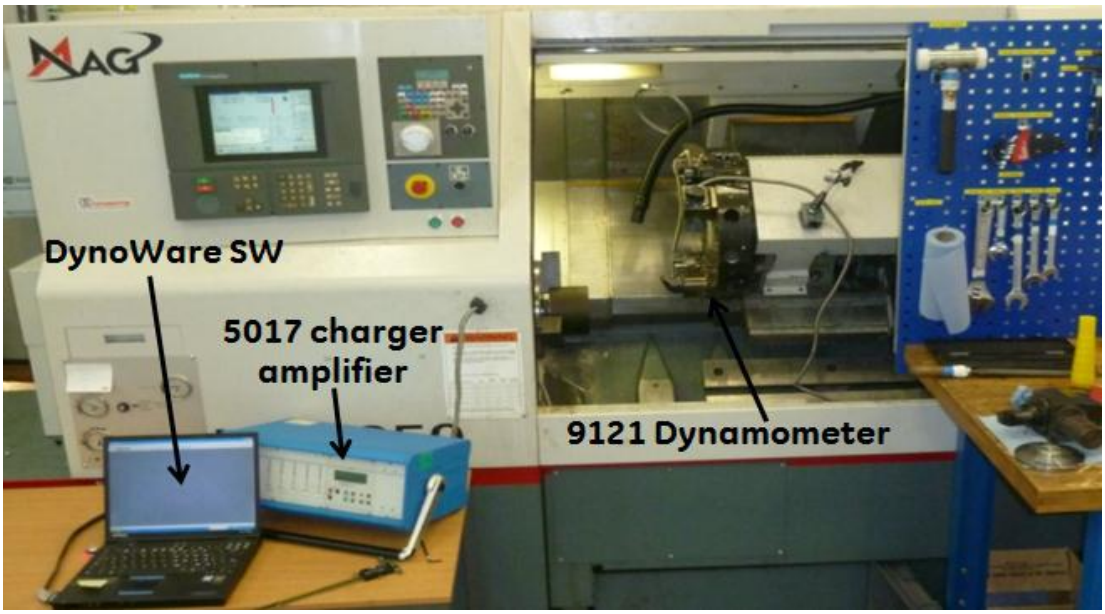

Figure 17: Cutting force measurement set up. Showing the Kistler charger amplifier, the dynamometer and the acquisition software.

The acquired data were filtered in Dynoware (window size=300) where a sample rate of 5000 Hz was set previous acquisitions. A measuring range of 1000 N was set for all channels.

An extraction system was also installed on the lathe machine tool to remove the small particles produced during the cutting trials, which reach dimensions smaller than one micron [44]. *Figure 18* shows the arrangement of the extraction system, dynamometer and tool.

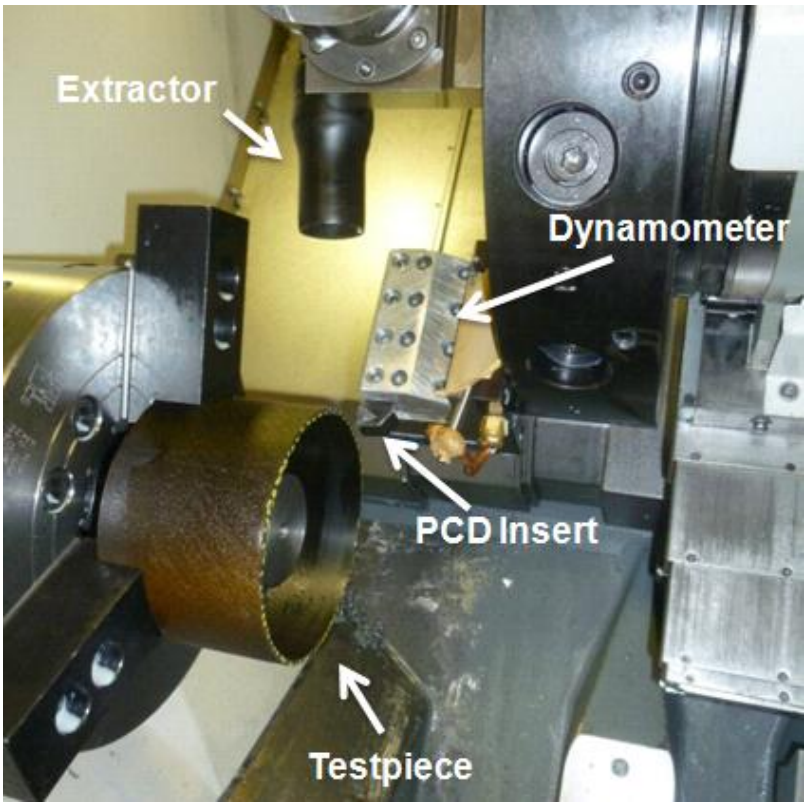

Figure 18: Machine tool set up. Showing the extraction system system, Kistler dynamometer, PCD Sandvik Coromant insert and UD-CFRP Test piece

Polished Sandvik Coromant TCMW 16T304FLP CD10 polycrystalline diamond (*PCD*) inserts were used for the cutting trials; *Appendix B*. These inserts have a clearance angle of 7º, a rake angle of 0º with a very sharp edge where no corner radius was applied. *PCD* inserts guarantee optimal hardness and thermal conductivity of the cutting tool as well as an excellent surface finishing and sharpness of the cutting edge reducing the friction between the chip and the tool [15], [45]. These factors play a significant role during the cutting process, making *PCD* inserts more suitable than carbide, which had shown insufficient wear resistance. On the other side their use is in some cases limited by their high tool costs and low geometrical flexibility [46].

During the experimental trials a fresh cutting edge was used for each test. Initially the surface speeds used during the tests were 40 m/min & 80 m/min, and the feed rates used were: 0.05, 0.1, 0.15 and 0.2 mm/rev. Each set of cutting trials were repeated one time to provide reliability in the trials, and before each test was performed an initial cut was done to clean the cutting surface of the work-piece.

To avoid any potential slipping between the work-piece and the sample holder during the cutting trials, jaws of suitable dimensions were used. Moreover, an internal support was used to compensate the jaws pressure when clamping the *CFRP* ring as shown in *Figure 19*.

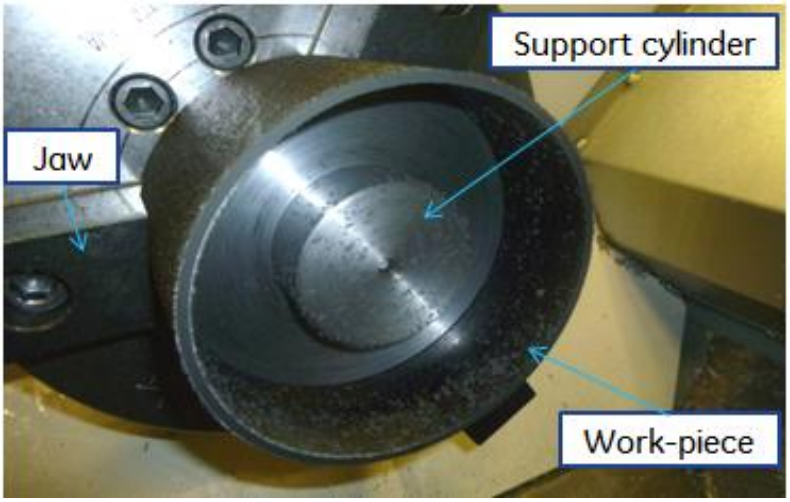

Figure 19: Test piece set up – jaws, work-piece and support cylinder.

After the test, swarf was collected for inspection using a microscope. The microscope system used was a *Sanyo VCC2972* with a high resolution camera mounted on a *Marcel Aubert CH2501 MA1200* lighting rig.

3.2 Experimental Results and Discussion

Figure 20 shows an example of typical results of cutting tests at 0 degree fibre orientation and 80m/min surface speed. The results indicated that feed forces were higher than cutting forces at low feed rates (*Figure 20*(a)); but when the tests were performed at higher feed rates the force results showed an opposite tendency, becoming the cutting forces higher than the feed forces (*Figure 20*(b)). This is attributed to the fact that, for the given initial test conditions (tool geometry, cutting parameters), the principal cutting force is determined by the chip section area, and therefore, by the feed rate, while the feed force is manly determined by the edge preparation and by the relative bouncing back phenomena [19]. These factors assume a relevant importance for low chip thickness values. Furthermore, in *Figure 20* can be noted that the feed forces did not reach a steady state; this behaviour was observed in other tests at longer cutting

times. This effect is related to the formation of a bigger corner radius which results increasing the pressing region and the forces on the feed direction.

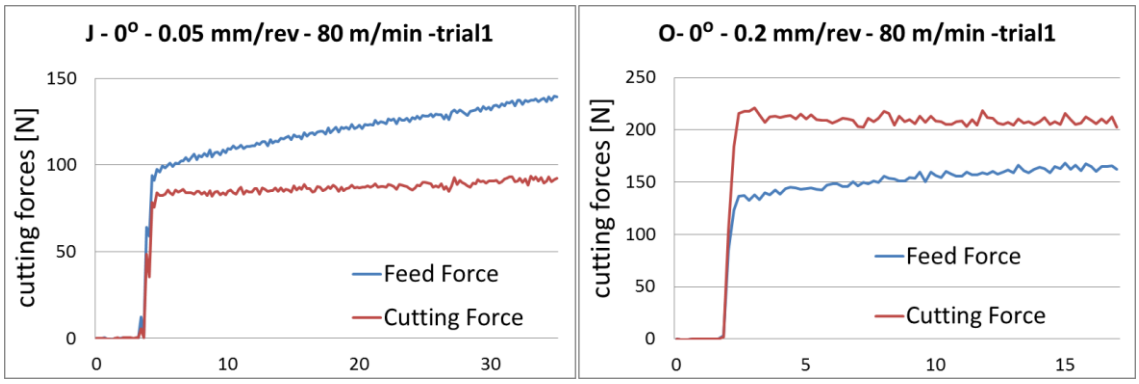

(a) (b)

Figure 20: Cutting force acquisition
(a) Cutting feed =0.05 mm/rev; (b) Cutting feed =0.2 mm/rev.

It should be highlighted that the surface quality and the chip formation showed some differences during the early stage of the cut and after a short period of time of the process. At the early stage of the cutting tests, it was observed that long chips and good surface quality was produced in the work-piece; this can be attributed to the fact that the insert cutting edge was sharp which allowed complete removal of all fibres. After cutting for a relatively short interval of time, the insert was not able to remove all fibres which produced chips of different sizes and poor surface quality in the work-piece. The tests also revealed that the fibres were easier to remove with higher feed rates (0.2 mm/rev), providing better surface quality.

For all the tested fibre orientation a correlation between the thrust force increment and the phase of the resultant force ($\beta-\alpha$) was created (*Appendix C*).

In *Figure 21* the direction of the resultant force is plotted for different fibre orientations.

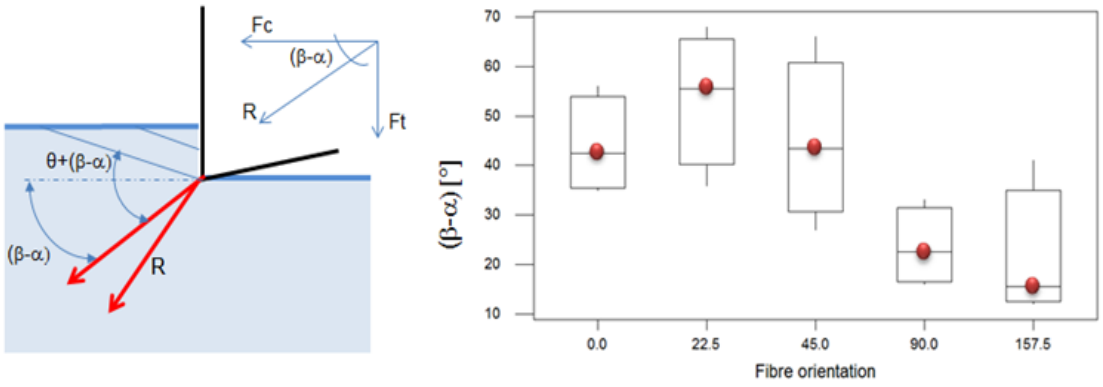

Figure 21: Resultant force angle (β–α) *for different fibre orientation work-piece*

Another main factor that affected the surface quality was the fibre orientation (*Figure 22*). The best surface quality was obtained when cutting fibres oriented at 157.5˚. This configuration produced the lowest cutting forces and no fibre pull-out was generated. Good surface quality was also obtained when cutting work-piece having fibre orientation at 0˚, although long uncut fibres remained on the machined surface. In this configuration the fibre-pull out was considered negligible for the integrity of the structure since the damage did not propagate in the bulk direction and could be easily removed.

When cutting 22.5˚ and 45˚ fibre orientation fibre pull-out was observed in the work-piece internal and the external diameter. In this configuration the fibres were free to bend aside while the matrix was completely removed. The length of the remaining fibre was short. However, this could have significant effects on the work-piece integrity since debonding could propagate from the uncut fibre into the work-piece. Poor surface quality was obtained for the 90˚ fibre orientation. In this arrangement the insert was not able to cut most of the fibre at the internal and external diameter of the work-piece, from which visible cracks are propagated with the bulk structure.

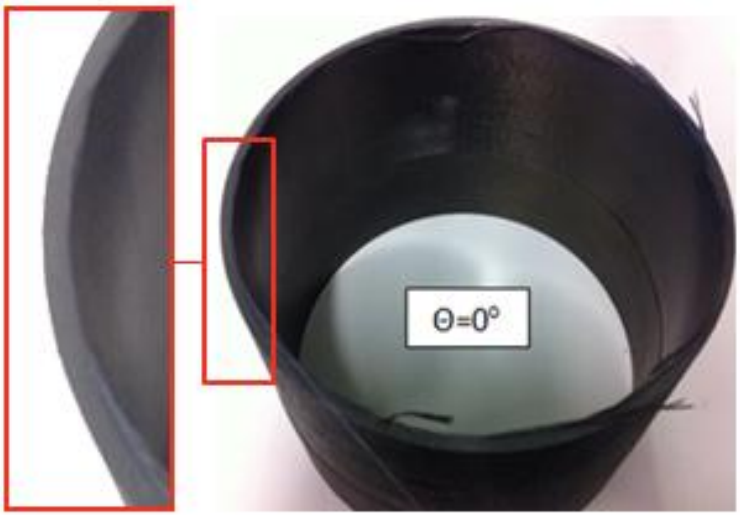

(a)

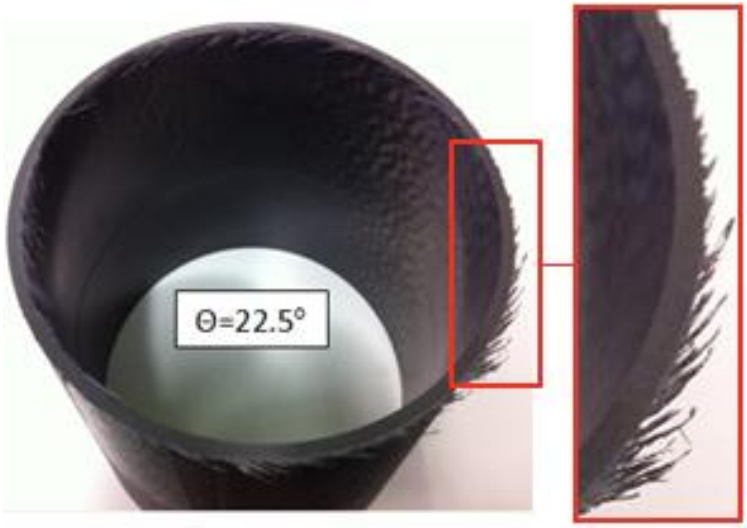

(b)

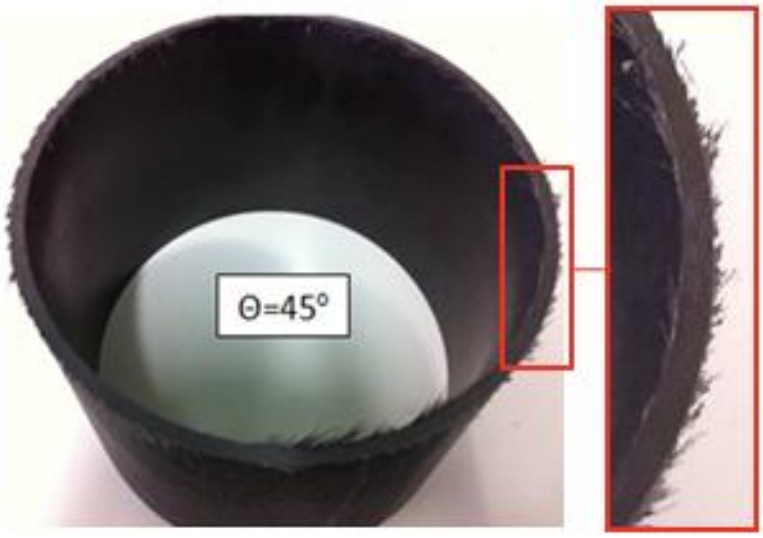

(c)

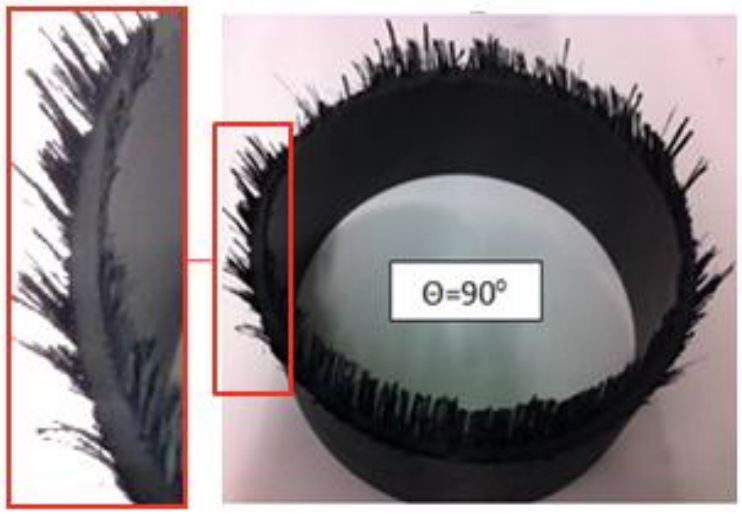

(d)

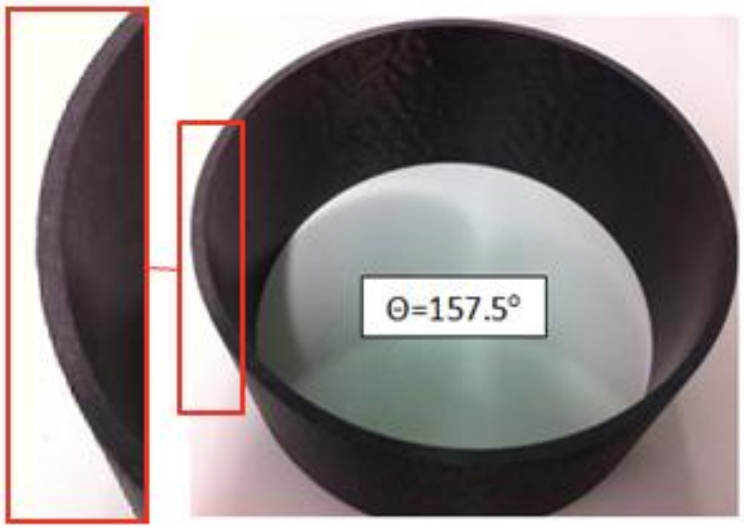

(e)

Figure 22: 0˚, 22.5˚, 45˚, 90˚ and 157.5˚fibre orientation cut work-pieces.

The tests performed at 135˚ fibre orientation failed during the machining trials as shown in *Figure 23.* Therefore, it was not possible to register any data during these tests. The failure of the samples could have been induced to the total cutting forces that were acting in the same direction of the fibre orientation leading a premature crack along the fibre matrix interface and a resultant delamination. It should be pointed that all tests collapsed even at very low feed rate of 0.008 mm/rev. Zang [10] and Zitoune et al [23] reported similar experimental results.

Figure 23: 135˚ fibre orientation work-piece.

Further tests were run to check the evolution of the cutting forces. *Figure 24* shows how the acquired forces evolved when cutting 0˚, 22.5˚, 45˚ and 90˚ fibre orientation at low feed rates. Several cutting trials were run at the lathe using the same insert to capture the effects of the tool wear on the cutting forces. From these tests it is notable that the abrasiveness of the *CFRP* material affects the tool condition, resulting in a continuous variation of the feed forces, while minor effects are played on the principal cutting force. This can be attributed to the formation of a bigger corner radius which increases the pressing region and the forces on the feed direction. It is notable that the orientation of the fibres affects both the cutting forces magnitude and its evolution.

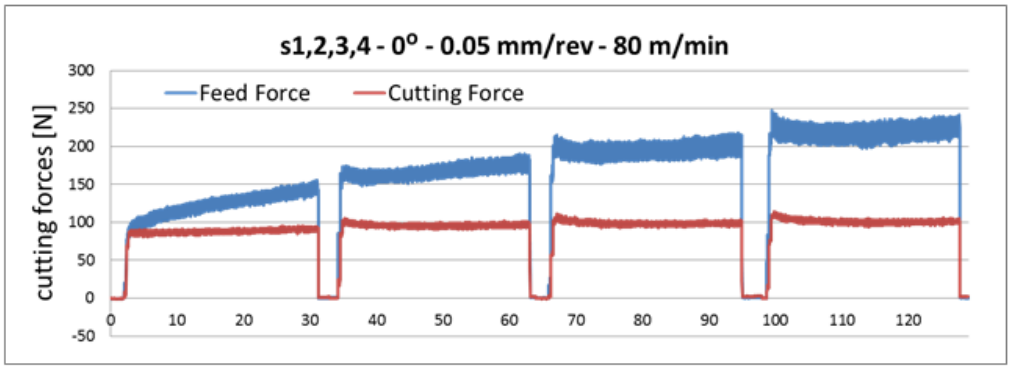

(a)

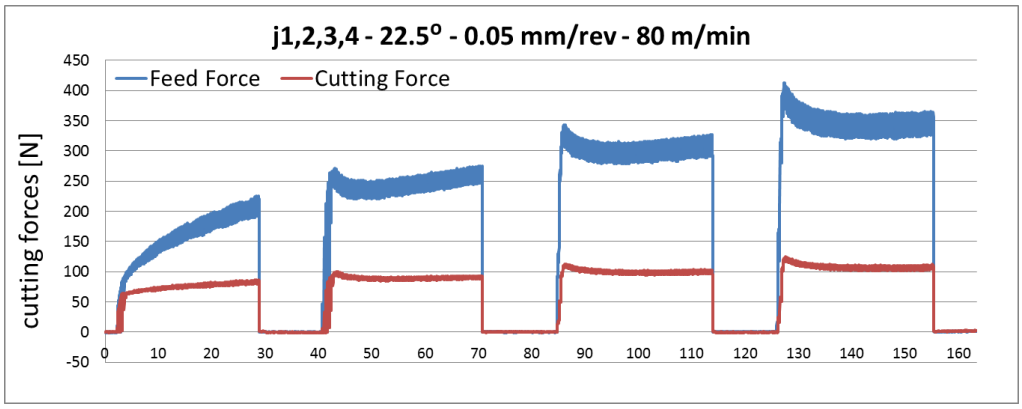

(b)

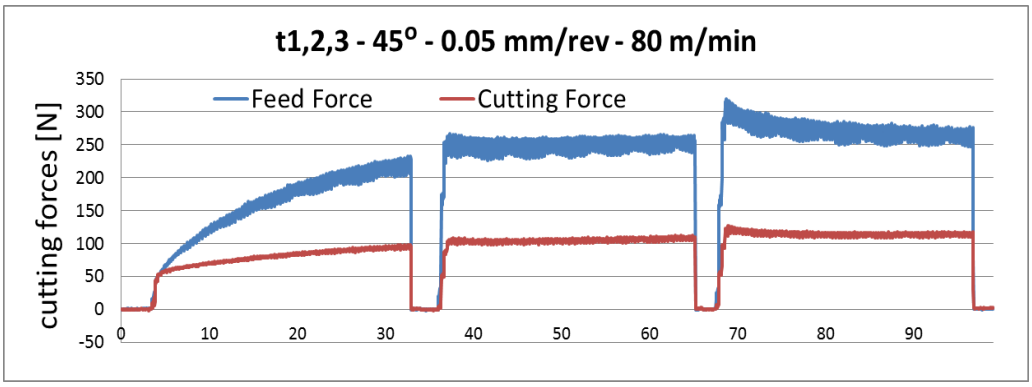

(c)

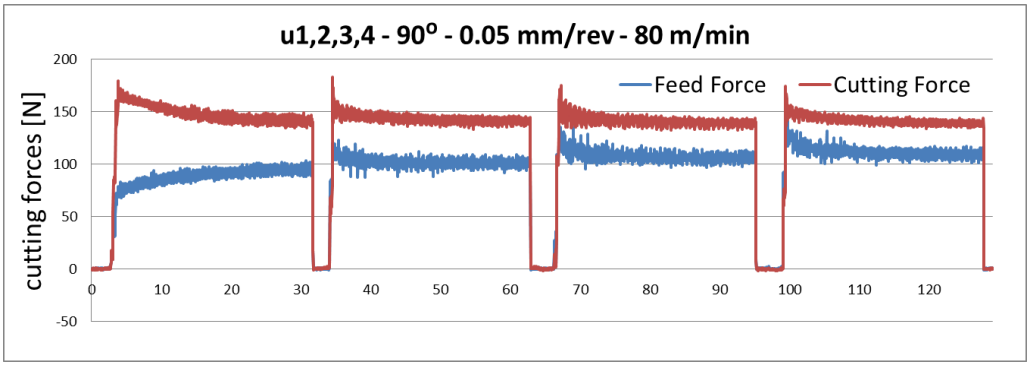

(d)

Figure 24: Cutting trials. Vc = 80 m/min, f=0.05 mm/rev; a) 0˚, b) 22.5˚, c) 45˚, d) 90˚ fibre orientation

A gradual loss of the tool capability to cut the fibres neatly was witnessed by Park et al [47]. They observed that in *CFRP*/Ti stack drilling different wear mechanisms took place. While the cutting edge was gradually affected by the abrasiveness of the fibre the Ti was responsible for the generation of flank wear.

In their study Wang et al [48] developed a hypothesis to explain the edge rounding wear in *CFRP* machining. They investigated the tool wear of uncoated, diamond coated and AlTiN coated carbide drills when drilling *CFRP*. The difference of *CFRP* wear mechanisms were attributed to the absence of the stagnant zone in the proximity of the edge preparation when cutting brittle materials. During the cutting of traditional metals, through continuous chip formation processes, the stagnant zone protects the cutting edge from the material flow, due to the low relative movement between the material to be removed and the edge preparation. This creates the formation of crater and flank wear as dominant wear types. On the other hand, when cutting brittle materials, as *CFRP*, the failure is attributed to fracture, which gradually affects the cutting edge until it is no longer able to cut the fibres neatly, leading to a rise of the cutting forces [48], [49].

An insert was examined by an electronic microscope before and after a machining trial to verify that the surfaces of the *PCD* insert were significantly altered. In *Figure 25* the insert is shown before and after a cut of 30 seconds. The rake and the relief faces are visible in *Figure 26*. It was observed that the cutting edge was affected during the machining operation, but the magnitude of such alteration cannot clearly be defined with the used electronic microscope. A further analysis, using higher resolution equipment, is therefore recommended to support these observations.

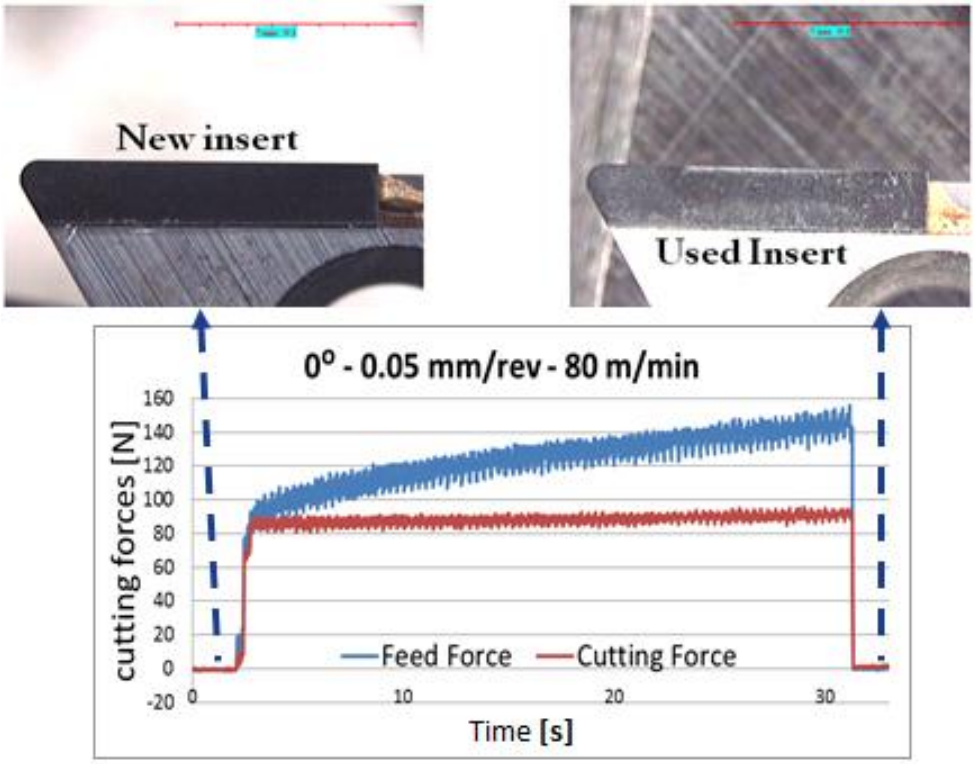

Figure 25: Cutting edge alteration after 30 seconds of cut. Vc = 80m/min, f=0.05 mm/rev.

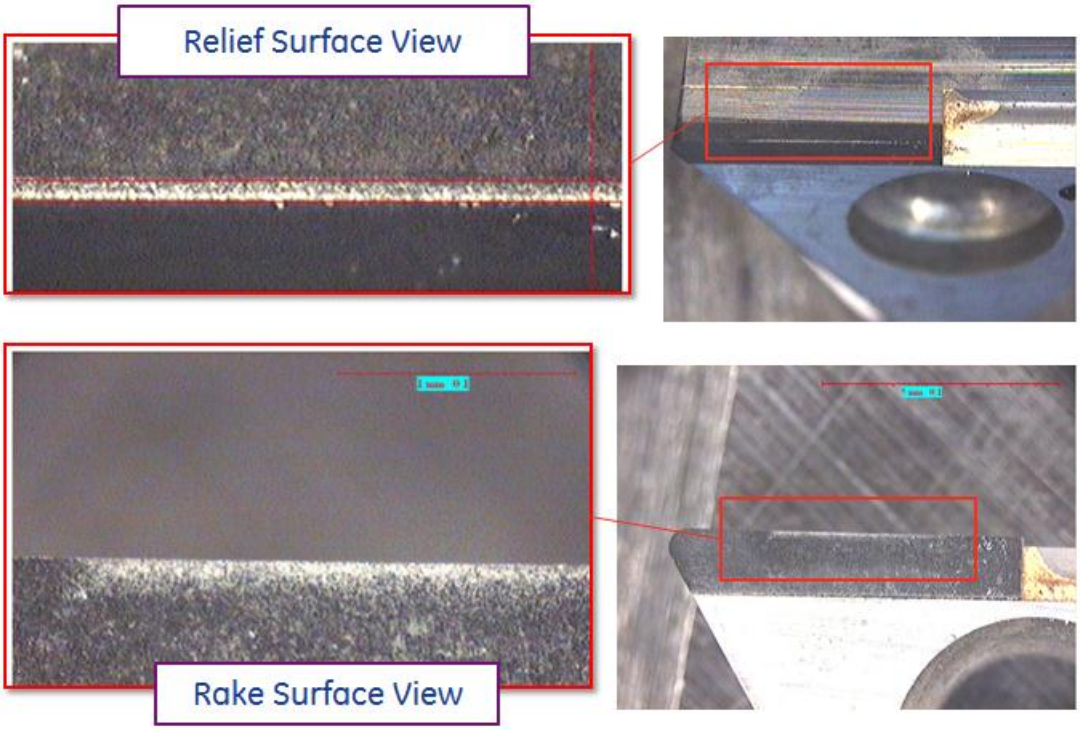

Figure 26: Rake and Relief surfaces alteration after 30 seconds of cut.

These results gave additional indication that when cutting *CFRP* materials the tool life should be determined taking into consideration the quality of the cut surface, which has shown to be very sensitive to any variations in the tool edge, and not by the magnitude of wear on the insert edge as per metals. No common methodologies have been developed yet to determinate the quality of the *CFRP* material cut surface as per metal [3], [5].

It should be pointed out that this behaviour has to be attributed to the alteration of the corner radius and not to temperature effects. Therefore, it has been considered as representative cutting force value the one within an interval of 1-3 seconds cut from the beginning of the test, where the cutting edge has not been altered yet. The cutting forces results are reported in *Appendix C.*

Figure 27 shows the cutting force results at four different feed rates and two different cutting speeds for 0˚ fibre orientation.

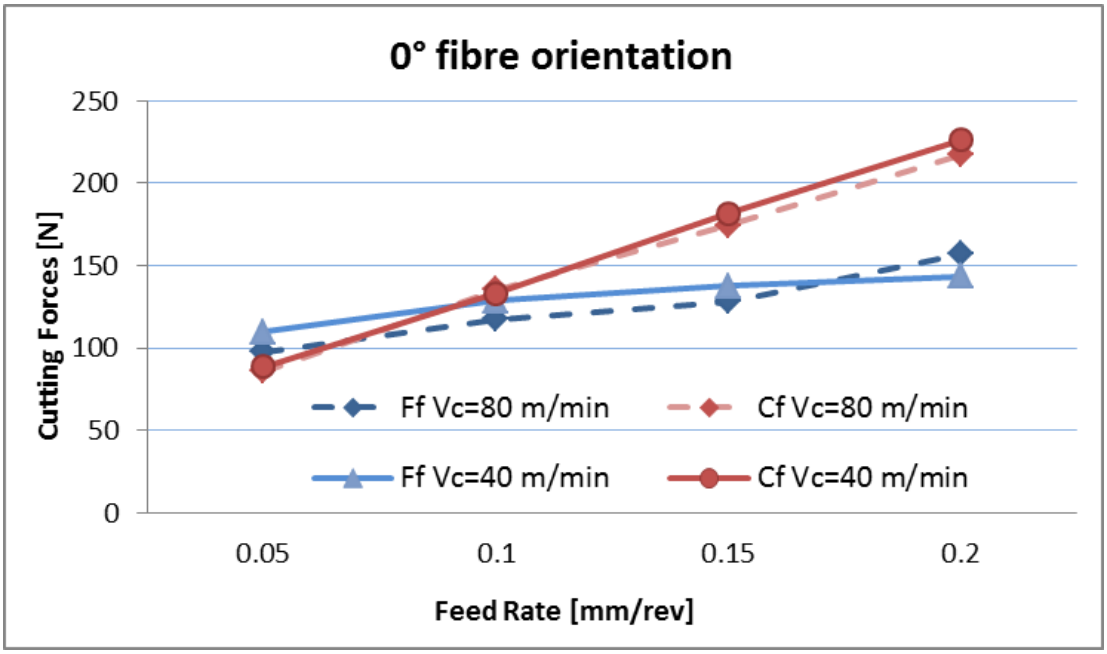

Figure 27: Cutting force for 0˚ fibres orientation. 40 Vs. 80 m/min (Appendix C).

In the main effect plot (*Figure 28*) the effect of each factor on principal cutting force, feed force and resultant force is shown.

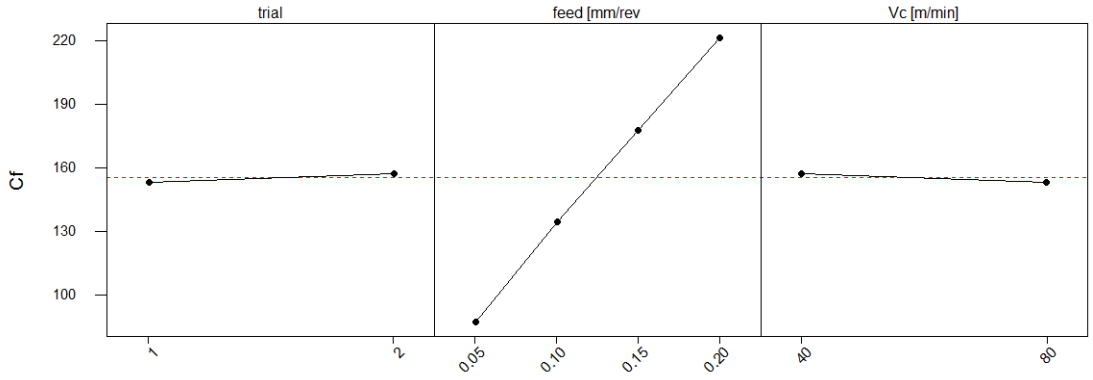

(a)

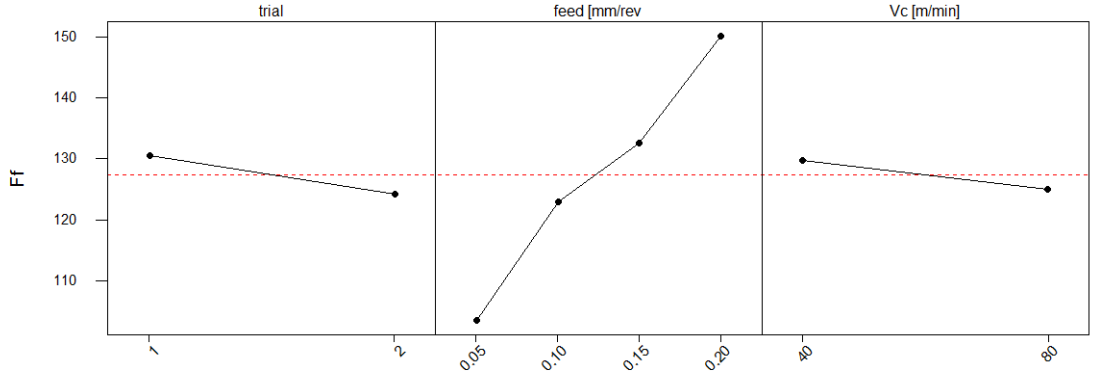

(b)

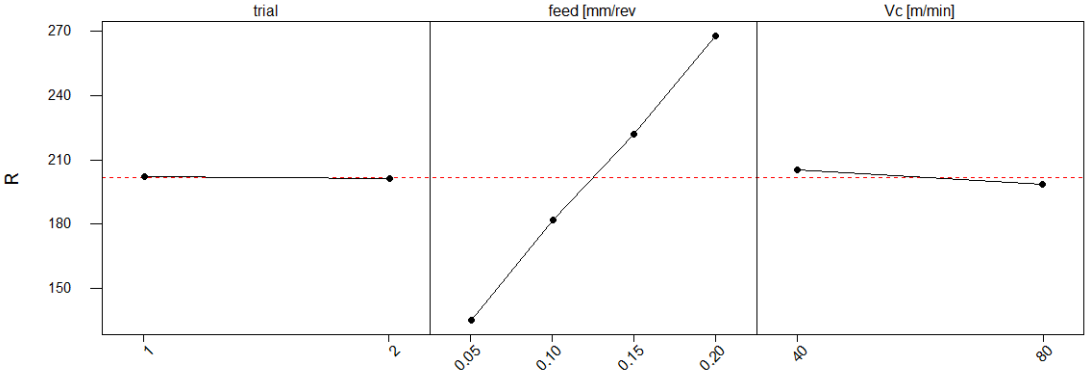

(c)

Figure 28: Main effect plot on:
a) Principal cutting force, b) Feed force, c) Resultant force (Appendix C).

The main effect plot highlights that the cutting forces are directly proportional to the feed rate, as also found by Mata [20], while a minor effect is played by the cutting speed, which will be kept constant (80 m/min) in future tests. Globally all the tests presented a good repeatability. From *Figure 27* it can be noticed that for low feed rates (f=0.05 mm/rev) the cutting forces are lower than the feed forces while this behaviour is inverted from 0.1 mm/rev of feed.

Figure 29 to *Figure 30* show the effects of the fibres orientation on the cutting forces and feed forces against different feed rates. In these graphs, the cutting times after 1-3 seconds and after 30 seconds were considered to capture the effects of the tool wear on the cutting forces. From the graphs it is easy to observe that both the feed rates and the fibre orientations affect the cutting forces.

When cutting 157.5° fibres orientation work-pieces the material presented brittle characteristics, generating a neat cut from which a small particles chip is obtained. This is due to the fact that the resultant force acts along the direction of the fibres where no plasticity is involved and rupture occurs once the yield stress is reached. In this configuration the work-piece has shown higher machinability since less energy is required to generate the chip, while the cut surface is the one having the best quality among all fibre orientations.

A similar scenario in terms of fibres-resultant force direction was obtained when cutting work-pieces oriented at 135° but, in this configuration, a fast destruction of the specimen, due to debonding which leaded to severe cracks, was obtained. Through experimental tests performed at a cutting speed of 80 m/min it is possible to exclude the Zitoune et al thesis that attributes the cracks generation to the low relative travel rate between the tool and the work-piece [32]. Further tests were performed reducing the feed rate, up to 0.008 mm/rev, to reduce the resultant force phase ($\beta-\alpha$ angle) but the same results were achieved. It is reasonable to believe that when cutting specimens oriented at 157.5° the whole bulk has the capability to withstand the force required to generate the chip. When fibre orientation is reduced to 135°, the fibres are lifted by the rake angle which, with the tool advancement and the increasing of the shear force, generates fibre/matrix separation. Due to the dynamicity of turning and to the structural

properties of the designed specimens the cracks in this configuration are more severe than the ones obtained when performing traditional quasi-static orthogonal cutting tests, although basic principles are similar. In their study Wang and Zhang demonstrated that no significant improvements were obtained when changing the rake angle to machine F593 specimens at 120° fibre orientation [18].

A force increment of up to 10 times was obtained when cutting test pieces with fibres oriented at 22.5°. In this configuration the highest increment of feed forces after 30 seconds of cut was achieved. This could be correlated to the big value of the resultant force angle ($\beta-\alpha$) during the cut. Long continuous chip was obtained for low feed rates while small particles were generated for higher feeds. A neat cut was initially obtained with the new tool and a good surface quality was achieved. A rapid flank wear occurred increasing the feed forces significantly. In this new scenario the fibres pull out occurred in correspondence to the internal and the external diameters of the work-piece.

Highest principal cutting forces were obtained when cutting 90° fibre orientation work-pieces where the advancement of the tool generate compressive stresses in the matrix direction. In this configuration, while the matrix was disintegrated, fibres underwent a bending deformation along the cutting speed direction. A non-continuous chip was obtained. From these tests seems that higher feed values produced less uncut fibres on the machined surface. This could be due to the consistency of the chip which helped to remove fibres and matrix together. Zitoune et al. stated that large chip thickness leads to fibres breakage [32].

When cutting 0° fibre orientation work-pieces a similar behaviour to the one found when cutting 157.5° work-pieces was obtained, although the cutting forces were significantly higher. Good surface quality was obtained although fibre pull out was left onto the cut surface.

Tests performed on specimens oriented at 45° presented a slight different scenario. As per the other fibre orientation work-pieces, the forces were directly proportional to the feed rate, but this behaviour was inverted after 30 seconds of cut, once flank wear occurred. The thrust forces, and consequently the resultant forces, grew significantly as the tool wear increased, which contributed to alter the ($\beta-\alpha$) angle during the cut. It was

then possible to correlate the flank wear with the alteration of the (β–α) angle and, consequently, with the increase of the cutting forces.

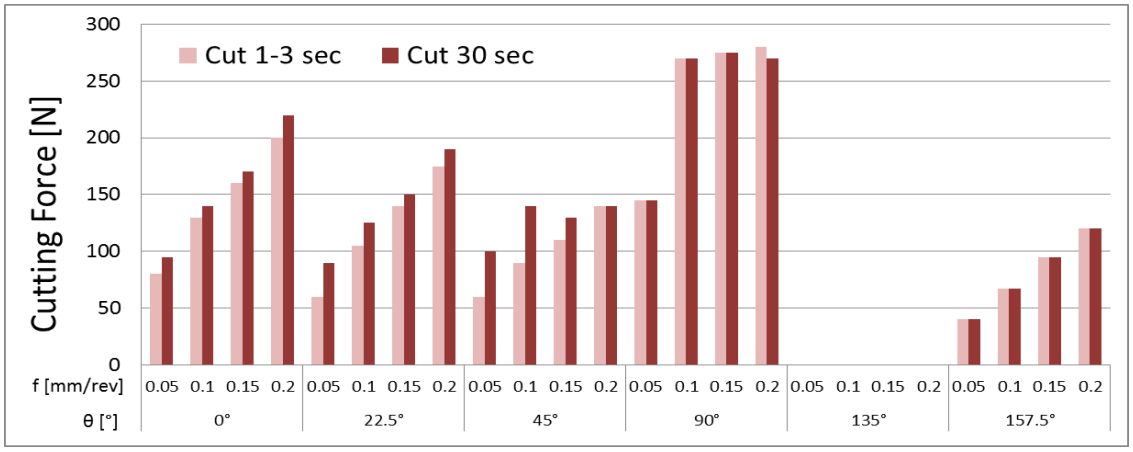

Figure 29: Cutting forces for different feed rates and fibre orientations after 1-3 seconds and 30 seconds of cutting time.

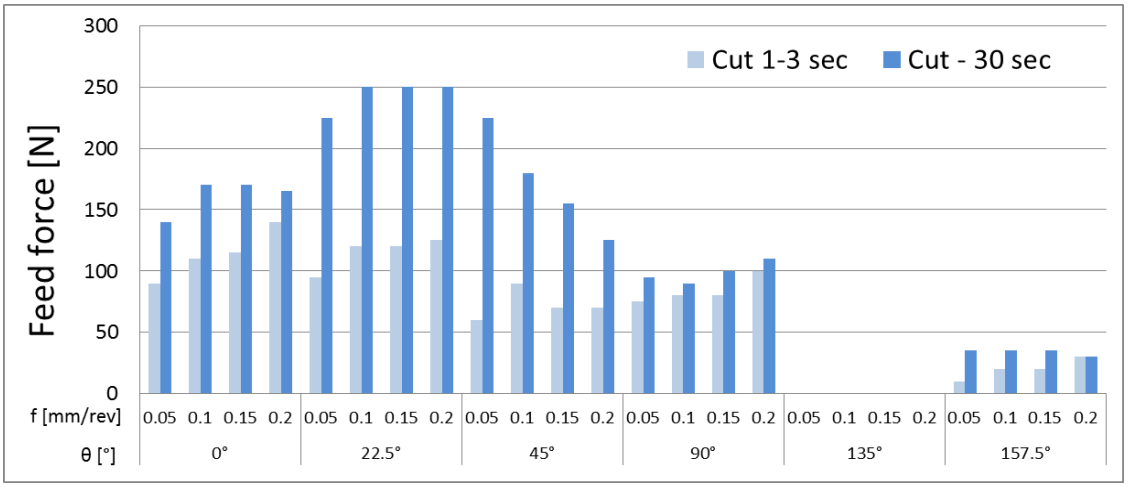

Figure 30: Thrust forces for different feed rates and fibre orientations after 1-3 seconds and 30 seconds of cutting time.

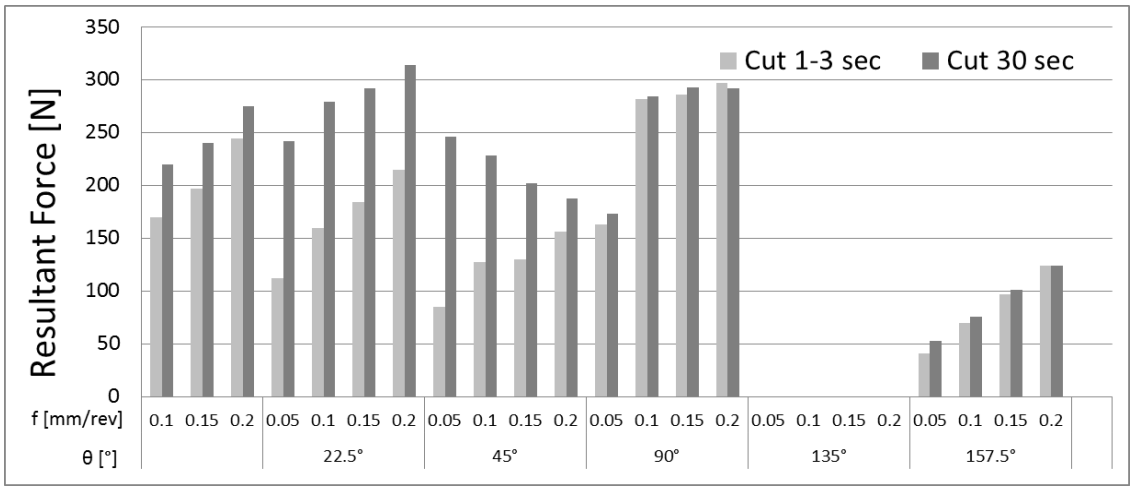

Figure 31: Resultant forces for different feed rates and fibre orientations after 1-3 seconds and 30 seconds of cutting time.

The trend of the acquired force components has been found to be in line with the results obtained by Arola et al. [21] where the influence of fibre orientation and tool geometry during orthogonal trimming of *UD-CFRP* was investigated (*Figure 32*).

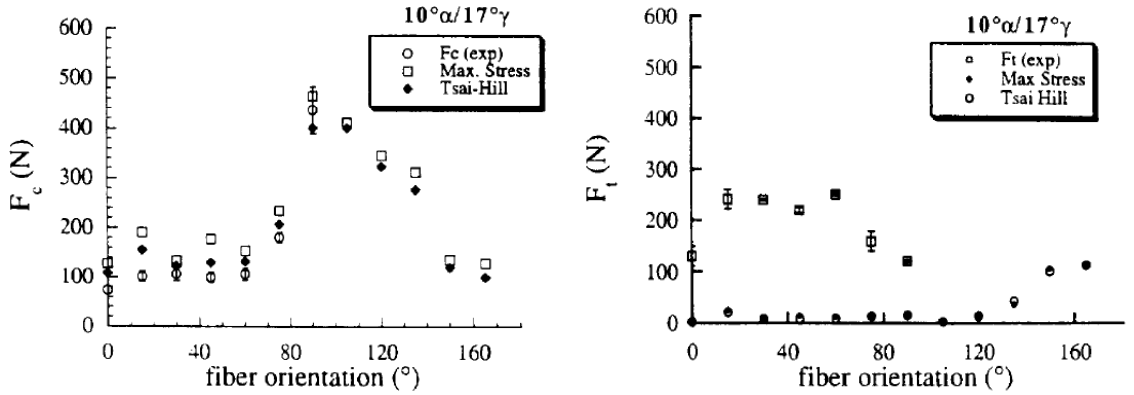

Figure 32: Comparison of Predicted and Experimental Force Responses from Arola [21].

To better relate turning with milling, where during the rotation of the tool the insert meets the fibres always at different angles, it is useful to consider the graphs from *Figure 33* to *Figure 34* where the change of the cutting forces is captured at different fibre orientations for a defined feed rate. Even during milling the fibre cutting angle at 90˚ represents a critical configuration where high cutting forces are generated and where fibres pull out is expected.

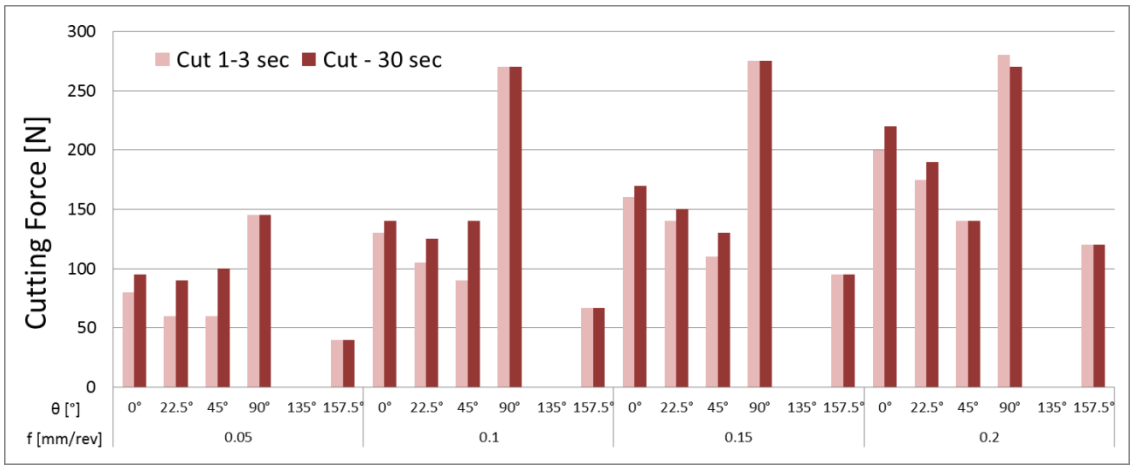

Figure 33: Cutting forces for different fibre orientations and defined feed rates after 1-3 seconds and 30 seconds of cutting time.

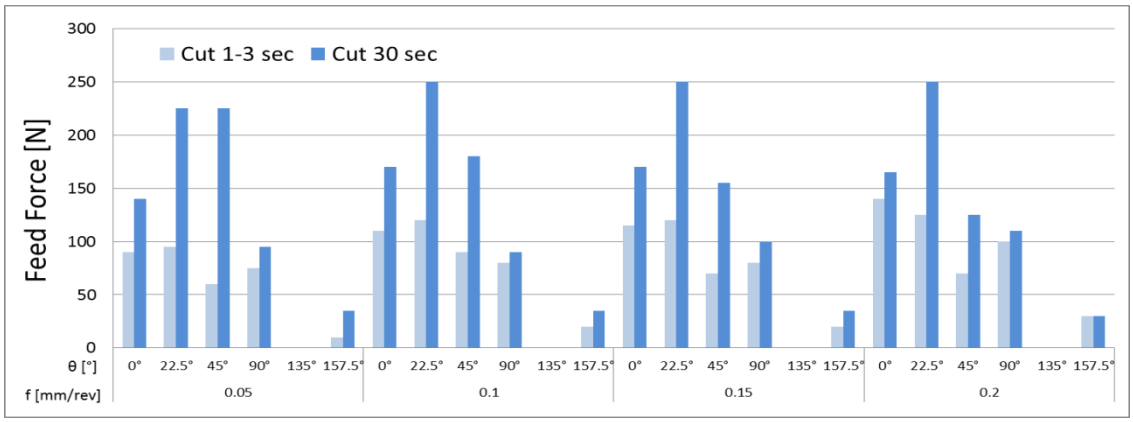

Figure 34: Feed forces for different fibre orientations and defined feed rates after 1-3 seconds and 30 seconds of cutting time.

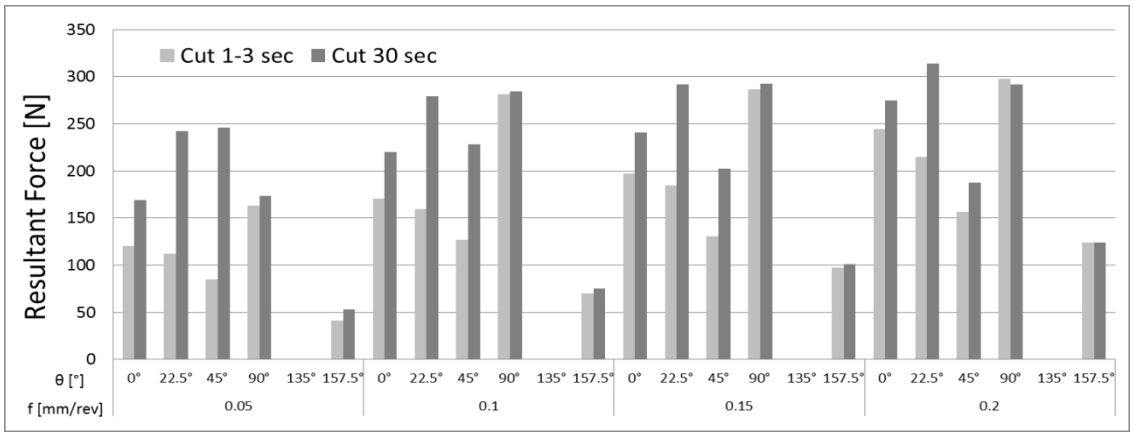

Figure 35: Resultant forces for different fibre orientations and defined feed rates after 1-3 seconds and 30 seconds of cutting time.

To obtain information related to the chip mechanisms formation the chips produced during the cutting trials were collected and inspected at the electronic microscope. As previously mentioned in **chapter 2**, composites machining produces heterogeneous chips in form of swarf with different shapes and dimensions. The small particles were subtracted during the tests by the extractor while the heaviest ones fallen down into the machine tool. The results showed that the cutting parameters and the fibre orientation highly affect the chip morphology.

When machining at a cutting speed of 80 m/min the chip size resulted to be inversely proportional to the feed rate (*Figure 36* and *Figure 37*) while the opposite behaviour was observed for cutting speed of 40 m/min, where the size of the chip grew for higher feed rates (*Figure 38*).

Being the cutting trials relative short in time and length, no burning was observed neither on the cut surface nor to the formed chip.

$\theta = 45^{\circ}$,

Vc = 80 m/min

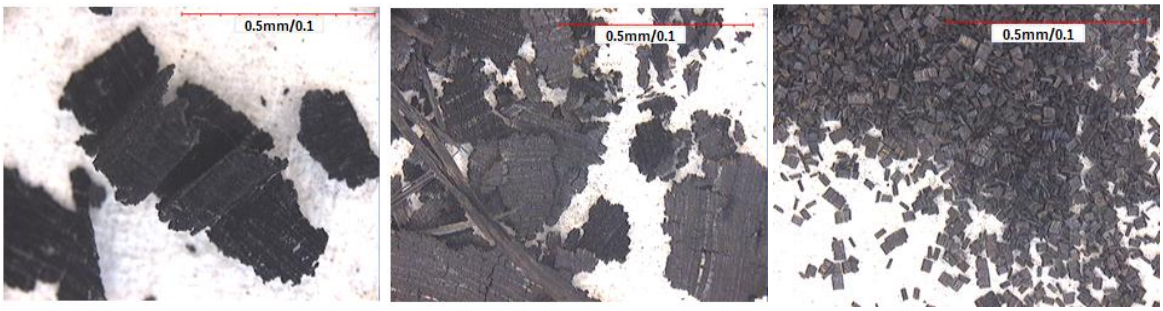

(a) (b) (c)

Figure 36: Generated chip – effects of feed for 45˚ fibre orientation and 80 m/min a) f = 0.05 mm/rev; b) f = 0.1 mm/rev; c) f = 0.2 mm/rev

$\theta = 0^{\circ}$

Vc = 80 m/min

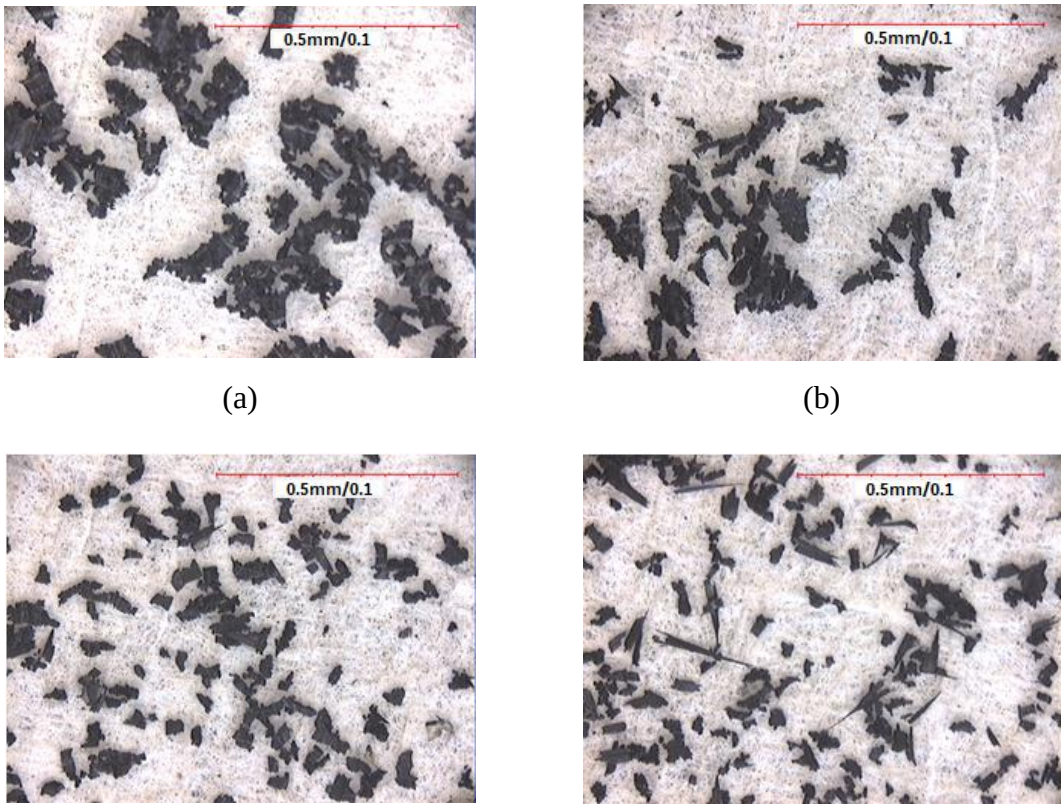

(a) (b)

(c) (d)

Figure 37: Generated chip - effects of feed for 0˚ fibre orientation and 80 m/min a) f = 0.05 mm/rev; b) f = 0.1 mm/rev; c) f = 0.15 mm/rev; d) f = 0.2 mm/rev

$\theta = 0^{\circ}$

Vc = 40 m/min

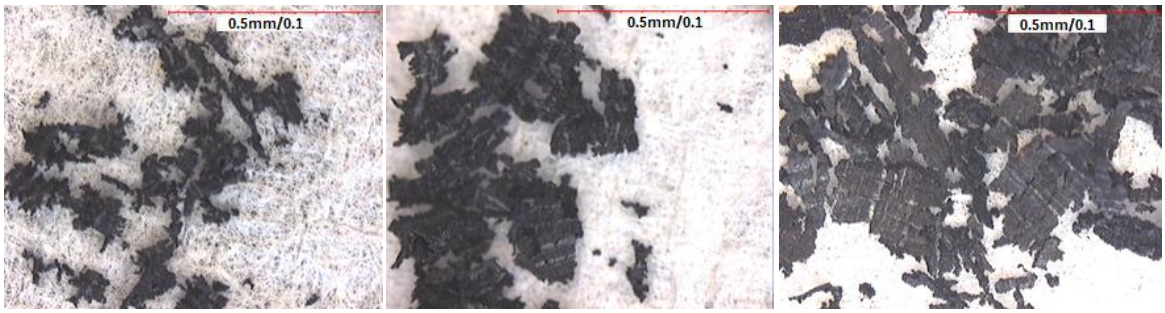

(a) (b) (c)

Figure 38: Generated chip - effects of feed for 0˚ fibre orientation and 40 m/min a) f = 0.05 mm/rev; b) f = 0.1 mm/rev; c) f = 0.2 mm/rev

3.3 Chapter Summary

This study focused on unidirectional composites work-pieces materials which lend themselves nicely to research, being the effects of process parameters easy to relate to different fibre orientations.

Orthogonal cutting was performed to simplify the analysis of the chip formation to a two dimensional problem.

The experimental test results showed that the feed rate had a major influence on the machining forces, while minor effects are played by the cutting speed. It was also observed that for low feed rates (f=0.05 mm/rev) the cutting forces are lower than the feed forces while this behaviour is inverted from 0.1 mm/rev feed. Experiment highlighted that the feed forces did not reach the steady state during the machining trials; this behaviour was attributed to the abrasiveness of the fibres which quickly altered the edge corner radius. This resulted in an increase of the pressing zone, which led to fibre bounce back of the pressed material and to a gradual increment of the thrust forces. Further tests (*Figure 25*) proved that when cutting *CFRP* materials the feed force does not stabilise due to a rapid progressive alteration of the cutting edge. In some cases the feed force values achieved after 30 seconds cut were twice as big as the forces recorded after 1-3 seconds, while minor changes of the principal cutting force values were observed.

Another key factor, which had a significant effect on cutting forces, was the orientation of the fibres. A sudden rise of the cutting forces was observed when cutting material at 0, 90 and 157.5 degrees fibre orientation, while a gradual increase was captured when cutting material with a 22.5 and 45 degrees fibre orientation.

Low cutting forces were captured when cutting work-pieces oriented at 157.5˚, while high principal cutting forces were recorded for 90 degrees fibre work-pieces after 1-3 seconds of cut, and for 22.5˚ after 30 second of cut.

For work-pieces having a fibre angle lower than 90 degrees ($0 \leq \theta < 90$) the initial feed force values were found to be higher than the cutting forces for low feed rates (f = 0.05

mm/rev). This trend was inverted for higher feed rate values were the cutting force became the principal component.

The best surface quality was observed when cutting 157.5 degrees fibre orientation, where no fibre pull out was generated. Similar behaviour was shown when cutting 0 degrees fibre orientation work-pieces, with the exception that long fibres pull out was visible on the machined surface. In this configuration the fibre pull-out is considered harmless for the integrity of the structure since the damage did not propagate in the bulk direction. Severe induce surface damage and fibre pull out took place when cutting 90 degrees fibre orientation work-pieces.

For all the tested fibre orientation a correlation between the increment of the thrust force and the phase of the resultant ($\beta - \alpha$) force was created.

CHAPTER 4 **FEM CUTTING MODEL**

4.1 LS-Dyna Composite Models

A realistic characterisation of the work-piece material is of primary importance in *FEM* simulations since these properties define the cutting forces and relative energy spent in cutting.

To describe the behaviour of the work material the stress at fracture needs to be considered to predict onset of damage. In some cases even the strain limits are required. A degradation scheme is then needed to reduce the material properties once failure initiates. The mechanical properties of MTM44-1 are reported in *Appendix A*.

In LS-Dyna the material models are referenced by a 3-digit number to identify the material designation and implemented element formulation [50]. Each material model has different associated attributes:

SRATE - *Strain rate effects*
FAIL - *Failure Criteria*
EOS - *Equation of state required for 3D solid and 2D continuum elements*
THERM - *Thermal effects*
ANISO - *Anisotropic orthotropic*
DAM - *Damage effects*
TENS - *Tension handled differently than compression in some manner*

Several LS-DYNA material models deal specifically with composite materials. Each material model utilises a different modelling strategy: failure criterion, degradation scheme, material properties.

CHAPTER 4 **FEM CUTTING MODEL**
- LS-Dyna Composite Models -

The most suitable LS-DYNA material models which deal specifically with composites are listed in *Table 3*:

Table 3 LS-Dyna composite material models

MAT 022	Composite damage. Do not include Hashin criteria
MAT 054 & MAT 055	Enhanced composite damage. Valid for thin shell element only. Chang-Chang and Hashin criterion can be applied
MAT058	Laminate composite fabric. It may be used to model composite materials with *UD* layers, complete laminates and woven fabrics. Implemented for shell and thick shell elements
MAT059	Shell composite failure. Implemented for shell and solid elements. Do not include Hashin criteria
MAT 158	Like MAT58 but includes strain rate effects
MAT 161 & MAT 162	Composite_MSC. Used to model progressive failure analysis for composite materials (*UD* and woven). An extra license is required for these MAT models. Hashin criterion are applied

MAT54 can be used to describe anisotropic, linear elastic behaviour of the undamaged material under plane strain stress. The different damage criteria are stress or strain related and introduces the nonlinearity into the material model.

The modelling consists of three distinct work-steps: pre-processing, solving, post processing. In the pre-processing the parts are modelled and meshed; the material is defined and associated to the single part while the boundary conditions are applied to the element and part sets. The tool geometry, the cutting parameters and the cutting condition used in the simulation are consistent with the ones used in the experimental tests. The work-piece and the tool are respectively modelled as *EOHM* and as a rigid body while the tool wear is neglected to reduce the complexity and runtime.

The orthogonal cutting was developed with the plane stress assumption and a displacement curve was used to be associated with the movement of the tool.

The units used in the LS-Dyna simulation are reported in *Table 4*.

Table 4 Consistent units

MASS	LENGTH	TIME	FORCE	STRESS	ENERGY
g	mm	ms	N	MPa	N-mm

A 2D model was developed for the cutting force analysis where the tool geometry was modelled as a rigid body to reduce the computational time, having a height and a width of 0.4 mm and meshed with 256 nodes. The tool rake angle and the clearance angle of the tool were 0 and 7 degrees respectively with no nose radius. The work-piece was created using 4N-Shell Mesh, having 1 mm of length, 0.5 mm height and consisting of 800 single elements with the dimension of 25 square microns each. To avoid penetration or contact problems the tool and the work-piece were initially spaced by 20 microns (*Figure 39*). The models were considered as dried cut because coolant was not used in the experimental tests.

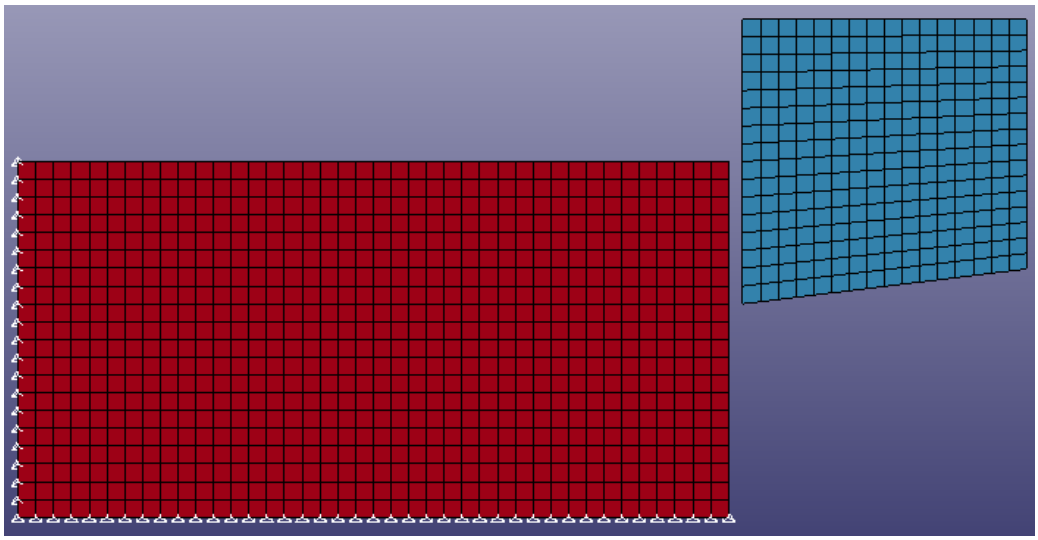

Figure 39: Work-piece and tool geometry in LS-Dyna.

MAT020_RIGID is used to characterise the insert material which was constrained and free to move along the X direction only.

MAT054-055_ENHANCED_COMPOSITE_DAMAGE is chosen among the materials in *Table 3* to characterise the linear elastic behaviour of the orthotropic *CFRP* samples. The stress-strain relations are described below by the Hooke's law:

$$[\sigma] = [D] * [\varepsilon] \tag{23}$$

where σ and ε are respectively the stress and the strain while D represents material stiffness parameters. In matrix form the derivation of the Hooke's law for orthotropic material can be written as:

$$\begin{Bmatrix} \sigma_{11} \\ \sigma_{22} \\ \sigma_{33} \\ \sigma_{12} \\ \sigma_{13} \\ \sigma_{23} \end{Bmatrix} = \begin{pmatrix} D1111 & D1122 & D1133 & 0 & 0 & 0 \\ D2211 & D2222 & D2233 & 0 & 0 & 0 \\ D3311 & D3322 & D3333 & 0 & 0 & 0 \\ 0 & 0 & 0 & D1212 & 0 & 0 \\ 0 & 0 & 0 & 0 & D1313 & 0 \\ 0 & 0 & 0 & 0 & 0 & D2323 \end{pmatrix} \begin{Bmatrix} \varepsilon_{11} \\ \varepsilon_{22} \\ \varepsilon_{33} \\ \gamma_{12} \\ \gamma_{13} \\ \gamma_{23} \end{Bmatrix} \tag{24}$$

Under plane stress conditions $\sigma_{31} = \sigma_{13} = \sigma_{32} = \sigma_{23} = 0$. In this case the Hooke's law takes form as:

$$\begin{Bmatrix} \sigma_{11} \\ \sigma_{22} \\ \sigma_{12} \end{Bmatrix} = \begin{pmatrix} D1111 & D1122 & 0 \\ D2211 & D2222 & 0 \\ 0 & 0 & D1212 \end{pmatrix} \begin{Bmatrix} \varepsilon_{11} \\ \varepsilon_{22} \\ \gamma_{12} \end{Bmatrix} \tag{25}$$

Specifying the terms of the elastic matrix stiffness:

$$\begin{Bmatrix} \sigma_{11} \\ \sigma_{22} \\ \sigma_{12} \end{Bmatrix} = \begin{pmatrix} \frac{E1}{(1-v12v21)} & \frac{v21E1}{(1-v12v21)} & 0 \\ \frac{v12\,E1}{(1-v12v21)} & \frac{E1}{(1-v12v21)} & 0 \\ 0 & 0 & G12 \end{pmatrix} \begin{Bmatrix} \varepsilon_{11} \\ \varepsilon_{22} \\ \gamma_{12} \end{Bmatrix} \tag{26}$$

Where E_i is the Young's modulus along axis i, G_{ij} is the shear modulus in direction j on the plane normal to direction i, and v_{ij} is the Poisson's ration that corresponds to a contraction in direction j when an extension is applied in direction i.

The parameters defined in the LS-Dyna material models are discussed in detailed in the next chapter.

The element type is defined as Shell element with Belytschko-Leviathan formulation which presented the best results in literature [51]. A constant shell element thickness of 3.7 mm was set to compare the *DOC* in the experiments.

Part list and node list were created to be associated with the boundary and other parameters.

In the current model the bottom edge (*uy=uz=urx=ury=urz=0*) and the left side (*ux=uz=urx=ury=urz=0*) of the work-piece were constrained while the tool moves towards the work-piece at constant velocity. The movement of the tool was defined through "prescribed_motion_rigid" where a curve function previously created was associated.

A 2D_AUTOMATIC-SURFACE-TO-SURFACE contact was set between the work-piece and the tool, having a constant friction coefficient of 0.3; according to Calzada [7] and based on the pin-on-disk tests performed by Mkaddem at 0° fibre orientation [29]. To obtain the resultant forces between the insert and the work-piece it is necessary to set up the respectively part lists as master and slave.

The output force values were extracted from "*RCFORC*" file, which contains the resultant contact forces for the slave and the master of the contact interface.

4.2 MAT054-055 Input Parameters

Some input data consist of parameters based on coupon tests while others are a mix of mathematical expedients and correction factors that cannot be measured experimentally since they may not have a physical meaning. These factors need to be defined by trials and errors.

The data that defines the material properties in *MAT054-055* are the material density, the Young's modulus (*EA, EB, EC*), the Poisson ratio (v_{ab}, v_{bc}, v_{ca}), the shear modulus

(G_{ab}, G_{bc}, G_{ca}) and the strength in the fibre and matrix direction, which is different for tension and compression (*Figure 40*) [43], [52].

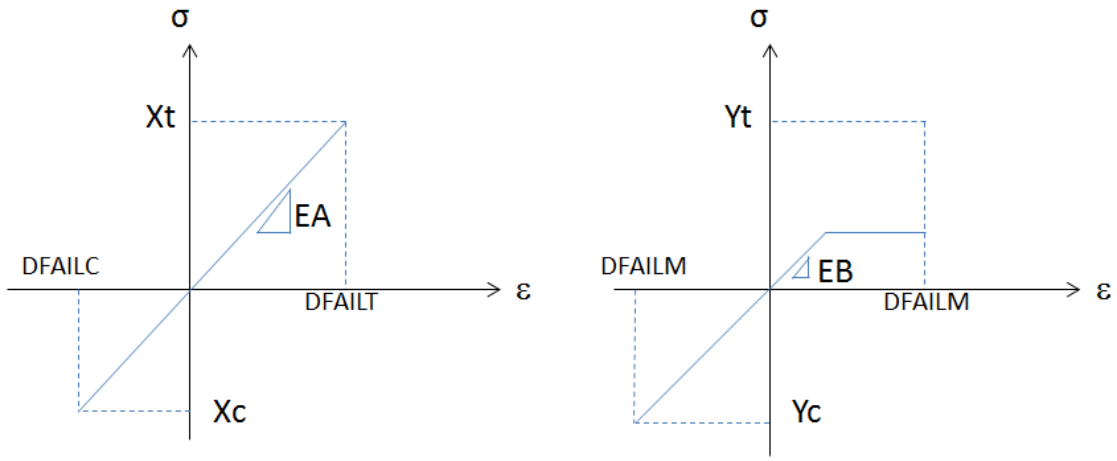

Figure 40: MAT54-55 Material properties.

The used Chang/Chang model is a stress related criteria, however sometimes it is desirable to limit the strain as well. MAT 054-055 offer the opportunity to limit the strain in the different directions using the parameters:

DFAILT – Maximum strain for fibre tension
DFAILC – Maximum strain for fibre compression
DFAILM – Maximum strain for matrix
DFAILS – maximum shear strain
EFS – effective strain

The tensile and compressive strength can be effected using the parameters *FBRT* and *YCFAC* which reduce it as a result of some compressive failure of the matrix. The elements can also fail if their time step decreases below a certain value given in *TFAIL*. In some cases it is related to the *EFS* which has no favourite direction. *SOFT* allows the modeller to reduce the Young's modulus and the strengths of the neighbouring elements to the failure.

The adopted shell element formulation is the Belytschko-Leviathan which was observed by Charoenphan to display the expected coupling between membrane and

bending/twisting deformations that occur in unbalanced and/or asymmetric composite materials [51].

The input parameters to be set up in *MAT54-55* are summarised in *Figure 41* and in *Table 5*, where the material properties, the strength and the strain limits, the element properties orientation, the softening and the reduction factors are set.

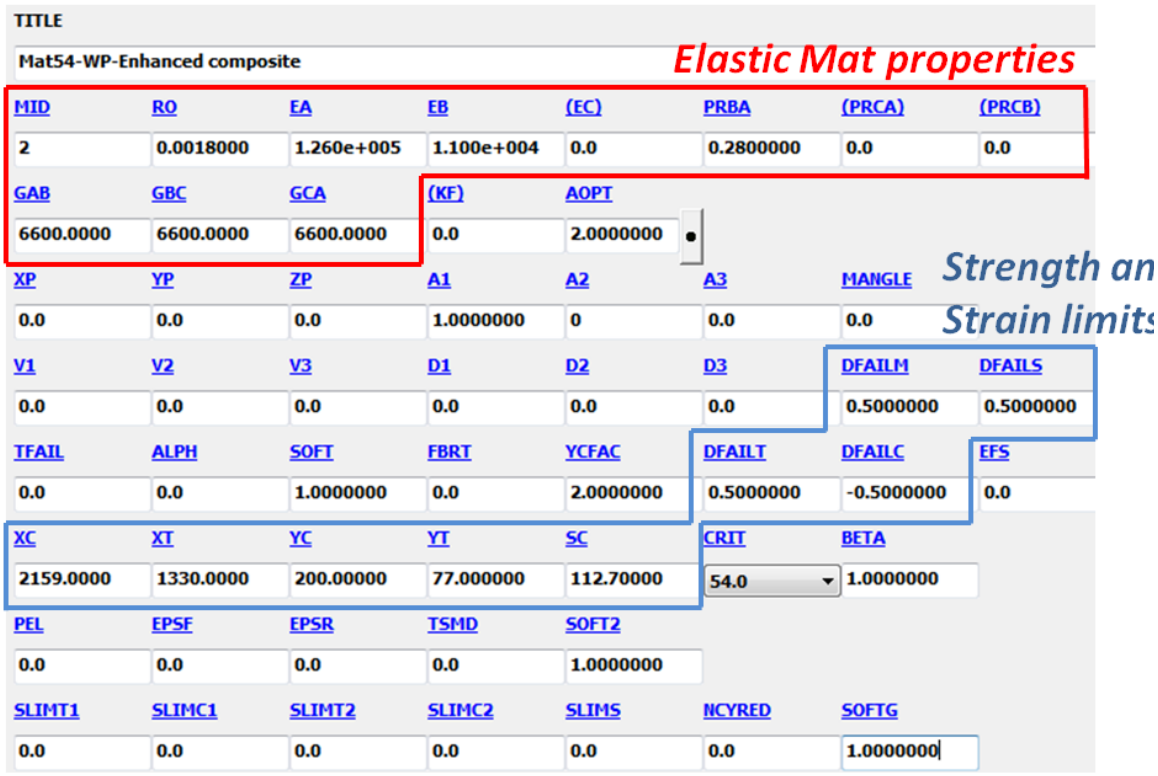

Figure 41: MAT054-055 input parameters.

Table 5 MAT54 input parameter definitions

Variable	**Definition**
MID	Mat identification number
RO	Mass
EA	young modulus- longitudinal direction
EB	young modulus- transverse direction
PRBA	Poisson's ratio vba
PRCA	Poisson's ratio vca
PRCB	Poisson's ratio vcb
GAB	Shear modulus Gab
GBC	Shear modulus Gbc
GCA	Shear modulus Gca
AOPT	Material axes optional parameter
A1 A2 A3	Vector component for material axes for AOPT=2
MANGLE	Material angle in degrees used when AOPT=3
V1 V2 V3	Vector component for material axes for AOPT=3
DFAILT	Strain limit for fibre tension
DFAILC	Strain limit for fibre compression
D1 D2 D3	Vector component for material axes for AOPT=2
DFAILM	Strain limit for matrix in tension and compression
DFAILS	Max shear strain
EFS	Effective failure strain
TFAIL	Time step size criteria for element deletion
ALPH	Shear stress non-linear term
SOFT	Crush front strength reducing parameter
FBRT	Softening tensile fibre factor after matrix failure
YCFAC	Softening compressive fibre factor after matrix failure
BETA	Weighing factor for shear term in tensile fibre mode
XC	Longitudinal compressive strength
XT	Longitudinal tensile strength
YC	Transverse compressive strength
YT	transverse tensile strength
SC	Shear strength
CRIT	Failure criterion used (MAT54, MAT55)

4.3 Dynamic Tensile Tests

Dynamic tensile tests were performed over three *CFRP* specimens to obtain the material behaviour data. The tests, respectively at 0, 45 and 90 degrees fibre orientation, were designed and performed at the Swinburne University in Melbourne while the composite samples were previously manufactured at the *AMRC* in Sheffield. The samples geometry and dimensions are visible in the *Appendix D*.

The tests highlighted that the specimen's geometry was not suited for *CFRP* materials analysis. Nevertheless it was still possible to perform the test with some changes in the specimens set up.

The three fibre orientations specimens were tested at a speed of 2 m/sec.

Good results were obtained when testing the 45 and 90 degrees samples while the strength limit was not reached for the 0 degree orientation where the sample was slipping from the clamping jaws when a force value of 16/20 kN was reached (*Figure 42*). This was attributed to the fact that the pressure applied by the clamping jaws on the specimen exceeded the strength of the material in that direction, deforming the clamped area, which could no longer provide the required support. This could be solved by a different design of the specimens.

The results provided valuable information to characterise the material in the 90 and 45 degrees orientations, while the longitudinal strength was not captured.

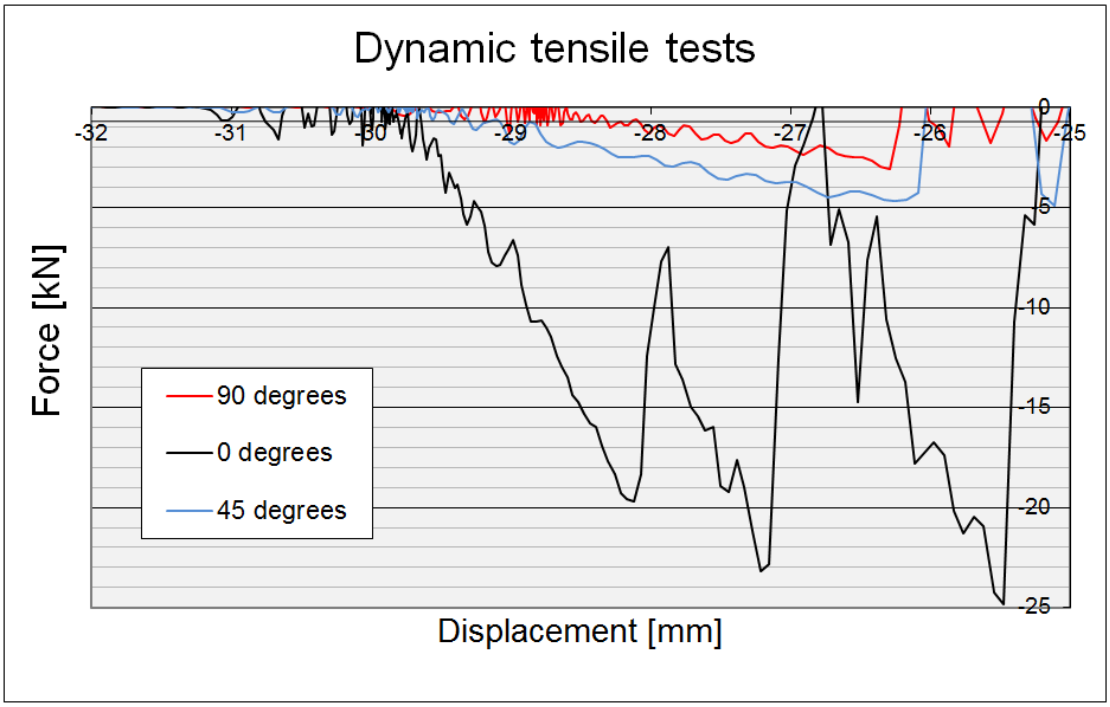

Figure 42: Dynamic tensile tests.

The tested specimens are shown in Figure 43 (*Appendix E*).

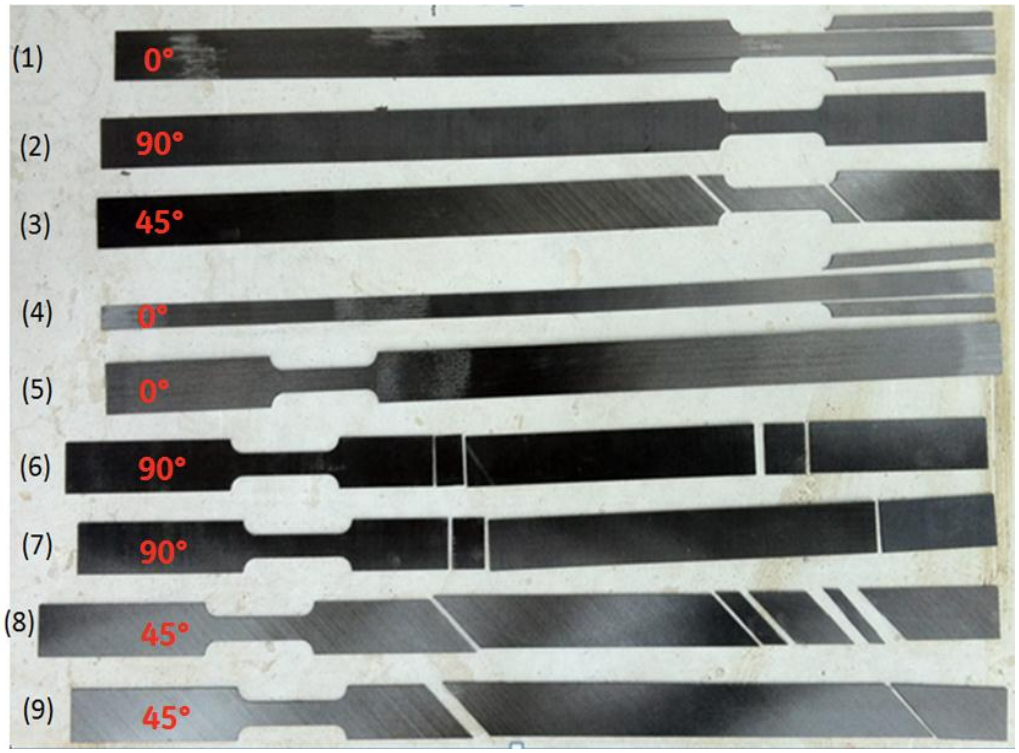

Figure 43: Tested unidirectional sample (Appendix E).

It is visible that in the initial tests (samples 1, 2, 3) the failure did not occur at the gauge length as expected when testing metals. The damage in these specimens occurred at the beginning of the radii which represents the weakest point where the onset of damage is generated. Once the damage occurs it always propagates along the fibre direction since the matrix and the shear strength represents the most critical strength when testing *CFRPs* material. When testing 0 degrees fibre orientation samples, the crack propagate along the fibre direction reaching the top of the sample where the fibre slipped from the jaws.

The results obtained from the initial tests cannot be accepted since the strength of the material is highly affected by the specimen geometry and the manufacturing process [11].

Suitable samples require a simple constant shape without any round features where the onset of damage could easily be generated and propagate.

To solve this problem it was decided to test the sample at the other end where a constant shape without curved geometry was available.

4.4 One Element Test

For a better understanding of the input parameters one element test simulations were performed (*Figure 44*).

EA = 1.289 GPa
EB = 1.289 GPa
v = 0.25
Xt = 2159 MPa
Xc = 1330 MPa
Yt = 49 MPa
Yc = 199 MPa
Sc = 154 MPa
Element length = 100 mm

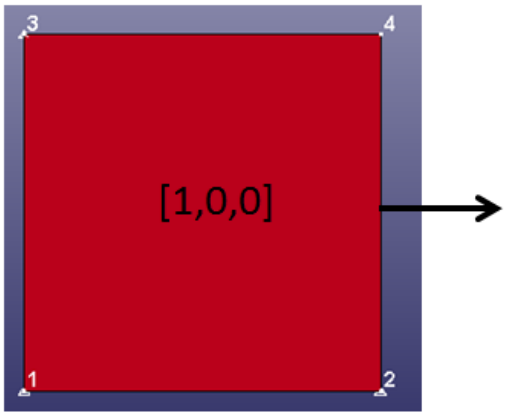

Figure 44: One element test

Node 1 is fully constrained in all directions while nodes 2 and 3 were left free to move respectively along the X and the Y directions. A displacement curve of 1.333 mm/ms (80 m/min) was applied to the node 2 and 4 along +X. In this configuration [1, 0, 0] being a traction applied along the fibre direction, the input parameters that control the stress-displacement curve are the longitudinal tensile strength (Xt=2159 MPa) and the strain limit of the fibre (DFAILT=0.02).

In *Figure 45* it is easy to notice that the stress of the element in the fibre direction increases until the longitudinal tensile strength value is reached. Then the stress remains constant until a strain of 2% is reached. The deletion of the element is managed by the strain limit which can be adjusted in the simulation to set linear elastic or elasto-plastic behaviour in the material. The same behaviour is observed along the matrix orientation.

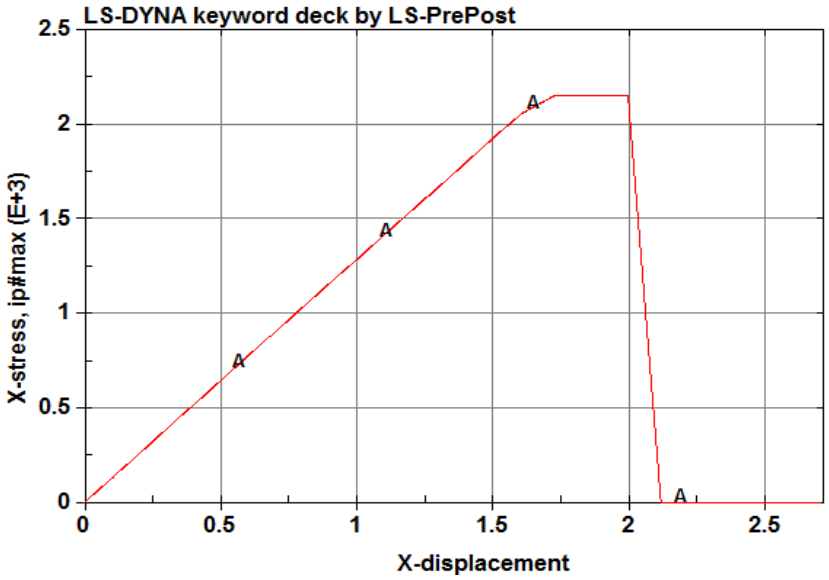

Figure 45: Stress-displacement curve.

The effect of the stress along the matrix direction can be considered through the parameters *FBRT* and *YCFAC*. Using *FBRT* the fibre tensile strength after matrix compressive failure can be reduced to $Xt^{*}=Xt * FBRT$. In the same way the fibre compressive strength after matrix compressive failure can be considered with the parameter: $Xc^{*}=Yc * YCFAC$.

4.5 FEM Results and Discussion

The outputs from the solver were imported in the postprocessor and analysed. The resultant forces were stored separately and needed to be imported in LS-Dyna through the "*ASCII*" option loading "*RCFORC*". Simulations with different fibre orientations were run to analyse the stresses, the strain and the cutting force values in X and Y direction. The forces along Z were checked and found to be zero validating the plane stress assumption.

The elastic material properties and the strengths of the material in the LS-Dyna material model were based on the dynamic tensile bar tests and according to the material properties in *Appendix A*.

In total, three fibre angle work-pieces were simulated at the following degrees: 0°, 45° and 90°.

In *Figure 46* an example of the predicted cutting forces is shown, when cutting 0 degrees fibre orientation work-piece. In the RCforc Data plot the principal cutting force and the feed force are respectively represented by the red (A) and the green (B) curves.

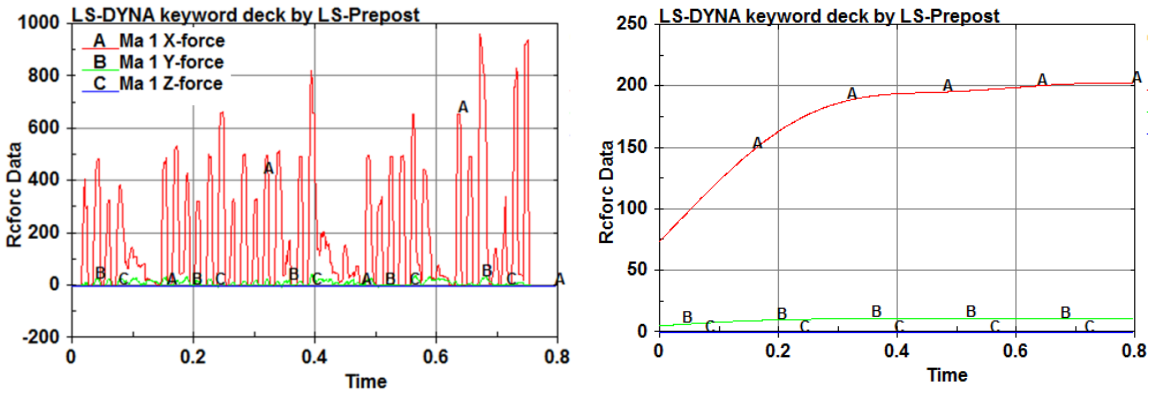

(a) (b)

Figure 46: Cutting force simulation results for 0° fibre orientation work-piece a) unfiltered b) filtered (SAE600).

The results achieved in the simulation were consistent with the results achieved by Krushnamoorthy et al [31] when an automatic contact surface is used and where the stresses in the elements grow till the failure criteria is met. Once the criterion is met the

elements are then deleted and the stresses drop to zero. A function SAE is chosen to filter the time-histories according to standard specifications SAE J211[32]. The SAE function implements a digital four-pole low pass filter. The algorithm uses a double-pass filtering option where the data is filtered twice, forward and then backward using the following equations where *X (t)* is the input data sequence and *Y (t)* is the filtered output sequence.

$$Y(t) = a_0 \cdot X(t) + a_1 \cdot X(t-1) + a_2 \cdot X(t-2) + b_1 \cdot Y(t-1) + b_2 \cdot Y(t-2) \quad (27)$$

The filter coefficients vary with the Channel Frequency Class (CFC) value and are calculated using the following formulas:

$$a_0 = \frac{\omega_a^2}{1 + \sqrt{2}\omega_a + \omega_a^2} \quad (28)$$

$$a_1 = 2a_0 \quad (29)$$

$$a_2 = a_0 \quad (30)$$

$$b_1 = \frac{-2\,(\omega_a^2 - 1)}{1 + \sqrt{2}\omega_a + \omega_a^2} \quad (31)$$

$$b_2 = \frac{-1 + \sqrt{2}\omega_a - \omega_a^2}{1 + \sqrt{2}\omega_a + \omega_a^2} \quad (32)$$

Where:

$$\omega_d = 2\pi * CFC * 2.0775 \quad (33)$$

$$\omega_a = \frac{\sin(\omega_a * T/2)}{\cos(\omega_a * T/2)} \quad (34)$$

The CFC was set equal to 600, as used by Krishnamoorthy et al [43]. In order to avoid the typical scatter at the beginning and at the end of the filtered time histories, a head and a tail are added to the original data sets consisting respectively of a simple

repetition of the first and last data value. Once the modified data sets are filtered the head and tail are deleted from the filtered curve.

In the current model a prediction of the principal cutting forces was achieved with an average accuracy of 18% while the thrust forces were highly underestimated (*Table 6* from *Appendix F*). This is mainly attributed to the bounce back phenomenon that is not described by the simulation [3], [12], [18], [19].

Table 6 Cutting forces: Tests vs. FEM simulation

Cutting Speed [m/min]	Feed Rate [mm/rev]	Forces [N]	Cutting Tests		FEM SAE600	
			0	45	0	45
80	0,05	Cf	80	60	58	41
		Ff	90	60	9	0
	0,1	Cf	130	90	106	66
		Ff	110	90	9	-3
	0,15	Cf	160	110	138	100
		Ff	115	70	8	-8
	0,2	Cf	200	140	203	121
		Ff	140	70	11,7	-13,9
40	0,05	Cf	90	57	62	45
		Ff	102	72	7	2
	0,1	Cf	130	-	114	69
		Ff	125	-	4	-5
	0,15	Cf	160	-	112	129
		Ff	140	-	13	10
	0,2	Cf	220	-	184	105
		Ff	150	-	13	-5

Figure 47 shows the prediction of the cutting forces for 0 degree fibre orientation tubes. The graph traces the evolution of the cutting forces according to the different cutting parameters; the trend of the forces corroborates with those in literature [6], [10]. The simulation results are generally underestimating the experimental cutting forces while the tendency of the forces in relation to the input parameters is correct and accurately described. The influence of the feed rates is linear and directly proportional to the cutting forces while the effects of cutting speed are negligible.

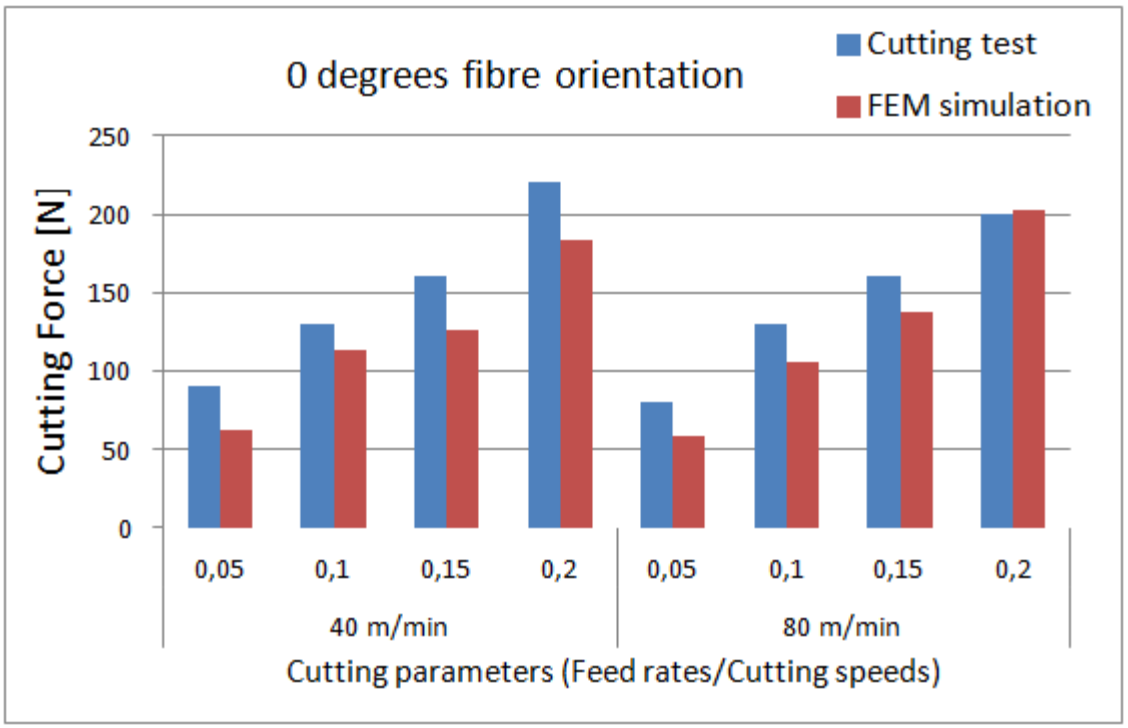

Figure 47: Cutting tests vs. FEM simulation
Cutting Forces when cutting 0 degrees fibre orientation work-piece

CHAPTER 5 **CONCLUSIONS**

The main aim of this study was to investigate the machinability of a *UD-CFRP* material under dynamic orthogonal cutting conditions. Representative cutting speeds and feeds were used to perform orthogonal turning operations; which enabled the use of a simplified analysis approach. As a result, a better understanding of how the process parameters affect the cutting forces was found. A second objective was to investigate the suitability of the Finite Element (FE) code LS-Dyna for predicting the force responses.

The complexities related to the *CFRPs* machining were highlighted during the experimental campaign were unidirectional tubes, oriented at 0°, 22.5°, 45°, 90°, 135° and 157.5°, were machined.

The orientation of the fibre in the *UD* lamina had proven to be the factor that mostly affects the machinability of composites. For this reason a good understanding of the chip formation mechanisms that take place in the micro-scale when cutting different fibre orientations is required. The dependency of the acquired cutting forces on the fibre orientation was accurately described in **chapter 3**.

Except when cutting work-piece having the fibres oriented at 157.5°, no significant effects are played by fibre orientation on the thrust forces. On the other hand the fibre orientation plays a significant role in determining the feed force values acquired after 30 seconds of cut.

Another key factor which had a significant effect on the machining forces was the feed rate, while minor effects were played by the cutting speed. A good repeatability was obtained during cutting trials.

Although *PCD* tools were used to withstand the high abrasiveness of the fibre, the absence of the stagnant zone when turning brittle material, as *CFRPs*, led to a rapid and gradual degradation of the cutting edge and to a reduction of its cutting capability. For this reason no steady state was reached by the cutting forces. However, it was observed that this phenomenon manly affects the thrust force. This was attributed to the fact that,

when cutting brittle materials fracture is the dominant failure mode, leading to the formation of a micro-wear which alters the tool cutting edge. This produces an increase of the contact surface between the insert and the work-piece. As a result the feed force rose gradually, while fibre pull out took place once the cutting edge was no longer able to cut the fibres neatly.

For all the tested fibre orientation a correlation between the thrust force increment and the phase of the resultant force ($\beta-\alpha$) was created. It was observed that while feed rate has a direct impact mainly on the magnitude of the resultant force, fibre orientation affects both its magnitude and direction.

A preliminary two dimensional macro-mechanic *FEM* analysis, using *EOHM* was developed in LS-Dyna to be compared with experimental results.

The trend of the principal cutting forces agreed with experimental results within a satisfactory level of accuracy while the thrust forces were highly underestimated. This underestimation could be attributed to the fact that the developed *FEM* model does not capture the elastic recovery of the material that takes place on the cut surface once the chip is formed. As a result of this bouncing back, a brushing action is generated between the relief face of the tool and the work-piece surface. The bouncing back phenomenon is therefore a key factor that determines the feed force values. Therefore, for an accurate prediction of both cutting force components, it is necessary to develop a model which has the capability to describe the elastic recovery after machining.

CHAPTER 6 **FUTURE WORK**

The complexities related to *CFRPs* machining were highlighted in this investigation. A basic understanding of the machinability aspects related to the *MTM 44-1* composite was developed. Due to the high number of factors involved in the cutting process and due to the complexities related to the topic, further studies are required to better relate machinability to fibre orientations, tooling and to cutting conditions.

It would be beneficial to extend the experimental campaign to study the effects that the rake angle has on the principal cutting forces as well as the effects the relief angle has on the feed forces. Moreover, the effects these cutting conditions have on chip formation mechanisms should be investigated.

Tool wear tests could be performed to identify tool life under give cutting conditions. This would provide information on how feed rate and cutting speed impact the tool life when cutting unidirectional work-piece at different fibre orientations.

Additional work is required to better relate the effects of the method of manufacturing to the structural integrity of *CFRP* material. Although surface roughness is the most often used method to characterise machined surfaces it is not sufficient to describe the surface integrity. Therefore the use of non-destructive tests along with a scanning electron microscope (SEM) is recommended to better investigate such aspects.

Further studies are required to correlate the increase in cutting forces with tool wear. Due to the high sharpness of *PCD* inserts, the use of high resolution optical measurement system, such as Alicona, is highly recommended. This would allow to capture the tool wear evolution and to relate it to the cutting forces increase. Such correlation could then be extended to the analysis of the cut surface in order to understand when fibre pull-out, cracking, delamination and burning occur. With the aid of a high speed camera this study could be extended to analyse the mechanisms of chip formation for different feed rates, cutting speeds, fibre orientations and tool wear.

The use of a thermal camera is also recommended to correlate cutting temperature with process parameters.

CHAPTER 6 **FUTURE WORK**

A further step would consists in extending the analysis to more realistic cutting conditions i.e. orthogonal milling, oblique milling, trimming, drilling, etc.

Being of more practical interest than unidirectional lamina, the machinability of multidirectional laminates should be investigated once the fundamental understanding of machining unidirectional composites is gained.

The current FE model is a basic set-up to demonstrate the capability of LS-Dyna to model the machinability of *CFRP* materials. Different optimizations could be performed as the use of different material models in LS-Dyna. The main limitation of this model is the prediction of the thrust force which is highly underestimated.

In the developed *FEM* model different coefficients of friction were not considered when modelling different fibre orientations. This should be implemented in future investigations. Tribological tests, such as pin on disc, should be performed using the examined *CFRP* material to support the modelling activity. A correlation between feed forces, coefficient of friction and tool wear should be investigated for different fibre orientation.

The material bouncing back was not described by the model and needs to be integrated in future work for a better modelling prediction. The use of a combined micro-macro mechanical approach, as the Cohesive Zone Model, is recommended to accurately describe material failure in close details. Given the capability of this approach to simulate the interface deboding between fibre and matrix, a prediction of the surface quality and the relative subsurface damage could be included. According to literature Abaqus is the most used and recommended software for this activity.

Other software as Third Wave Systems' AdvantEdge software should be examined to investigate software capability to simulate material removal cutting processes of *CFRP* materials.

Bibliography

[1] C. R. Dandekar and Y. C. Shin, "Modeling of machining of composite materials: A review," *International Journal of Machine Tools and Manufacture,* vol. 57, no. 0, pp. 102-121, 2012.

[2] J. Ferreira, N. Coppini and F. Levy Neto, "Characteristics of carbon–carbon composite turning," *Journal of Materials Processing Technology,* vol. 109, no. 1-2, pp. 65-71, 2001.

[3] J. Y. Sheikh-Ahmad, Machining of Polymer Composites, New York: Springer, 2009.

[4] ASM International Handbook Committee, Composites - Volume 21, ASM International, 2001.

[5] S. K. Mazumdar, Composites Manufacturing – Materials, Product and Process Engineering, Boca Raton: CRC Press LLC, 2002.

[6] L. Lasri, M. Nouari and M. El Mansori, "Modelling of chip separation in machining unidirectional FRP composites by stiffness degradation concept," *Composites Science and Technology,* vol. 69, no. 5, pp. 684-692, 2009.

[7] K. A. Calzada, "Modeling and interpretation of fiber orientation-based failure mechanisms in machining of carbon fiber-reinforced polymer composites," *Journal of Manufacturing Processes,* vol. 14, no. 2, pp. 141-149, 2012.

[8] M. V. Kini and A. Chincholkar, "Effect of machining parameters on surface roughness and material removal rate in finish turning of ±30° glass fibre reinforced polymer pipes," *Materials & Design,* vol. 31, no. 7, pp. 3590-3598, 2010.

Bibliography

[9] A. Sahraie Jahromi and B. Bahr, "An analytical method for predicting cutting forces in orthogonal machining of unidirectional composites," *Composites Science and Technology*, vol. 70, no. 16, pp. 2290-2297, 2010.

[10] L. Zhang, "Cutting composites: a discussion on mechanics modeling," *Journal of Materials Processing Technology*, vol. 209, no. 1, pp. 4548-4552, 2009.

[11] P. Ghidossi, M. El Mansori and F. Pierron, "Edge machining effects on the failure of polymer matrix composite coupons," *Composites Part A: Applied Science and Manufacturing*, vol. 35, no. 7-8, pp. 989-999, 2004.

[12] M. Ramulu, "Machining and surface integrity of fibre-reinforced plastic composites," *Sadhana*, vol. 22, no. 3, pp. 449-472, June 1997.

[13] J. Mackerle, "Finite-element analysis and simulation of machining: a bibliography (1976–1996)," *Journal of Materials Processing Technology*, vol. 89, no. 1-3, pp. 17-44, 1998.

[14] J. Mackerle, "Finite element analysis and simulation of machining: an addendum: A bibliography (1996–2002)," *International Journal of Machine Tools and Manufacture*, vol. 43, no. 1, pp. 103-114, 2003.

[15] M. C. Shaw, Metal Cutting Principles, Oxford: Oxford University Press, 2005.

[16] P. Ponces Camanho, "Failure criteria for fibre-reinforced polymer composites," 2002. [Online]. Available: http://paginas.fe.up.pt/~stpinho/teaching/feup/y0506/fcriteria.pdf. [Accessed 2014].

[17] A. Koplev, A. Lystrup and T. Vorm, "The cutting process, chips, and cutting forces in machining CFRP," *Composites*, vol. 14, no. 4, pp. 371-376, 10 1983.

Bibliography

[18] D. H. Wang, M. Ramulu and D. Arola, "Orthogonal cutting mechanisms of graphite/epoxy composite. Part II: multi-directional laminate," *International Journal of Machine Tools and Manufacture,* vol. 35, no. 12, pp. 1639-1648, 12 1995.

[19] X. M. Wang and L. Zhang, "An experimental investigation into the orthogonal cutting of unidirectional fibre reinforced plastics," *International Journal of Machine Tools and Manufacture,* vol. 43, no. 10, pp. 1015-1022, 2003.

[20] F. Mata, V. N. Gaitonde, S. R. Karnik and D. J. P., "Influence of cutting conditions on machinability aspects of PEEK, PEEK CF 30 and PEEK GF 30 composites using PCD tools," *Journal of Materials Processing Technology,* vol. 209, no. 4, pp. 1980-1987, 2009.

[21] D. Arola and M. Ramulu, "Orthogonal cutting of fiber-reinforced composites: A finite element analysis," *International Journal of Mechanical Sciences,* vol. 39, no. 5, pp. 597-613, 1997.

[22] D. Nayak, I. Singh, N. Bhatnagar and P. Mahajan, "An analysis of machining induced damages in FRP Composites – A micromechanics Finite Element Approach," *Materials Processing and Design: Modeling, Simulation and Applications,* pp. 327-331, 2004.

[23] R. Zitoune, F. Collombet and F. Lachaud, "Experiment–calculation comparison of the cutting conditions representative of the long fiber composite drilling phase," *Composites Science and Technology,* vol. 65, no. 3-4, pp. 455-466, 2005.

[24] J. Norman F. Knight, "User-Defined Material Model for Progressive Failure Analysis," NASA, Hampton, 2006.

[25] G. Venu Gopala Rao, P. Mahajan and N. Bhatnagar, "Micro-mechanical modeling of machining of FRP composites – Cutting force analysis," *Composites Science and Technology,* vol. 67, no. 3-4, pp. 579-593, 2007.

Bibliography

[26] G. Venu Gopala Rao, P. Mahajan and N. Bhatnagar, "Machining of UD-GFRP composites chip formation mechanism," *Composites Science and Technology,* vol. 67, no. 11-12, pp. 2271-2281, 2007.

[27] G. Venu Gopala Rao, P. Mahajan and N. Bhatnagar, "Three-dimensional macro-mechanical finite element model for machining of unidirectional-fiber reinforced polymer composites," *Materials Science and Engineering: A,* vol. 498, no. 1-2, pp. 142-149, 2008.

[28] A. Mkaddem, I. Demirci and M. El Mansori, "A micro–macro combined approach using FEM for modelling of machining of FRP composites: Cutting forces analysis," *Composites Science and Technology,* vol. 68, no. 15-16, pp. 3123-3127, 2008.

[29] A. Mkaddem and M. El Mansori, "Finite element analysis when machining UGF-reinforced PMCs plates: Chip formation, crack propagation and induced-damage," *Materials & Design,* vol. 30, no. 8, pp. 3295-3302, 2009.

[30] D. Iliescu, D. Gehin, I. Iordanoff, F. Girot and M. Gutierrez, "A discrete element method for the simulation of CFRP cutting," *Composites Science and Technology,* vol. 70, no. 1, pp. 73-80, 2010.

[31] C. Santiuste, X. Soldani and M. H. Miguelez, "Machining FEM model of long fiber composites for aeronautical components," *Composite Structures,* vol. 92, no. 3, pp. 691-698, 2010.

[32] R. Rentsch, O. Pecat and E. Brinksmeier, "Macro and micro process modeling of the cutting of carbon fiber reinforced plastics using FEM," *Procedia Engineering,* vol. 10, no. 0, pp. 1823-1828, 2011.

[33] M. El-Hofy, S. Soo, D. Aspinwall, W. Sim, D. Pearson and P. Harden, "Factors Affecting Workpiece Surface Integrity in Slotting of CFRP," *Procedia Engineering,* vol. 19, no. 0, pp. 94-99, 2011.

Bibliography

[34] Y. Karpat and N. Polat, "Mechanistic force modeling for milling of carbon fiber reinforced polymers with double helix tools," *Manufacturing Technology,* vol. 62, no. 1, pp. 95-98, 2013.

[35] R. Rentsch, O. Pecat and E. Brinksmeier, "Macro and micro process modeling of the cutting of carbon fiber reinforced plastics using FEM," *Procedia Engineering,* vol. 10, no. 0, pp. 1823-1828, 2011.

[36] O. Klinkova, J. Rech, S. Drapier and J.-M. Bergheau, "Characterization of friction properties at the workmaterial/cutting tool interface during the machining of randomly structured carbon fibers reinforced polymer with carbide tools under dry conditions," *Tribology International,* vol. 44, no. 12, pp. 2050-2058, 2011.

[37] A. Mondelin, B. Furet and J. Rech, "Tribology International," *Tribology International,* vol. 43, no. 9, pp. 1665-1673, 2010.

[38] D. Arola, M. Ramulu and D. Wang, "Chip formation in orthogonal trimming of graphite/epoxy composite," *Composites Part A: Applied Science and Manufacturing,* vol. 27, no. 2, pp. 121-133, 1996.

[39] D. Wang, M. Ramulu and D. Arola, "Orthogonal cutting mechanisms of graphite/epoxy composite. Part II: multi-directional laminate," *International Journal of Machine Tools and Manufacture,* vol. 35, no. 12, pp. 1639-1648, 1995.

[40] J. Donea, A. Huerta, J. Ponthot and A. Rodrıguez-Ferran, "Arbitrary Lagrangian–Eulerian Methods," in *Encyclopedia of Computational Mechanics*, Liege, John Wiley & Sons, 2004, pp. 1-25.

[41] U.S. Department of Transportation - Federal Aviation Administration, "Comparative Evaluation of Failure Analysis Methods for Compostes Laminates," Office of Aviation Research, Washington, 1996.

[42] P. Mohite, "Hashin Failure Criteria for Unidirectional Fiber Composites," Department of Aerospace Engineering, Kanpur, 2009.

Bibliography

[43] P. Feraboli, B. Wade, F. Deleo, M. Rassaian, M. Higgins and A. Byar, "LS-DYNA MAT54 modeling of the axial crushing of a composite tape sinusoidal specimen," *Composites Part A: Applied Science and Manufacturing,* vol. 42, no. 11, pp. 1809-1825, 2011.

[44] P. Holt and M. Horne, "Dust from carbon fibre," *Environmental Research,* vol. 17, no. 2, pp. 276-283, 1978.

[45] P. Philbin and S. Gordon, "Characterisation of the wear behaviour of polycrystalline diamond (PCD) tools when machining wood-based composites," *Journal of Materials Processing Technology,* Vols. 162-163, no. 0, pp. 665-672, 2005.

[46] C. Dold, M. Henerichs, L. Bochmann and K. Wegener, "Comparison of Ground and Laser Machined Polycrystalline Diamond (PCD) Tools in Cutting Carbon Fiber Reinforced Plastics (CFRP) for Aircraft Structures," *Procedia CIRP,* vol. 1, no. 0, pp. 178-183, 2012.

[47] K.-H. Park, A. Beal, D. (.-W. Kim, P. Kwon and J. Lantrip, "Tool wear in drilling of composite/titanium stacks using carbide and polycrystalline diamond tools," *Wear,* vol. 271, no. 11-12, pp. 2826-2835, 2011.

[48] X. Wang, P. Y. Kwon, C. Sturtevant, D. (.-W. Kim and J. Lantrip, "Tool wear of coated drills in drilling CFRP," *Journal of Manufacturing Processes,* vol. 15, no. 1, pp. 127-135, 2013.

[49] K. Nakayama, M. Arai and T. Kanda, "Machining Characteristics of Hard Materials," *CIRP Annuals - Manufacturing Technology,* vol. 37, no. 1, pp. 89-92, 1988.

[50] Livermore Software Technology Corporation, "LS-Dyna-Keyword User's Manual," Livermore Software Technology Corporation, Livermore, 2007.

Bibliography

[51] S. Charoenphan, L. C. Bank and M. E. Plesha, "Use of LS-DYNA shell elements in the analysis of composite plates with unbalanced and unsymmetric layups," [Online]. Available: http://www.dynalook.com/international-conf-2000/session8-4.pdf.

[52] K. Schweizerhof, K. Weimar, T. Munz and T. Tottner, "Crashworthiness Analysis with Enhanced Composite Material Models in LS Dyna – Merits and Limits," University of Karlsrube, Karlsrube.

[53] A. Koplev, A. Lystrup and T. Vorm, "The cutting process, chips, and cutting forces in machining CFRP," *Composites*, vol. 14, no. 4, pp. 371-376, 1983.

[54] K. Nakayama, M. Arai and T. Kanda, "Machining Characteristics of Hard Materials," *CIRP Annals - Manufacturing Technology,* vol. 37, no. 1, pp. 89-92, 1988.

Appendix A **UMECO MTM 44-1 Matrix Resin Data Sheet**

UMECO MTM®44-1
MATRIX RESIN

Product Description

MTM®44-1 is a high performance, toughened epoxy matrix system optimised for low pressure vacuum-bag Out-of-Autoclave (OoA) processing in both prepreg and film infusion formats. MTM44-1 can also be autoclave cured.

MTM44-1 can be cured in a single cycle. Following gelation at 130°C (266°F), the cure cycle can be continued to completion at 180°C (356°F). Alternatively, after an extended initial cure at 130°C (266°F), a free-standing post-cure can be carried out at 180°C (356°F).

Following a full 180°C (356°F) cure, MTM44-1 will exhibit a dry/wet Tg of 190°C (374°F)/150°C (302°F) and a high level of damage tolerance.

MTM44-1 offers low density, excellent Tg retention under wet conditions and a high level of damage tolerance, thus making it particularly suited to the production of both primary and secondary structures for aircraft.

Features

- 130°C (266°F) initial cure.
- Full properties achieved after a 180°C (356°F) post-cure.
- 21 days out life.
- Available in film format for resin film infusion (RFI) processing.
- Available in partially and selectively impregnated fabric formats for OoA vacuum processing.
- Available as fully impregnated unidirectional prepreg for OoA and autoclave processing.
- 190°C (374°F) dry Tg achieved after a 180°C (356°F) cure.
- 150°C (302°F) wet Tg achieved after a 180°C (356°F) cure.
- Excellent damage tolerance.
- HTA®240 fully compatible OoA adhesive film.
- Low density, providing at least a 3% weight saving when compared to standard aerospace matrices.

Umeco Structural Materials (Derby) Ltd.
Composites House, Sinclair Close,
Heanor Gate Industrial Estate,
Heanor, Derbyshire, DE75 7SP, UK
Telephone: +44 (0)1773 766200
Facsimile: +44 (0)1773 530245
Internet: www.umeco.com

PDS1189/03.12/7c

Registered Office
Registered No. 2264869 England

Instructions for Use

The prepreg should be removed from the freezer, thawed and allowed to reach room temperature before removal from the protective polythene bag.

The level of tack increases with temperature; the material is designed to have optimum tack for lay-up between 18°C and 24°C (64°F and 75°F).

Prepreg should be cut to shape using templates and laid up in accordance with design instructions. It is common practice to kit cut and re-freeze material to maximise its out life.

Care must be taken to ensure the prepreg conforms exactly to the tool shape, especially around internal corners.

Note:
MTM44-1 prepregs supplied for vacuum bag processing with woven and non-crimp fabric (NCF) reinforcements are delivered in a partially impregnated form.

Experience has shown that improved laminate surface quality is achieved when the prepreg is laminated with the drier side towards the mould.

During the lay-up process, the laminate stack should be debulked at regular intervals to ensure that the prepreg conforms exactly to the tool's shape, especially around internal corners, thus preventing bridging in corners and ensuring good consolidation over the entire surface area. The lay-up should be covered with a perforated release film (P3) plus a suitable breather and a low cost membrane and placed under vacuum for approximately 5 to 10 minutes. It is recommended that the lay-up is debulked every 3 or 4 plies.

Note:
Excessive debulking of woven or NCF formats can close air channels in the laminate stack. This can impede air release during final cure and could be detrimental to final laminate quality.

Recommended Bagging Arrangement

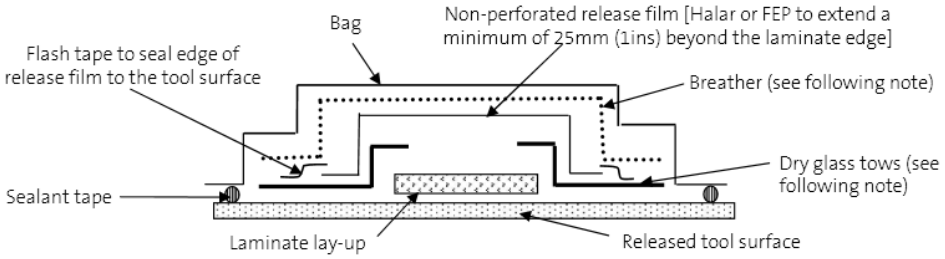

Glass Tows Detail
Placing dry glass tows at 0.5m (20in) intervals around the edge of the laminate will provide air paths under the release film and into the breather (depicted above).

It is recommended that dry fabric strips such as peel ply or glass are strategically placed around the periphery when laminating unidirectional (UD) material.

Release Film Detail
The release film may be taped down to the tool surface with flash tape.

Breather Detail
Apply one layer of heavyweight breather fabric over the entire lay-up. Extra plies may be fitted at valve positions. To prevent bridging in the curing laminate, special care should be taken to ensure that the breather is fitted well into corners.

The highest available vacuum, typically 980mbar (29in Hg), must be used during cure. Check vacuum integrity using a gauge positioned diametrically opposite to the position of the vacuum port.

A vacuum drop test should be performed prior to curing the part. The test must show no more than a 68mbar (2in Hg) pressure loss within 10 minutes after the vacuum is removed.

Exotherm

MTM44-1 is a reactive formulation which can undergo severe exothermic heat build up during the initial curing process if incorrect curing procedures are followed.

Great care must be taken to ensure that safe heating rates, dwell temperatures and lay-up/bagging procedures are adhered to, especially when moulding solid laminates in excess of 10mm (0.4in) thick. The risk of exotherm increases with lay-up thickness and increasing temperature. It is strongly recommended that the user carries out representative trials of all relevant circumstances to allow a safe cure cycle to be specified. It is also important to recognise that the model or tool material and its thermal mass, combined with the insulating effect of breather/bagging materials, can affect the risk of exotherm in particular cases.

If in doubt, contact the Group's technical support staff for advice on modified cure cycles for thick laminates, especially those greater than 10mm (0.4in) thick.

Umeco Structural Materials (Derby) Ltd.
Composites House, Sinclair Close,
Heanor Gate Industrial Estate,
Heanor, Derbyshire, DE75 7SP, UK
Telephone: +44 (0)1773 766200
Facsimile: +44 (0)1773 530245
Internet: www.umeco.com

PDS1189/03.12/7c

Registered Office
Registered No. 2264869 England

Initial Cure

	Vacuum Bag Processing*	Autoclave Processing
Ramp Rate	1 to 2°C/minute (1.8 to 3.6°F/minute)	1 to 2°C/minute (1.8 to 3.6°F/minute)
Pressure	N/A	3 to 7bar
Vacuum Pressure	>0.75bar	>0.75bar
Cure Time	2 hours dwell @ 130°C (266°F) + 2 hours @ 180°C (356°F) (no post-cure) * or 4 hours @ 130°C (266°F) + free-standing post-cure	4 hours @ 130°C (266°F) or 2 hours @180°C (356°F)

*Further information relating to vacuum bag processing can be found in Umeco technical data sheet TDS1012

Post-Cure

Components must be post-cured to develop the maximum Tg and mechanical properties. Following a 130°C (266°F) cure, the material will still be in a relatively low state of cure. To develop full mechanical performance, it is necessary to post-cure parts to 180°C (356°F).

- Parts may be loaded into a pre-heated oven or rapidly heated to 130°C (266°F).
- Heat from 130°C (266°F) at a rate of 0.3°C (0.55°F)/minute to 180°C (356°C).
- Maintain temperature at 180°C -0/+5°C (356°F -0/+9°F) for 2 hours -0/+30 minutes.
- Cool at a rate of 2°C (3.5°F)/minute to 70°C (158°F).

Note:
Large components should be adequately supported to avoid distortion.

Appendix A

UMECO MTM 44-1 Matrix Resin Data Sheet

Physical Properties

Resin Gel Time	140 minutes at 130°C (266°F)	
Viscosity	200 Pa.s at 80°C (176°F) 10 Pa.s at 130°C (266°F) 6 Pa.s at 140°C (284°F) 1.5 Pa.s at 160°C (320°F)	
Cured Resin Density	1.18 g/cm³	
Glass Transition Temperature (DMTA onset, SACMA)	Dry: 190°C (374°F) Wet**: 155°C (311°F) Skydrol**: 190°C (374°F)	
	Conditioning Environment	**% Moisture Content**
Moisture Pick-Up (cast resin)	@ 25°C (77°F)/60%RH	1.46% ± 0.01%
	@ 60°C (140°F)/60%RH	1.45% ± 0.05%
Moisture Pick-Up (MTM®44-1/M55J 32% resin weight)	@ 25°C (77°F)/60%RH	0.39% ± 0.02%
	@ 60°C (140°F)/60%RH	0.39% ± 0.01%

**14 days immersion at 70°C (158°F)

Mechanical Properties

All data for laminates cured to 180°C (356°F) for 2 hours.

Representative Mechanical Data for Aerospace Reinforcements: Oven Vacuum Bag Curing

Test	Test Method	145gsm 12k HTS5631 UD	268gsm 24k IMS5131 UD	283gsm 3k HTA5131 CF0604 5-HS Fabric
0° Tensile Modulus - GPa (msi)	D3039	128.9 (18.6)	174.6 (25.3)	62.6 (9)
0° Tensile Strength - MPa (ksi)	D3039	2159 (313)	2738 (397)	927 (134.4)
0° Compression Modulus - GPa (msi)	ASTM D695 (mod)	123.2 (17.8)	147.2 (21.3)	59.4 (8.6)
0° Compression Strength - MPa (ksi)	ASTM D695 (mod)	1330 (192.8)	1459 (211.5)	729 (105.7)
In-Plane Shear Modulus - GPa (msi)	D3518	4.11 (0.6)	3.60 (0.5)	3.98 (0.58)
In-Plane Shear Strength - MPa (ksi)	D3518	112.7 (16.3)	76 (11)	133 (19.3)
0° Flexural Modulus - GPa (msi)	CRAG	121.9 (17.7)	154.9 (22.4)	57.1 (8.2)
0° Flexural Strength - MPa (ksi)	200	1958 (238.9)	1874 (271.7)	1181 (171.2)
0° ILSS - MPa (ksi)	D2344	106.6 (15.4)	109.4 (15.8)	75.4 (10.9)

Mechanical testing using ASTM test methods, except flexurals.
Unidirectional data normalised to 60% Vf, and fabric data to 55% Vf.
All data for room temperature/dry test condition for laminates cured to 180°C (356°F).

Umeco Structural Materials (Derby) Ltd.
Composites House, Sinclair Close,
Heanor Gate Industrial Estate,
Heanor, Derbyshire, DE75 7SP, UK
Telephone: +44 (0)1773 766200
Facsimile: +44 (0)1773 530245
Internet: www.umeco.com

PDS1189/03.12/7c

Registered Office
Registered No. 2264869 England

Appendix A

UMECO MTM 44-1 Matrix Resin Data Sheet

Hot/Wet Laminate Performance

Test	Test/Condition	Stitched NCF HTS5631 UD	134gsm 12k HTS5631 UD	285gsm 6k HTA5131 2x2 Twill Fabric
0° ILSS MPa (ksi)	Room Temperature/Dry	96 (13.9)	94 (13.6)	69 (10)
	120°C (248°F)/Dry	68 (9.86)	58 (8.4)	48 (6.9)
	120°C (248°F)/Wet	50 (7.25)	50 (7.25)	39 (5.6)

Mechanical testing using EN2563 test method.
Wet = Equilibrium at 70°C (158°F)/85% R.H.

Representative Open Hole Compression Strength

Test	Test/Condition	134gsm 12k HTS5631 UD	268gsm 24k IMS5131 UD	285gsm 6k HTA5131 2x2 Twill Fabric
OHC (MPa) – Quasi-isotropic	Room Temperature/dry	311	304	319

Unidirectional data normalised to 60% Vf, and fabric data to 55% Vf.

Compression Strength after Impact (CSAI) Data

Test	Test/Condition	32-ply 145gsm 12k HTS5631 UD	16-ply 268gsm 24k IMS5131 UD	16-ply 283gsm 3k HTA5131 CF0604 5-HS Fabric
CSAI (MPa) – Quasi-isotropic	Room Temperature/dry	259 (32 J)	247 (28 J)	329 (33.5 J)

Mechanical testing using SRM 2R-94 test method, with an impact of 6.7J/mm (Joules per mm thickness of laminate).
Unidirectional data normalised to 60% Vf, and fabric data to 55% Vf.
(J) = Actual impact energy for test laminate.

Outgassing Data:

MTM44-1/M55J, 32% Rw, Cure 2 hours at 180°C (356°F)

Total Mass Loss (TML) %	Recovered Mass Loss (RML) %	Water Vapour Release (WVR) %	Collected Volatile Condensable Material (CVCM) %
0.307	0.056	0.251	0.002
Test Method ECSS-Q-ST-70-02C			

PDS1189/03.12/7c

Appendix A

UMECO MTM 44-1 Matrix Resin Data Sheet

Out Life and Storage

Storage at -18°C (0°F)	12 months
Out life at 21°C (70°F)	21 days

When not in use, MTM44-1 prepregs should be stored in a sealed polyethylene bag in a freezer. When material is removed from the freezer, it is essential that the roll be allowed to thaw and reach room temperature before the bag is opened. For example, the thaw time for a 15Kg (35lb) roll taken from -18°C (0°F) storage into a 21°C (70°F) room is typically between 4 and 6 hours. Unless the material is fully thawed, condensation may form on the surface. Moisture within a curing laminate may be detrimental to final part quality and appearance.

When materials are returned to the freezer they must be resealed to prevent ingress of moisture.

Health and Safety

MTM44-1 contains epoxy resin which can cause allergic reactions by skin contact. Avoid prolonged or repeated skin contact. Gloves and protective clothing must be worn.

Wash the skin thoroughly with soap and water or resin removing cream after handling. Do not use solvents for cleaning the skin.

Use mechanical exhaust ventilation when heat curing the resin system.

For further information, consult ACM (Material) Safety Data Sheet.
(M)SDS 413

Umeco Structural Materials (Derby) Ltd.
Composites House, Sinclair Close,
Heanor Gate Industrial Estate,
Heanor, Derbyshire, DE75 7SP, UK
Telephone: +44 (0)1773 766200
Facsimile: +44 (0)1773 530245
Internet: www.umeco.com

PDS1189/03.12/7c

Registered Office
Registered No. 2264869 England

Appendix B **Sandvik Coromant Inserts Code-Key**

GENERAL TURNING Inserts –Code Key

Inserts for general turning

Inserts, metric

C	N	M	G	12	04	08	–			–	PF
1	2	3	4	5	6	7		8	9		12

Inserts, inch

C	N	M	G	4	3	2	–			–	PF
1	2	3	4	5	6	7		8	9		12

Inserts, advanced cutting materials, metric

C	N	M	G	12	04	08	–	T	010	20
1	2	3	4	5	6	7		8	10	11

Inserts, advanced cutting materials, inch

C	N	G	A	4	3	2	–	T	03	20
1	2	3	4	5	6	7		8	10	11

1 Insert shape

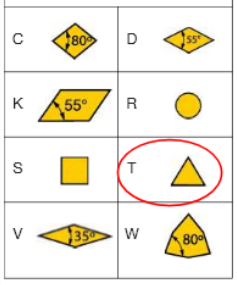

2 Insert clearance angle

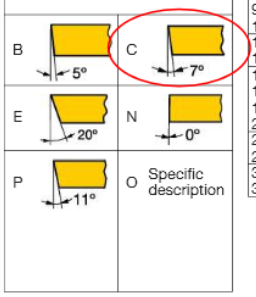

3 Tolerances, metric

Class	*s*	*iC* / *iW*
G	±0.13	±0.025
M	±0.13	±0.05 –±0.15[1]
U	±0.13	±0.08 –±0.25[1]
E	±0.025	±0.025

[1] Varies depending on the size of *iC*. See below.

Inscribed circle *iC* mm	Tolerance class M	U
3.97 5.0 5.56 6.0 6.35 8.0 9.525 10.0	±0.05	±0.08
12.0 12.7	±0.08	±0.13
15.875 16.0 19.05 20.0	±0.10	±0.18
25.0 25.4	±0.13	±0.25
31.75 32.0	±0.15	±0.25

3 Tolerances, inch

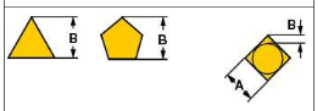

A: Theoretical diameter of the insert
T: Thickness of the insert.
B: See figures.

Tolerances in inch

Clas	B:	A:	T:
A	±.0002	±.001	±.001
B	.0002	.001	.005
C	.0005	.001	.001
D	.0005	.001	.005
E	.001	.001	.001
F	.0002	.0005	.001
G	.001	.001	.005
H	.0005	.0005	.001
J	.0002	.002-.005	.001
K	.0005	.002-.005	.001
L	.001	.002-.005	.001
M	.002-.005	.002-.005	.005
U	.005-.012	.005-.010	.005
N	.002-.010	.002-.004	.001

A 16

SANDVIK Coromant

Appendix B

Sandvik Coromant Inserts Code-Key

Inserts for general turning

4 Insert type

A		Q	
G		R	
M		T	
N		W	
P		X	Special design

5 Insert size

Inscribed circle, inch

R S T W

Inscribed circle is indicated in 1/8".

Cutting edge length, metric

iC mm	*iC* inch	C	D	R	S	T	V	W	K
3.18	1/8"					05			
3.97	5/32"					06			
5.0				05					
9.525	3/8"					09			
6.0			06						
6.35	1/4"	06	07			11	11		
8.0				08					
9.525	3/8"	09	11	09	09	16	16	06	16[3]
10.0				10					
12.0				12					
12.7	1/2"	12	15	12	12	22	22	08	
15.875	5/8"	16		15	15	27			
16.0				16					
19.05	3/4"	19		19	19	33			
20.0				20					
25.0				25[1]					
25.4	1"	25		25[2]	25				
31.75	1/4"			31					
32				32					

[3] For insert shape K (KNMX, KNUX) only the theoretical cutting edge length is indicated.
[1] Metric base design
[2] Inch base design

6 Insert thickness, *s* mm, inch

Metric			Inch		
01	s =	1.59	1.	s =	.0625
T1	s =	1.98	(1.2)	s =	.075
02	s =	2.38	(1.5)	s =	3/32
03	s =	3.18	2	s =	1/8
T3	s =	3.97	(2.5)	s =	5/32
04	s =	4.76	3	s =	3/16
05	s =	5.56	4	s =	1/4
06	s =	6.35	5	s =	5/16
07	s =	7.94	6	s =	3/8
09	s =	9.52	6.3	s =	.394
10	s =	10.00	7.6	s =	.475
12	s =	12.00			

7 Nose radius, r_ε mm, inch

Metric:	Inch:	Actual
00 = 0	00	Round
01 = 0.1	03	.004
02 = 0.2	0	.008
04 = 0.4	1 = 1/64	.0156
05 = 0.5		
08 = 0.8	2 = 1/32	.0312
10 = 1.0		
12 = 1.2	3 = 3/64	.047
15 = 1.5		
16 = 1.6	4 = 1/16	.0625
24 = 2.4	6 = 3/32	.094
32 = 3.2	8 = 1/8	.125

Note: See example for approximation of metric nose radius. 16=1.6mm=.063≈ .0625

8 Cutting edge condition

F	Sharp cutting edge
A	ER treated cutting edge
E	ER treated cutting edge
T	Negative land
K	Double negative lands
S	Negative land and ER treated

9 Hand of tool

R	Feed	
L	Feed	
N	Feed	Feed

10 Chamfer width metric, inch

$b_{\gamma n}$

Metric:

010	bγn = 0.10
025	bγn = 0.25
070	bγn = 0.70
150	bγn = 1.50
200	bγn = 2.00

Inch:

03	bγn = .003
08	bγn = .008
30	bγn = .030
60	bγn = .060
80	bγn = .080

For more information, see code key on page A66

11 Chamfer angle

γ_n

15 γn = 15°
20 γn = 20°

12 Manufacturer's option

The ISO code consists of nine symbols including 8 and 9 which are used only when required. In addition the manufacturer may add further three symbols e. g.

- WF = Wiper – finishing
- WMX = Wiper, medium machining
- PF = ISO P – finishing
- PR = ISO P – roughing

Appendix B

Sandvik Coromant Inserts Code-Key

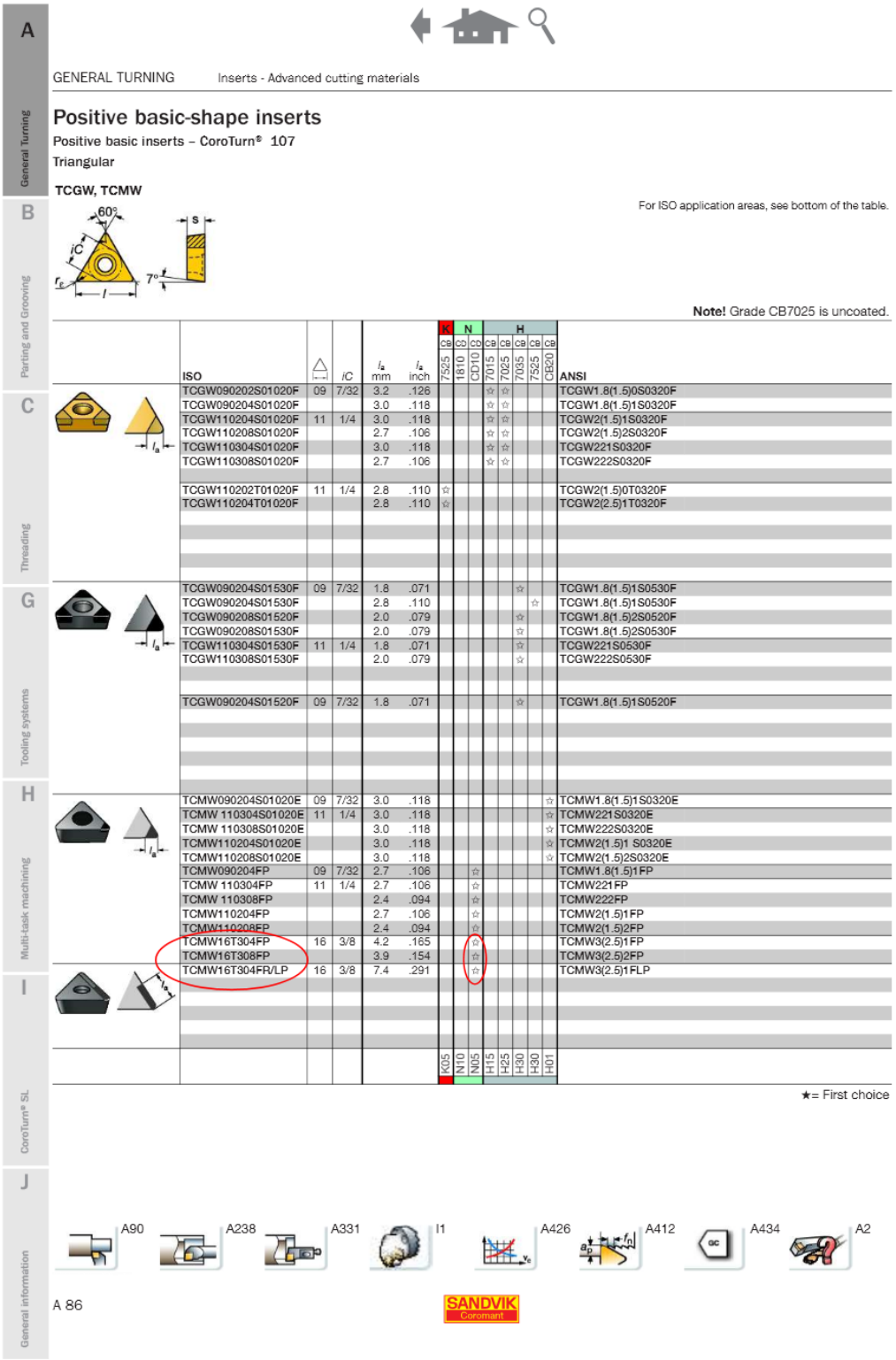

A

General Turning

GENERAL TURNING Inserts - Advanced cutting materials

Positive basic-shape inserts

Positive basic inserts – CoroTurn® 107

Triangular

TCGW, TCMW

For ISO application areas, see bottom of the table.

Note! Grade CB7025 is uncoated.

ISO		iC	l_e mm	l_e inch	K CB 7525	N CB 1810	N CD CD10	H CB 7015	H CB 7025	H CB 7035	H CB 7525	H CB CB20	ANSI
TCGW090202S01020F	09	7/32	3.2	.126				☆	☆				TCGW1.8(1.5)0S0320F
TCGW090204S01020F			3.0	.118				☆	☆				TCGW1.8(1.5)1S0320F
TCGW110204S01020F	11	1/4	3.0	.118				☆	☆				TCGW2(1.5)1S0320F
TCGW110208S01020F			2.7	.106				☆	☆				TCGW2(1.5)2S0320F
TCGW110304S01020F			3.0	.118				☆	☆				TCGW221S0320F
TCGW110308S01020F			2.7	.106				☆	☆				TCGW222S0320F
TCGW110202T01020F	11	1/4	2.8	.110	☆								TCGW2(1.5)0T0320F
TCGW110204T01020F			2.8	.110	☆								TCGW2(2.5)1T0320F
TCGW090204S01530F	09	7/32	1.8	.071						☆			TCGW1.8(1.5)1S0530F
TCGW090204S01530F			2.8	.110							☆		TCGW1.8(1.5)1S0530F
TCGW090208S01520F			2.0	.079						☆			TCGW1.8(1.5)2S0520F
TCGW090208S01530F			2.0	.079						☆			TCGW1.8(1.5)2S0530F
TCGW110304S01530F	11	1/4	1.8	.071						☆			TCGW221S0530F
TCGW110308S01530F			2.0	.079						☆			TCGW222S0530F
TCGW090204S01520F	09	7/32	1.8	.071						☆			TCGW1.8(1.5)1S0520F
TCMW090204S01020E	09	7/32	3.0	.118								☆	TCMW1.8(1.5)1S0320E
TCMW 110304S01020E	11	1/4	3.0	.118								☆	TCMW221S0320E
TCMW 110308S01020E			3.0	.118								☆	TCMW222S0320E
TCMW110204S01020E			3.0	.118								☆	TCMW2(1.5)1 S0320E
TCMW110208S01020E			3.0	.118								☆	TCMW2(1.5)2S0320E
TCMW090204FP	09	7/32	2.7	.106			☆						TCMW1.8(1.5)1FP
TCMW 110304FP	11	1/4	2.7	.106			☆						TCMW221FP
TCMW 110308FP			2.4	.094			☆						TCMW222FP
TCMW110204FP			2.7	.106			☆						TCMW2(1.5)1FP
TCMW110208FP			2.4	.094			☆						TCMW2(1.5)2FP
TCMW16T304FP	16	3/8	4.2	.165			☆						TCMW3(2.5)1FP
TCMW16T308FP			3.9	.154			☆						TCMW3(2.5)2FP
TCMW16T304FR/LP	16	3/8	7.4	.291			☆						TCMW3(2.5)1FLP

K05	N10	N05	H15	H25	H30	H30	H01

★= First choice

A90 A238 A331 I1 A426 A412 A434 A2

SANDVIK Coromant

Appendix C **Cutting Trials Factorial Design Results**

PHASE 1

Factorial Design

General Factorial Design

Factors: 2 Factor Levels: 4, 2
Runs: 16 Replicates: 2

Cutting trials data acquisition

feed	Vc	trial	Cf	Ff
[mm/rev]	[m/min]		[N]	[N]
0.05	40	1	91	111
0.05	80	1	85	98
0.1	40	1	130	132
0.1	80	1	135	119
0.15	40	1	178	140
0.15	80	1	172	125
0.2	40	1	219	143
0.2	80	1	216	176
0.05	40	2	86	108
0.05	80	2	87	97
0.1	40	2	136	125
0.1	80	2	136	116
0.15	40	2	185	135
0.15	80	2	177	131
0.2	40	2	233	144
0.2	80	2	218	138

Appendix C

Cutting Trials Factorial Design Results

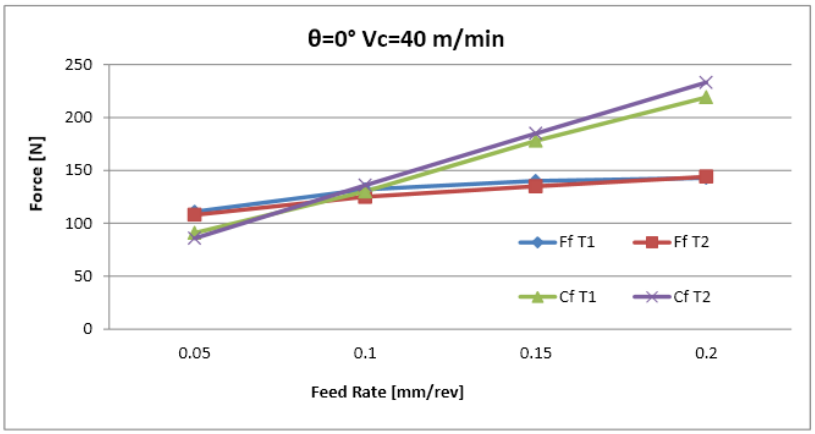

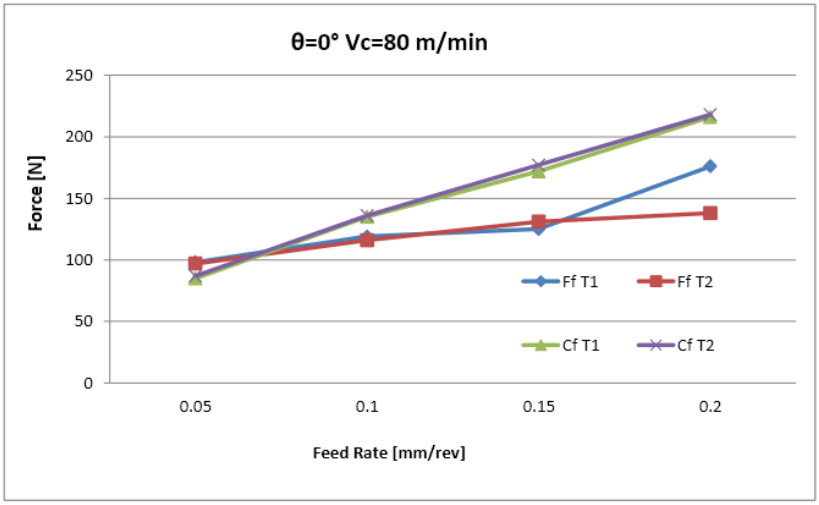

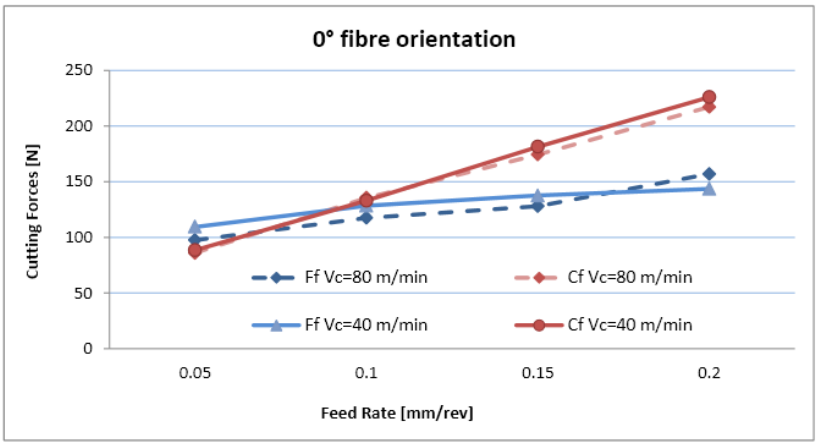

Appendix C

Cutting Trials Factorial Design Results

Variable	N	Mean	Median	TrMean	StDev	SE Mean
Cf	16	155.2	154.0	154.7	51.7	12.9
Ff	16	127.34	128.00	126.04	19.80	4.95
R	16	201.9	198.9	201.5	50.9	12.7

Variable	Minimum	Maximum	Q1	Q3
Cf	85.0	233.0	100.8	208.1
Ff	97.00	176.00	112.25	139.50
R	129.7	278.6	152.3	250.6

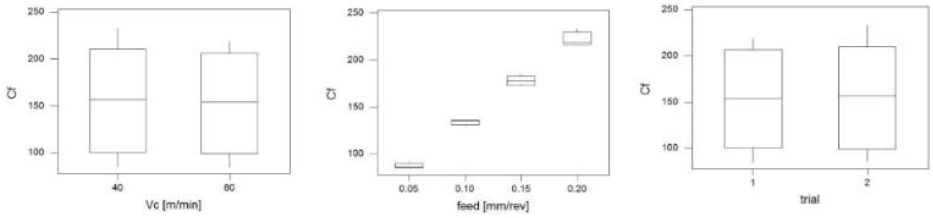

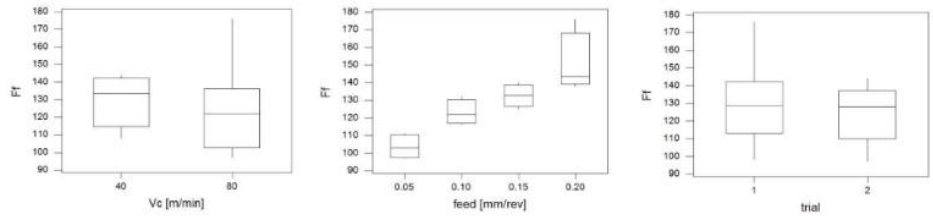

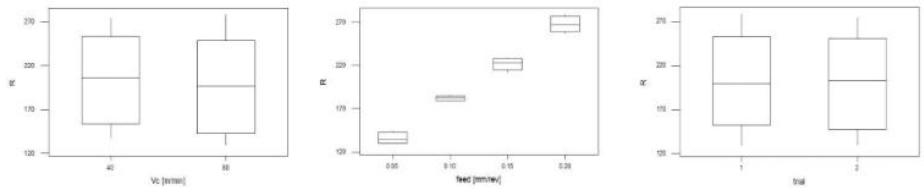

Appendix C

Cutting Trials Factorial Design Results

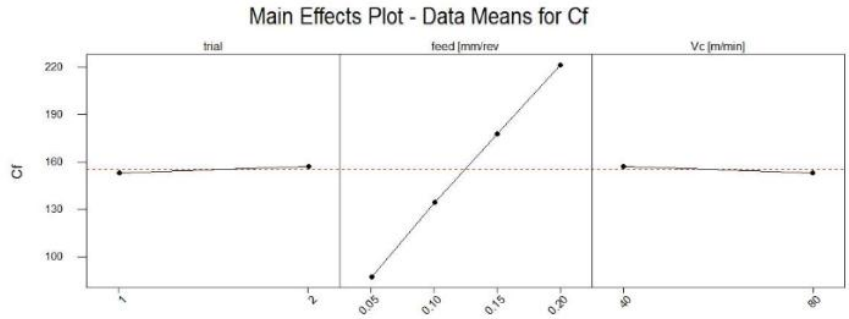

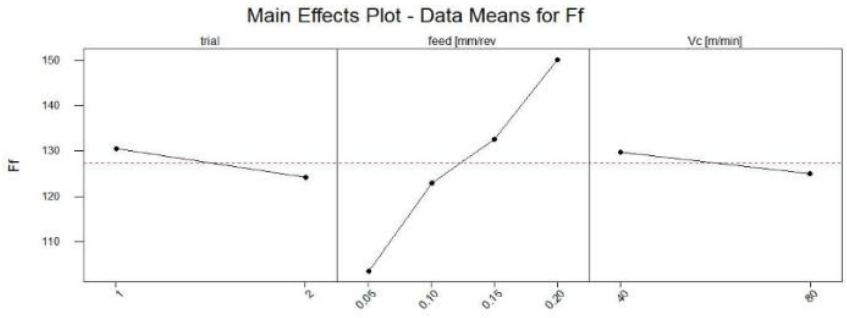

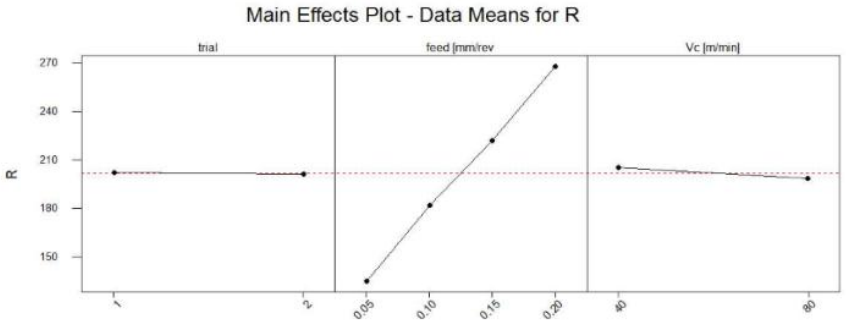

Appendix C

Cutting Trials Factorial Design Results

PHASE 2

θ	Feed	Thrust Force		Cutting Force		Resultant force	
[°]	[mm/rev]	[N]		[N]		[N]	
		1-3 sec	30 sec	1-3 sec	30 sec	1-3 sec	30 sec
0°	0.05	90	140	80	95	120	169
	0.1	110	170	130	140	170	220
	0.15	115	170	160	170	197	240
	0.2	140	165	200	220	244	275
22.5°	0.05	95	225	60	90	112	242
	0.1	120	250	105	125	159	280
	0.15	120	250	140	150	184	292
	0.2	125	250	175	190	215	314
45°	0.05	60	225	60	100	85	246
	0.1	90	180	90	140	127	228
	0.15	70	155	110	130	130	202
	0.2	70	125	140	140	157	188
90°	0.05	75	95	145	145	163	173
	0.1	80	90	270	270	282	285
	0.15	80	100	275	275	286	293
	0.2	100	110	280	270	297	292
135°	0.05	NA	NA	NA	NA	NA	NA
	0.1	NA	NA	NA	NA	NA	NA
	0.15	NA	NA	NA	NA	NA	NA
	0.2	NA	NA	NA	NA	NA	NA
157.5°	0.05	10	35	40	40	41	53
	0.1	20	35	67	67	70	76
	0.15	20	35	95	95	97	101
	0.2	30	30	120	120	124	124

Appendix C

Cutting Trials Factorial Design Results

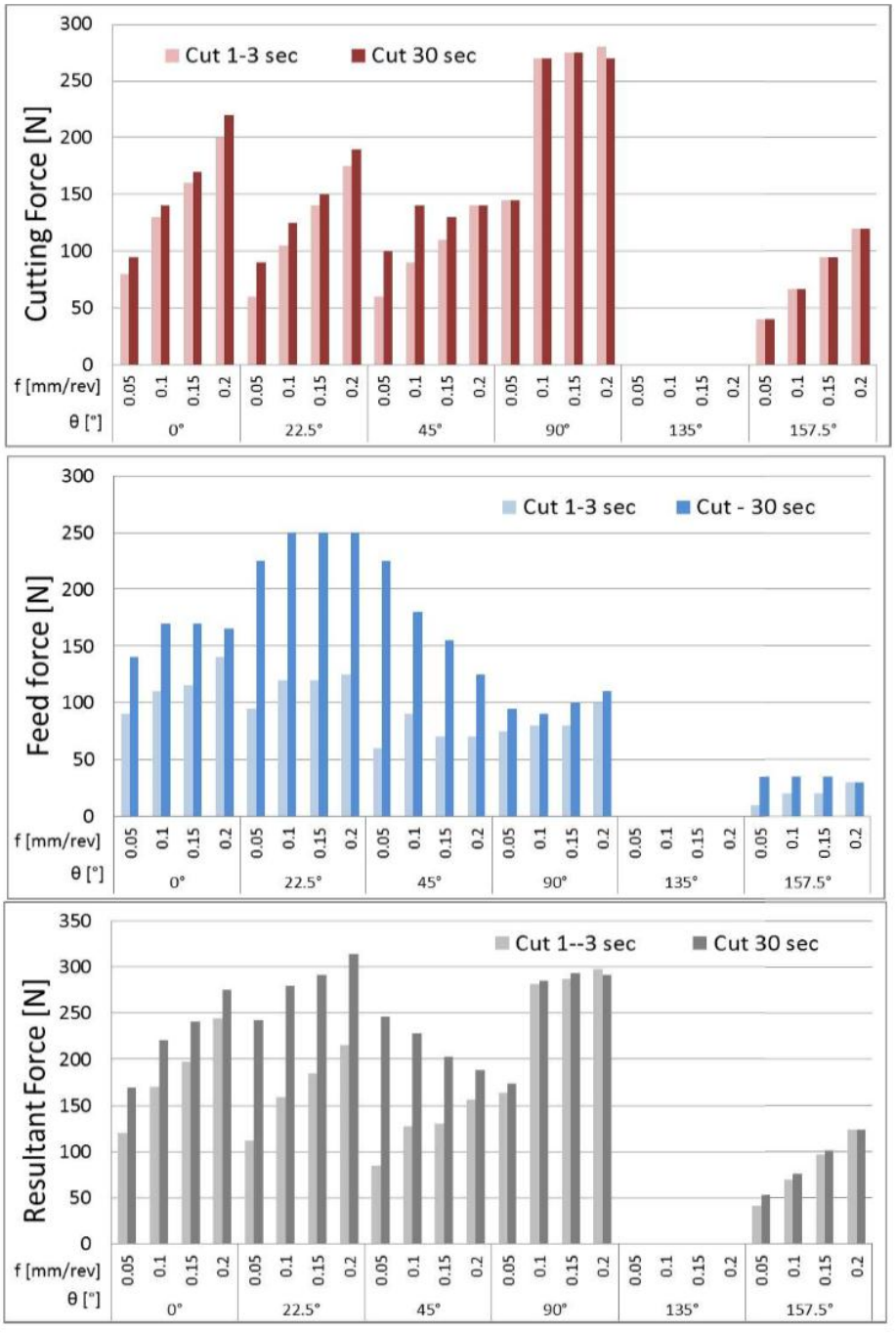

Appendix C

Cutting Trials Factorial Design Results

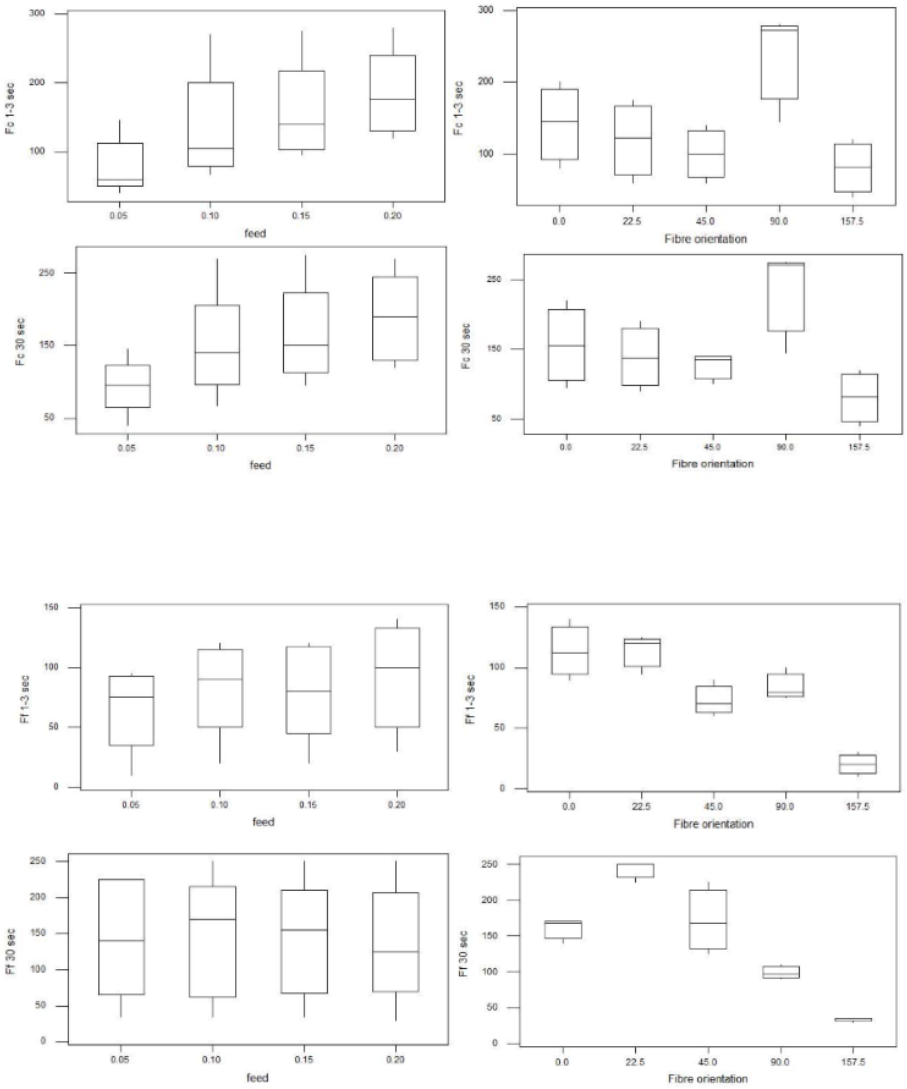

Appendix C

Cutting Trials Factorial Design Results

Feed	θ	Thrust Force		Cutting Force		Resultant force	
[mm/rev]	[°]	[N]		[N]		[N]	
		1-3 sec	30 sec	1-3 sec	30 sec	1-3 sec	30 sec
0.05	0°	90	140	80	95	120	169
	22.5°	95	225	60	90	112	242
	45°	60	225	60	100	85	246
	90°	75	95	145	145	163	173
	135°	NA	NA	NA	NA	#VALUE!	#VALUE!
	157.5°	10	35	40	40	41	53
0.1	0°	110	170	130	140	170	220
	22.5°	120	250	105	125	159	280
	45°	90	180	90	140	127	228
	90°	80	90	270	270	282	285
	135°	NA	NA	NA	NA	#VALUE!	#VALUE!
	157.5°	20	35	67	67	70	76
0.15	0°	115	170	160	170	197	240
	22.5°	120	250	140	150	184	292
	45°	70	155	110	130	130	202
	90°	80	100	275	275	286	293
	135°	NA	NA	NA	NA	#VALUE!	#VALUE!
	157.5°	20	35	95	95	97	101
0.2	0°	140	165	200	220	244	275
	22.5°	125	250	175	190	215	314
	45°	70	125	140	140	157	188
	90°	100	110	280	270	297	292
	135°	NA	NA	NA	NA	#VALUE!	#VALUE!
	157.5°	30	30	120	120	124	124

Appendix C

Cutting Trials Factorial Design Results

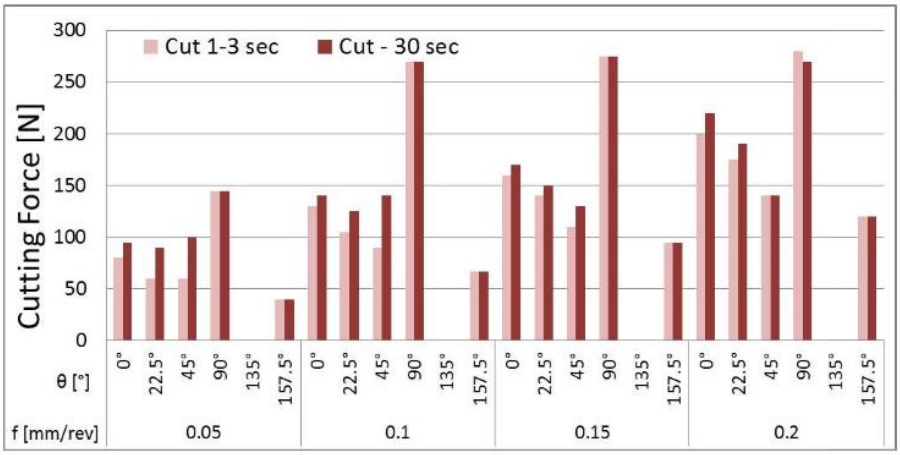

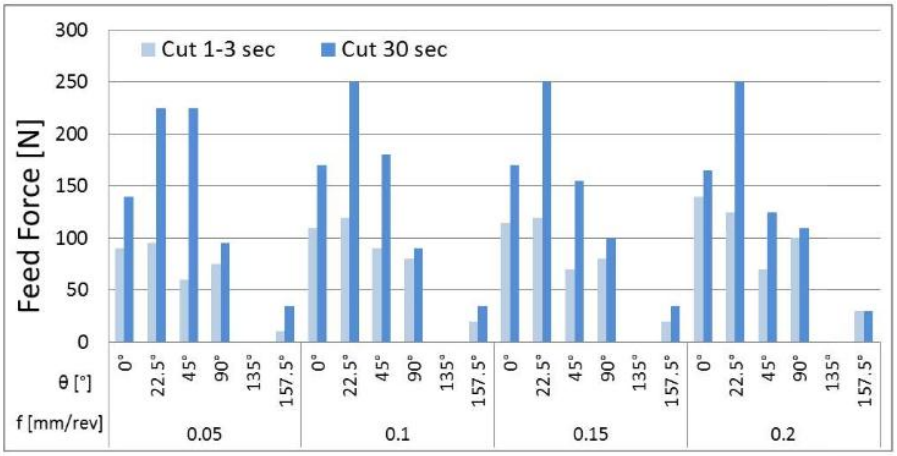

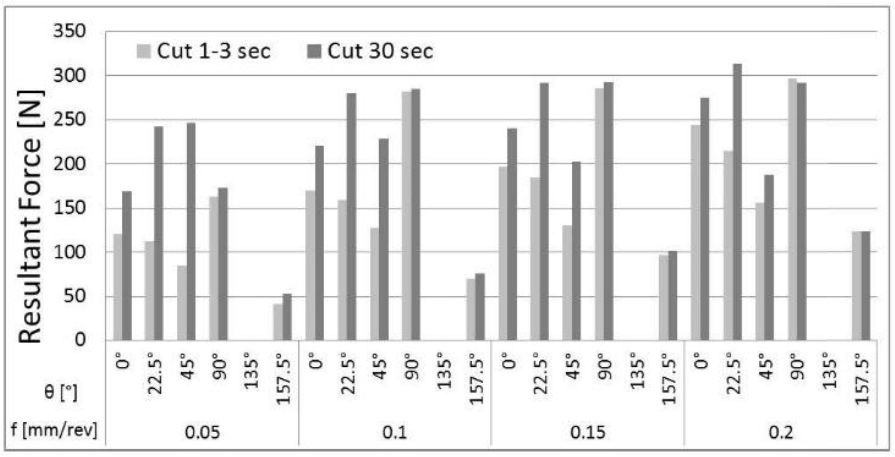

Appendix C

Cutting Trials Factorial Design Results

Geometrical considerations on resultant force direction

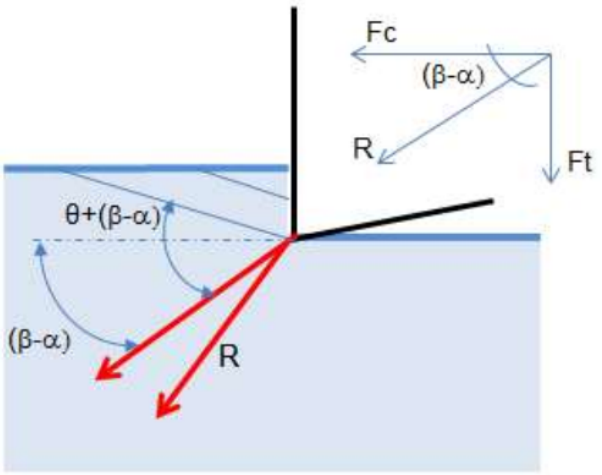

		Tool wear condition			
	[s]	1-3		30	
θ	[°]	0		0	
f	[mm/rev]	0.05	0.2	0.05	0.2
β-α	[°]	48	35	0	0
θ+(β−α)	[°]	48	35	0	0
θ	[°]	22.5		22.5	
f	[mm/rev]	0.05	0.2	0.05	0.2
β-α	[°]	0	0	0	0
θ+(β−α)	[°]	23	23	23	23
θ	[°]	45		45	
f	[mm/rev]	0.05	0.2	0.05	0.2
β-α	[°]	0	0	0	0
θ+(β−α)	[°]	45	45	45	45
θ	[°]	90		90	
f	[mm/rev]	0.05	0.15	0	0.1
β-α	[°]	0	16	0	0
θ+(β−α)	[°]	90	106	90	90
θ	[°]	157.5		157.5	
f	[mm/rev]	0.1	0.15	0.05	0.2
β-α	[°]	17	12	0	0
θ+(β−α)	[°]	-6	-11	-23	-23

Appendix C

Cutting Trials Factorial Design Results

(β–α) [°]				
Cut. time	**1-3 sec**		**30 sec**	
θ	**min**	**max**	**min**	**max**
0°	48	35	56	37
22.5°	58	36	68	53
45°	45	27	66	42
90°	27	16	33	18
157.5°	17	12	41	14

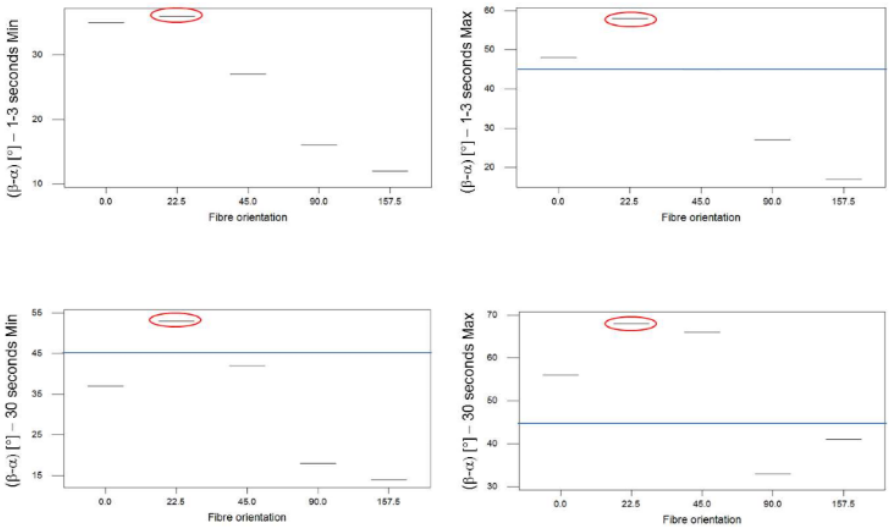

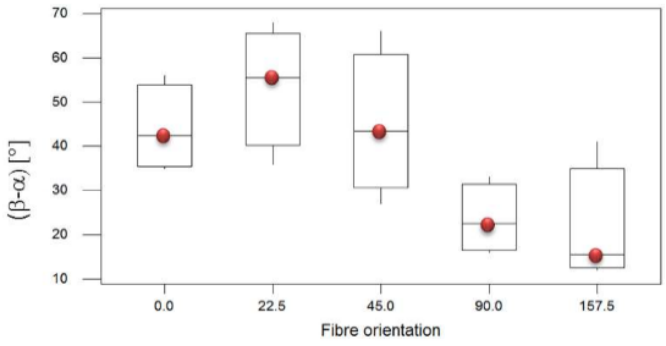

θ	Feed	Thrust Force		
[°]	[mm/rev]	[N]		
		1-3 sec	30 sec	Δ
0°	0.05	90	140	50
	0.1	110	170	60
	0.15	115	170	55
	0.2	140	165	25
22.5°	0.05	95	225	130
	0.1	120	250	130
	0.15	120	250	130
	0.2	125	250	125
45°	0.05	60	225	165
	0.1	90	180	90
	0.15	70	155	85
	0.2	70	125	55
90°	0.05	75	95	20
	0.1	80	90	10
	0.15	80	100	20
	0.2	100	110	10
135°	0.05	NA	NA	#VALUE!
	0.1	NA	NA	#VALUE!
	0.15	NA	NA	#VALUE!
	0.2	NA	NA	#VALUE!
157.5°	0.05	10	35	25
	0.1	20	35	15
	0.15	20	35	15
	0.2	30	30	0

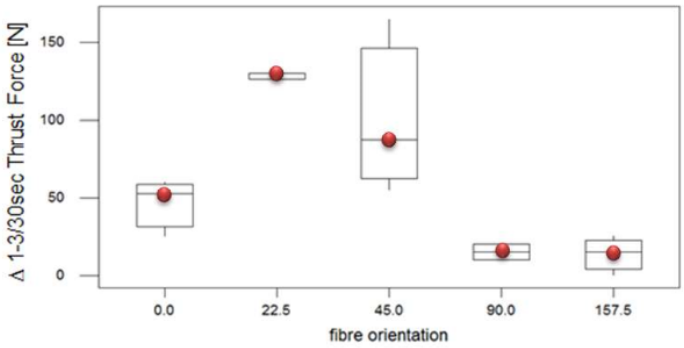

Appendix D

Specimen Engineering Drawing

Appendix D **Specimen Engineering Drawing**

Recommended Specimen for VHS Fast Jaw Grips

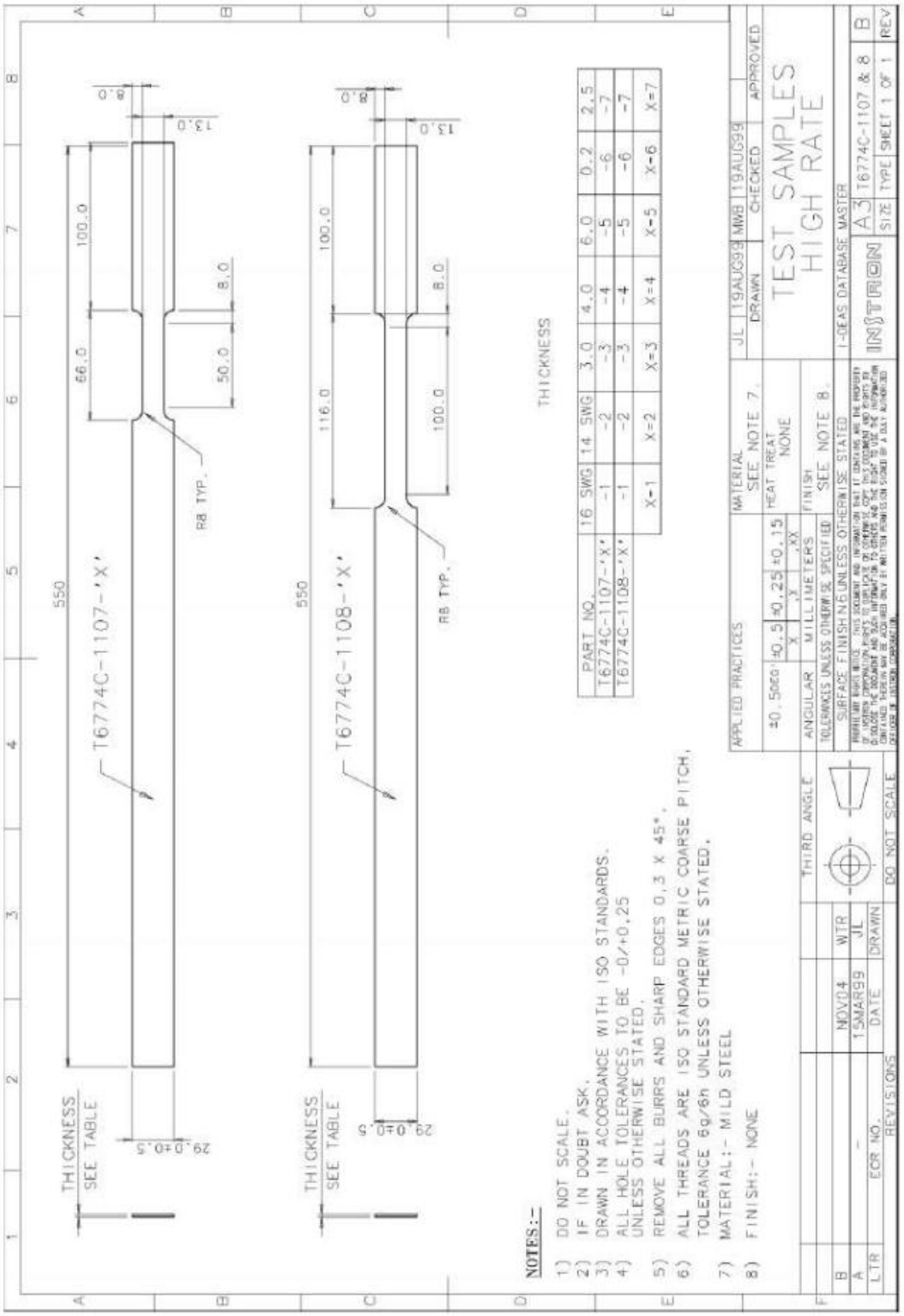

Appendix E **Tested Samples**

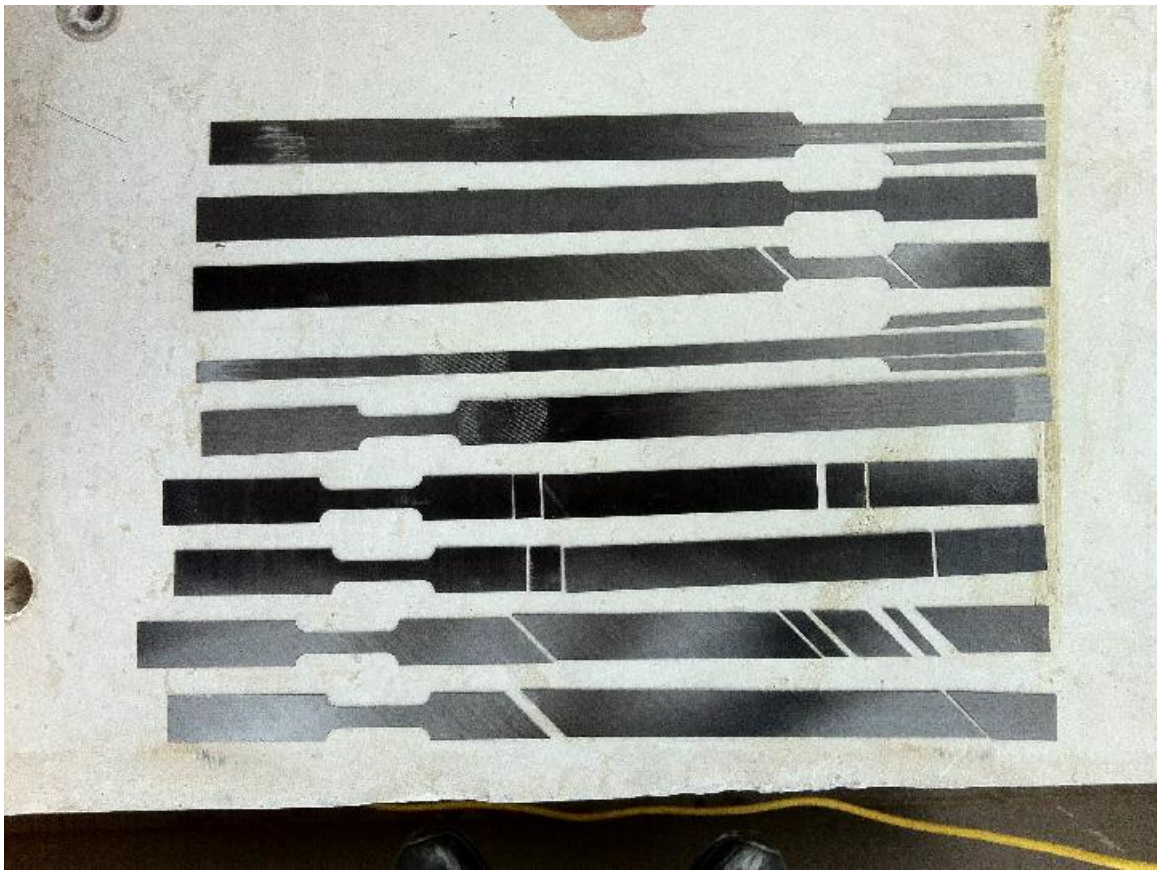

Appendix F **LS-DYNA Cutting Force Simulation**

		Simulation SAE600			
	θ	0°		45°	
Vc	f	Vc	Vf	Vc	Vf
80	0.05	58	9	41	0
	0.1	106	9	66	-3
	0.15	138	8	100	-8
	0.2	203	11.7	121	-13.9
40	0.05	62	7	45	2
	0.1	114	4	69	-5
	0.15	112	13	129	10
	0.2	184	13	105	-5

WP-Insert v8

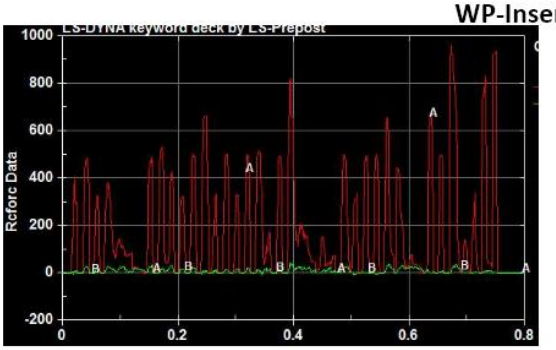

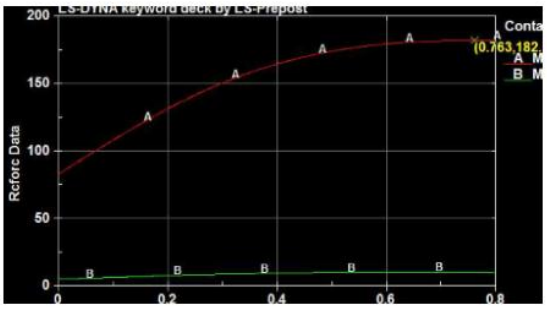

Vc Filtered
180= 116 N
300= 182 N
600= 203 N

Vf Filtered
180= 3.56 N
300= 10.8N
600= 11.7 N

80 m/min
0.2 mm/rev

Mat prop as v5, v6 and v7
A finer mesh was used

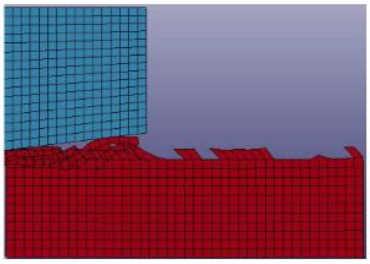

Appendix F

LS-DYNA Cutting Force Simulation

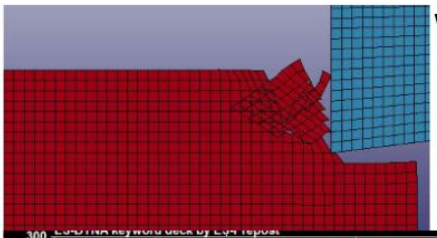

WP-Insert v11

80 m/min
0.2 mm/rev

A1	A2	A3
1.0000000	-1.0000000	0.0

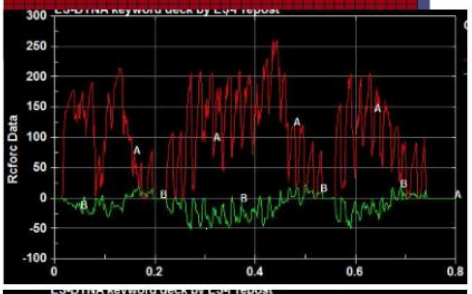

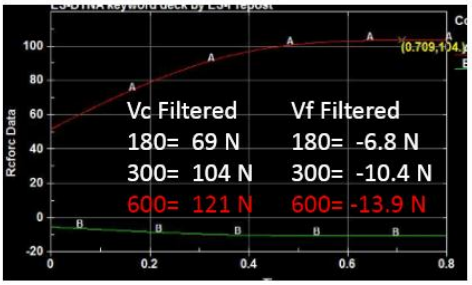

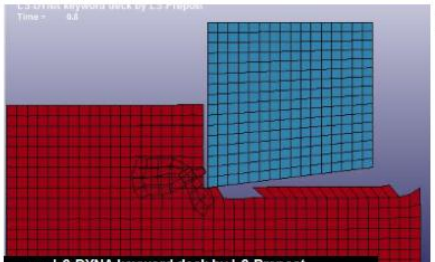

WP-Insert v12 (from v8)

40 m/min
0.2 mm/rev

A1	A2	A3
1.0000000	0.0	0.0

Vc Filtered
180= 109 N
300= 162 N
600= 184 N

Vf Filtered
180= 8 N
300= 12 N
600= 13 N

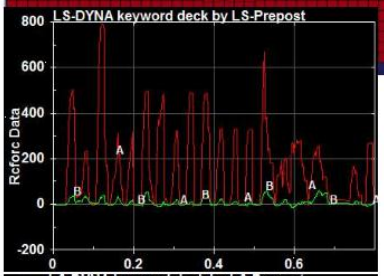

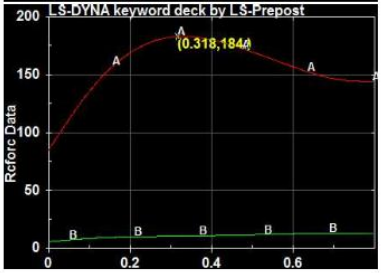

Appendix F

LS-DYNA Cutting Force Simulation

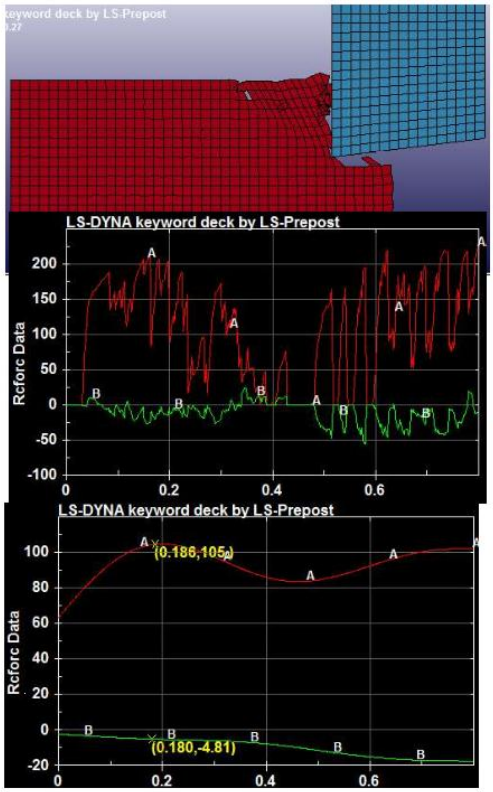

WP-Insert v15

40 m/min
0.2 mm/rev

A1	A2	A3
1.0000000	-1.0000000	0.0

Vc Filtered	Vf Filtered
180= 65 N	180= -5 N
300= 95 N	300= -10 N
600= 105 N	600= -5 N

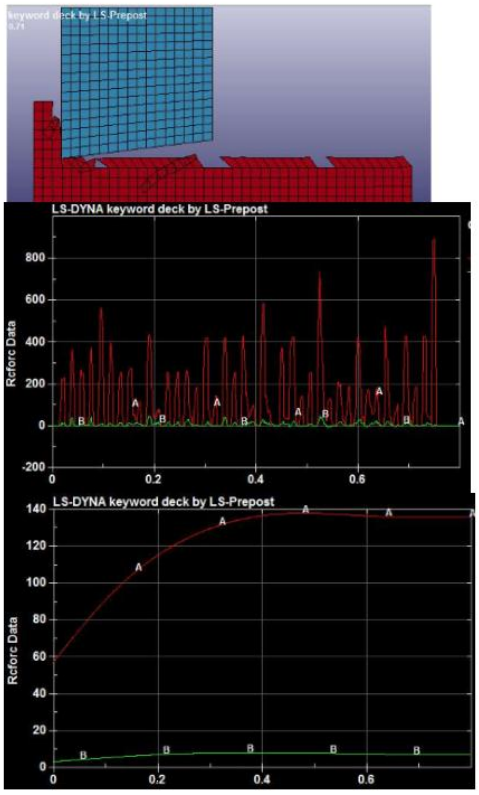

WP-Insert v16

80 m/min
0.15 mm/rev

A1	A2	A3
1.0000000	0.0	0.0

Vc Filtered	Vf Filtered
180= 82 N	180= 5 N
300= 127 N	300= 7 N
600= 138 N	600= 8 N

Appendix F

LS-DYNA Cutting Force Simulation

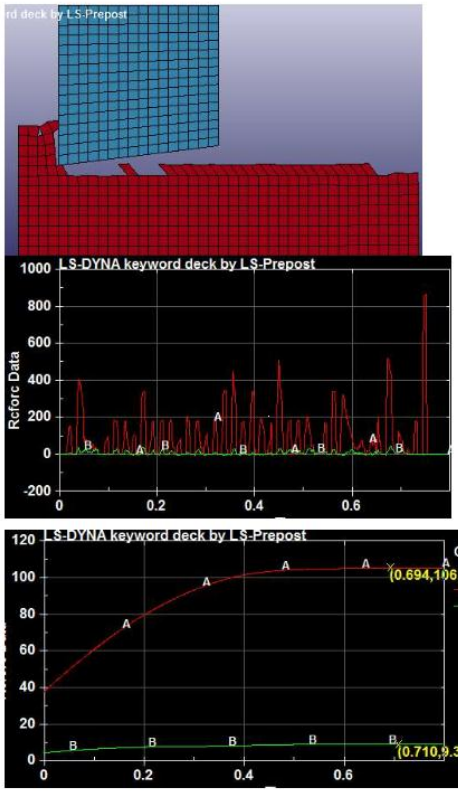

WP-Insert v17

80 m/min
0.1 mm/rev

A1	A2	A3
1.0000000	0.0	0.0

Vc Filtered	Vf Filtered
180= 60 N	180= 6 N
300= 95 N	300= 9 N
600= 106 N	600= 9 N

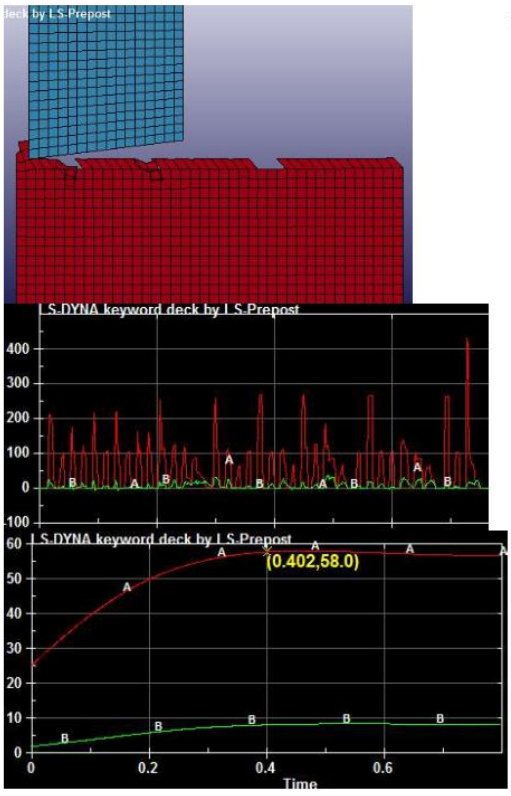

WP-Insert v18

80 m/min
0.05 mm/rev

A1	A2	A3
1.0000000	0.0	0.0

Vc Filtered	Vf Filtered
180= 35 N	180= 5 N
300= 54 N	300= 7 N
600= 58 N	600= 9 N

Appendix F

LS-DYNA Cutting Force Simulation

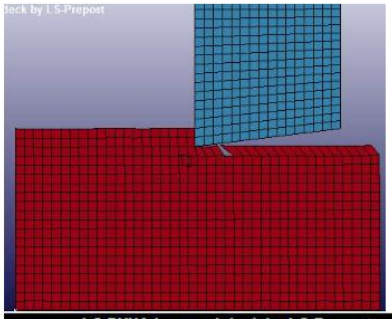

WP-Insert v19

40 m/min
0.05 mm/rev

A1	A2	A3
1.0000000	0.0	0.0

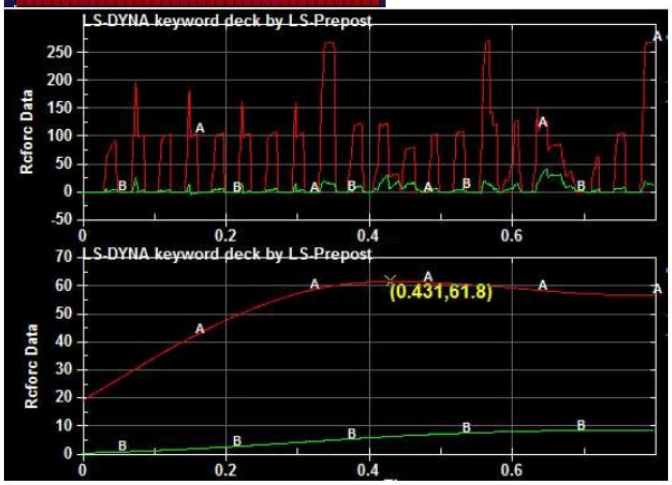

Vc Filtered	Vf Filtered
180= 34 N	180= 3 N
300= 54 N	300= 6 N
600= 62 N	600= 7 N

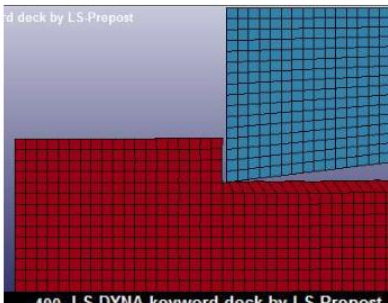

WP-Insert v20

40 m/min
0.10 mm/rev

A1	A2	A3
1.0000000	0.0	0.0

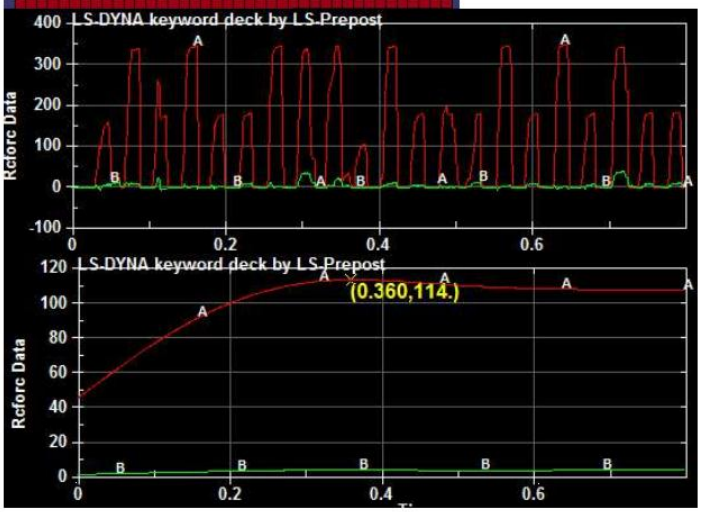

Vc Filtered	Vf Filtered
180= 67 N	180= 2 N
300= 105 N	300= 4 N
600= 114 N	600= 4 N

Appendix F

LS-DYNA Cutting Force Simulation

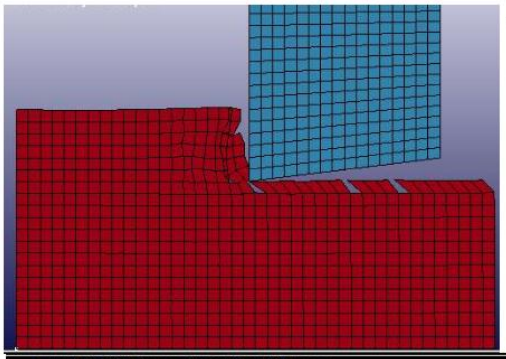

WP-Insert v21

40 m/min
0.15 mm/rev

A1	A2	A3
1.0000000	0.0	0.0

Vc Filtered
180= 70 N
300= 106 N
600= 112 N

Vf Filtered
180= 7 N
300= 10 N
600= 13 N

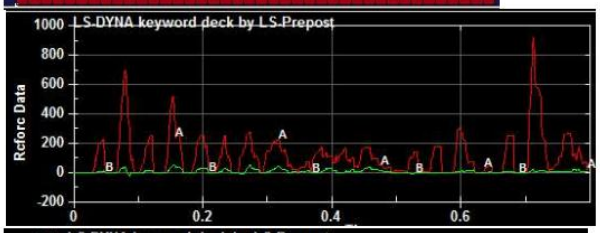

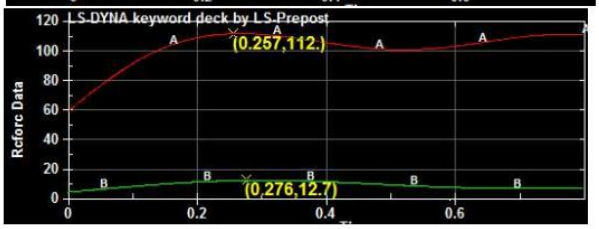

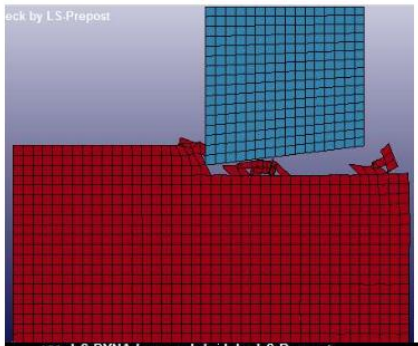

WP-Insert v22

40 m/min
0.05 mm/rev

A1	A2
1.0000000	-1.0000000

Vc Filtered
180= 25 N
300= 39 N
600= 45 N

Vf Filtered
180= 1 N
300= 2 N
600= 2 N

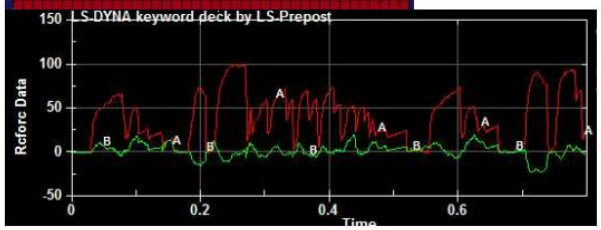

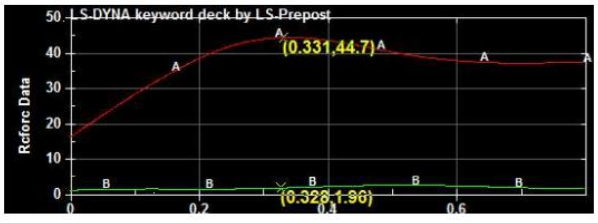

Appendix F

LS-DYNA Cutting Force Simulation

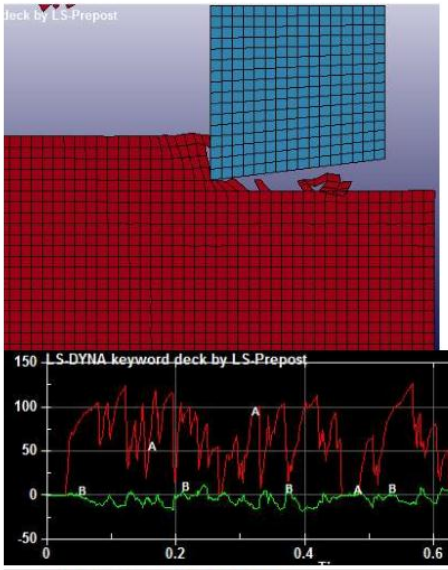

WP-Insert v23

40 m/min
0.1 mm/rev

A1	A2
1.0000000	-1.0000000

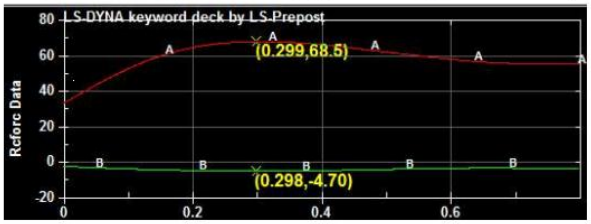

Vc Filtered	Vf Filtered
180= 41 N	180= -3 N
300= 61 N	300= -4 N
600= 69 N	600= -5 N

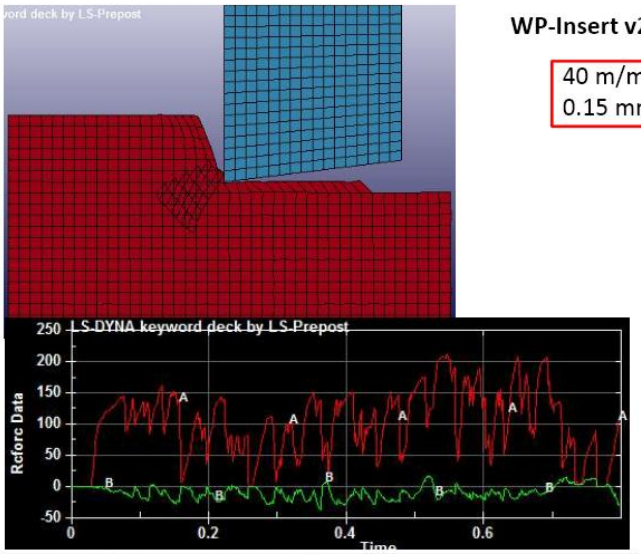

WP-Insert v24

40 m/min
0.15 mm/rev

A1	A2
1.0000000	-1.0000000

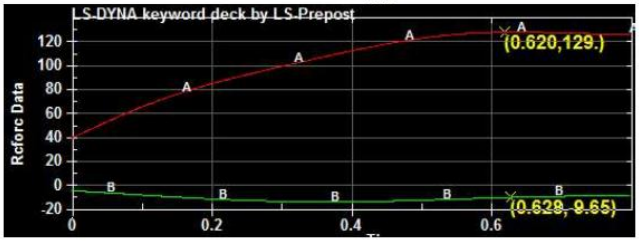

Vc Filtered	Vf Filtered
180= N	180= N
300= N	300= N
600= 129 N	600= 10 N

Appendix F

LS-DYNA Cutting Force Simulation

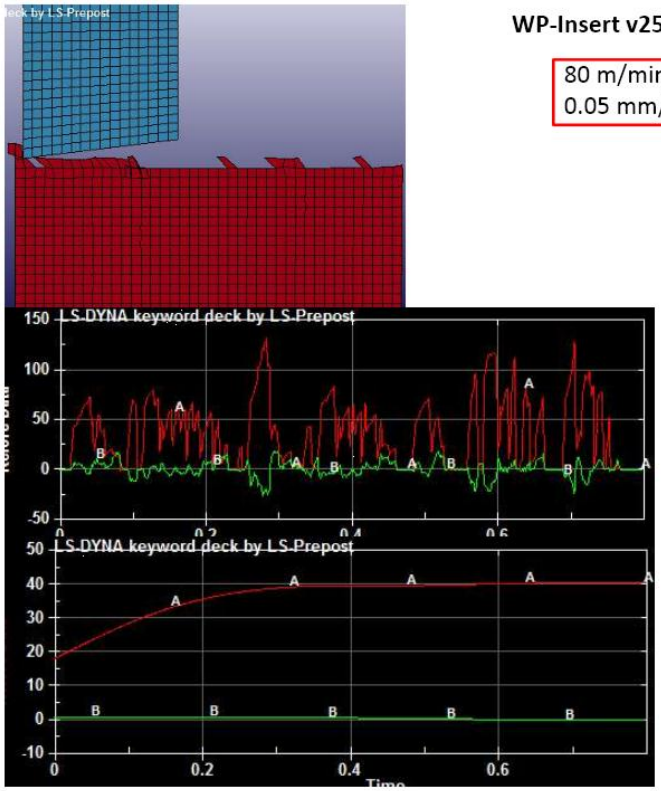

WP-Insert v25

80 m/min
0.05 mm/rev

A1	A2
1.0000000	-1.0000000

Vc Filtered	Vf Filtered
180= 24 N	180= 0 N
300= 38 N	300= 0 N
600= 41 N	600= 0 N

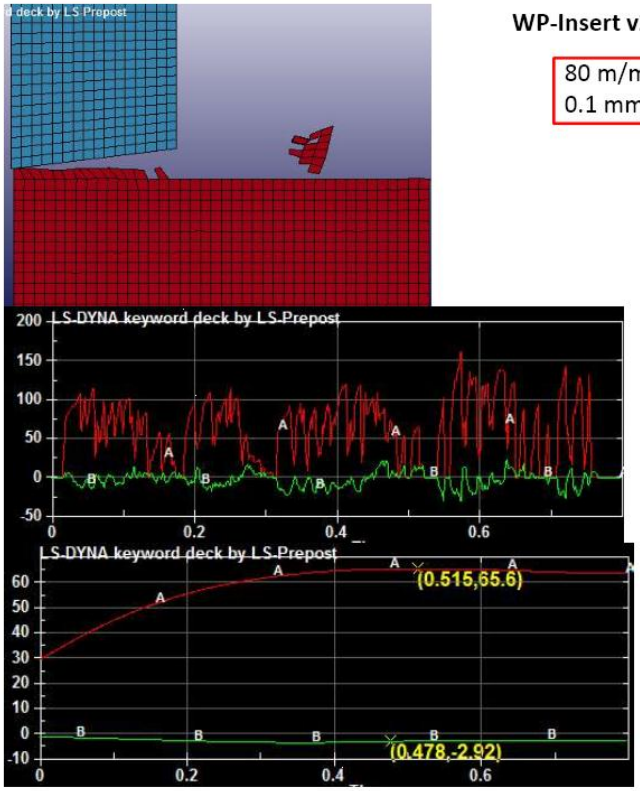

WP-Insert v26

80 m/min
0.1 mm/rev

A1	A2
1.0000000	-1.0000000

Vc Filtered	Vf Filtered
180= 39 N	180= -2 N
300= 61 N	300= -3 N
600= 66 N	600= -3 N

Appendix F

LS-DYNA Cutting Force Simulation

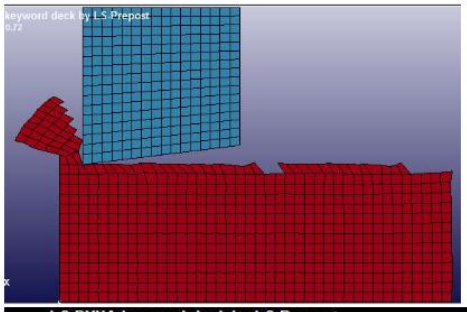

WP-Insert v27

80 m/min
0.15 mm/rev

A1	A2
1.0000000	-1.0000000

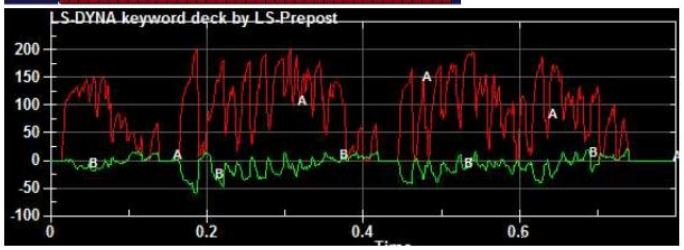

Vc Filtered	Vf Filtered
180= 58 N	180= -5 N
300= 90 N	300= -7 N
600= 100 N	600= -8 N